A STUDY ON IONIC CONDUCTIVITY OF ALGINATES DOPED WITH AMMONIUM NITRATE AS APPLICATION FOR SOLID BIOPOLYMER ELECTROLYTES

NUR MUHITUL JALILAH BINTI RASALI

MASTER OF SCIENCE

UNIVERSITI MALAYSIA PAHANG

UNIVERSITI MALAYSIA PAHANG

DECLARATION OF THESIS AND COPYRIGHT

Author's Full Name : NUR MUHITUL JALILAH BINTI RASALI

Date of Birth : 21/01/1992

Title : A STUDY ON IONIC CONDUCTIVITY OF ALGINATES DOPED WITH AMMONIUM NITRATE AS APPLICATION FOR SOLID BIOPOLYMER ELECTROLYTES

Academic Session : SEM 2 2018/2019

I declare that this thesis is classified as:

☐ CONFIDENTIAL (Contains confidential information under the Official Secret Act 1997)*

☐ RESTRICTED (Contains restricted information as specified by the organization where research was done)*

☑ OPEN ACCESS I agree that my thesis to be published as online open access (Full Text)

I acknowledge that Universiti Malaysia Pahang reserves the following rights:

1. The Thesis is the Property of Universiti Malaysia Pahang
2. The Library of Universiti Malaysia Pahang has the right to make copies of the thesis for the purpose of research only.
3. The Library has the right to make copies of the thesis for academic exchange.

Certified by:

_____ _____
(Student's Signature) (Supervisor's Signature)

_____ _____
New IC/Passport Number Name of Supervisor
Date: Date:

NOTE: * If the thesis is CONFIDENTIAL or RESTRICTED, please attach a thesis declaration letter.

SUPERVISOR's DECLARATION

I hereby declare that I have checked this thesis and in my opinion, this thesis is adequate in terms of scope and quality for the award of the degree of Master of Science.

_____

(Supervisor's Signature)

Full Name   : DR AHMAD SALIHIN BIN SAMSUDIN

Position   : SENIOR LECTURER

Date   :

STUDENT'S DECLARATION

I hereby declare that the work in this thesis is based on my original work except for quotations and citations which have been duly acknowledged. I also declare that it has not been previously or concurrently submitted for any other degree at Universiti Malaysia Pahang or any other institutions.

_____

(Student's Signature)

Full Name   : NUR MUHITUL JALILAH BINTI RASALI

ID Number   : MSM 16005

Date   :

A STUDY ON IONIC CONDUCTIVITY OF ALGINATES DOPED WITH AMMONIUM NITRATE AS APPLICATION FOR SOLID BIOPOLYMER ELECTROLYTES

NUR MUHITUL JALILAH BINTI RASALI

Thesis submitted in fulfillment of the requirements

for the award of the degree of

Master of Science

Faculty of Industrial Sciences & Technology

UNIVERSITI MALAYSIA PAHANG

JULY 2019

ACKNOWLEDGEMENTS

ABSTRAK

Penemuan baru dalam bidang sistem elektrolit adalah sangat luas terutamanya dalam penyimpanan tenaga yang menggunakan bahan-bahan hijau. Peranti elektrokimia adalah penting berikutan sumbangannya yang besar sebagai penyimpan tenaga khususnya bagi sektor industri. Pada masa kini, penggunaan polimer sintetik terus meningkat tetapi polimer ini mahal dan tidak mesra alam sekitar. Oleh itu, system elektrolit biopolimer pepejal (SBEs) dipilih sebagai salah satu elektrolit jenis baharu yang menggunakan polimer semulajadi sebagai polimer perumah. Kajian ini dijalankan untuk mengkaji kekonduksian dan pengangkutan ionik SBEs sistem untuk membangunkan elektrolit biopolimer jenis baharu. Dalam kajian ini, sistem SBEs berasaskan alginat menggunakan pelbagai peratus berat ammonium nitrat sebagai bahan dop penderma proton telah berjaya dihasilkan melalui kaedah tuangan larutan. Beberapa teknik seperti spektroskopi inframerah transformasi Fourier (FTIR), belauan sinar-X (XRD) spektroskopi impedans elektrik (EIS), pengukuran nombor pemindahan (TNM)), dan analisis termogravimetrik (TGA) dijalankan untuk mencirikan kajian ini. Analisis FTIR mengesahkan bahawa interaksi telah berlaku antara kumpulan karboksilat (COO^-) daripada alginate dan H^+ di mana terdapat perubahan pada puncak di nombor gelombang 1415 cm^{-1} dan 1598 cm^{-1} yang berpadanan dengan $C=O$ dan CO^- dalam alginate, 1062 cm^{-1} yang sepadan dengan C-O-C, dan 3393 cm^{-1} yang sepadan dengan kumpulan OH^-. Kelincahan (μ) dan pekali resapan (D) didapati mempengaruhi daya kekonduksian ionik dalam sistem SBEs seperti yang diamati melalui teknik nyahkonvolusi-IR. Analisis belauan sinar-X (XRD) mendedahkan bahawa sampel 25 wt.% NH_4NO_3 merupakan sampel yang paling amorfus dan matriks polimer menyebabkan perubahan pada keadaan bahan daripada semi-kristal kepada sifat amorfus. Daripada analisis TGA, peningkatan kestabilan terma bertambah dengan penambahan NH_4NO_3. Kekonduksian ionik sistem SBEs telah diukur menggunakan EIS dengan julat frekuensi daripada 50 Hz hingga 1 MHz dan mencapai kekonduksian ionik maksimum pada suhu ambien (303 K) dengan 5.56×10^{-5} S cm^{-1} untuk sampel yang mengandungi 25 wt.% NH_4NO_3. Sistem SBEs didapati mematuhi kelakuan Arrhenius dengan $R^2{\sim}1$ di mana semua sampel diaktifkan secara termal dengan peningkatan suhu dan sampel yang menunjukkan kekonduksian tertinggi mempunyai nilai tenaga pengaktifan E_a yang paling rendah (0.11 eV). Analisis model mekanisme konduksi mencadangkan model loncatan penghalang berkorelasi (CBH) untuk sistem alginate-NH_4NO_3 SBEs. Sampel alginate-NH_4NO_3 SBEs dengan kekonduksian tertinggi mempunyai nombor pemindahan, t_{ion} bersamaan 0.97, yang menunjukkan bahawa spesies konduksi adalah kation. Tujuan penghasilan sistem SBEs ini adalah untuk digunakan sebagai penyimpan tenaga seperti bateri atau super kapasitor pada masa hadapan.

ABSTRACT

There are numerous new discoveries in the field of electrolytes system especially in energy storage using green materials. Electrochemical devices are essential due to their huge contribution in energy storage, especially for the industrial sector. Nowadays, the usage of synthetic polymer keep increasing but these polymers are costly and not environmental friendly. Therefore, the solid biopolymer electrolytes (SBEs) system have been chosen as one of the new types of electrolytes that use natural polymer as a host polymer. This research was undertaken to investigate the conductivity and ionic transport of SBEs to develop a new type of biopolymer electrolyte. In the present research, SBEs system was developed based on alginate as the host polymer doped with various weight percentages of ammonium nitrate as a proton donor and prepared using the solution casting method. Several techniques, such as Fourier transform infrared (FTIR) spectroscopy, X-ray and diffraction (XRD), electrical impedance spectroscopy (EIS), transference number measurement (TNM) and thermogravimetric analysis (TGA) were performed to characterize this present work. FTIR analysis confirmed that interaction has occurred between the carboxylate group (COO$^-$) from alginate and H$^+$ where there were changes in the peaks at wavenumbers 1415 cm^{-1} and 1598 cm^{-1} that corresponded to C=O and C-O$^-$ in alginate, 1062 cm^{-1} that corresponded to C–O–C, and 3393 cm^{-1} that corresponded to the OH-group. The mobility (μ) and diffusion coefficient (D) were found to influence the ionic conductivity in the SBE system as observed via IR-deconvolution technique. X-ray diffraction analysis (XRD) revealed that the 25 wt.% NH$_4$NO$_3$ was the most amorphous sample, and the polymer matrix resulted in the change of state of the material from semi-crystalline to amorphous in nature. From TGA analysis, the thermal stability increased with the addition of NH$_4$NO$_3$. The ionic conductivity of the SBEs system was measured using EIS with a frequency range from 50 Hz to 1 MHz and achieved the maximum ionic conductivity at ambient temperature (303 K) with 5.56 $\times$ 10^{-5} S cm^{-1} for the sample containing 25 wt.% of NH$_4$NO$_3$. The SBEs system was found to obey the Arrhenius behavior with R^2~1 where all samples were thermally activated with increasing temperature with the highest conducting sample showing the lowest value of activation energy E_a (0.11 eV). The conduction mechanism model suggested a correlated barrier hopping (CBH) model for the alginate-NH$_4$NO$_3$ SBEs system. The alginate-NH$_4$NO$_3$ SBEs system sample with the highest conductivity had a transference number, t_{ion} of 0.97, which further indicated that the conduction species is a cation. In the future, this SBE system is aimed to be used for energy storage, including as a battery or supercapacitor.

TABLE OF CONTENT

LIST OF TABLES

LIST OF FIGURES

LIST OF SCHEMES

LIST OF SYMBOLS

2θ	Bragg angle
^{o}C	degree celcius
E_a	activation energy
wt. %	weight percentage
k	Boltzman constant
t	thickness
T	temperature
R_b	bulk resistance
σ	conductivity
R^2	regression
ε_r	dielectric constant
ε_i	dielectric loss
ε_o	permittivity of free space
f	frequency
M_r	real modulus
M_i	imaginary modulus
Z_i	imaginary part of the complex permittivity
Z_r	real part of complex permittivity
μ_+	cationic ionic mobility
μ_-	anionic ionic mobility
D_+	cationic diffusion coefficient
D_-	anionic diffusion coefficient

LIST OF ABBREVIATIONS

AC	Alternating current
AF	ammonium fluoride
CA	Cellulose acetate
CBH	correlated barrier hopping
CH_3COONH_4	ammonium acetate
CMC	Carboxyl methyl cellulose
CPEs	Composite polymer electrolytes
CuTF	copper trifluoromethanesulfonate
DTAB	Dodecyltrimethyl ammonium bromide
EIS	Electrochemical Impedance Spectroscopy
ES	Ethylene sulphite
FTIR	Fourier Transform Infrared Spectrometer
GEs	Gel electrolytes
GPE	Gel polymer electrolyte
HEC	hydroxyethyl cellulose
HFP	co-hexafluoropropylene
HNT	halloysite nanotube
LC	lignocellulose
LiTf	lithium triflate
$LiCF_3SO_3$	lithium trifluoromethanesulfonate
$LiClO_4$	lithium perchlorate
MC	methyl cellulose
NH_4BF_4	ammonium tetrafluroborate
NH_4I	ammonium iodide
NH_4NO_3	ammonium nitrate
$(NH_4)SCN$	ammonium thiocyanate
$NH_4SO_3CF_3$	ammonium trifluoromethane sulfonate
NSPT	non-overlapping small polaron tunneling
OA	oleic acid
OLPT	overlapping-large polaron tunneling
PEI	polyetherimide

PEG	polyethylene glycol
PEO	poly(ethylene oxide) (PEO)
PEs	polymer electrolytes
PMMA	poly(methyl methacrylate)
PVA	poly (vinyl alcohol)
PVDF	poly(vinylidene fluoride)
PVP	poly(vinylpyrrolidinone)
QMT	quantum mechanical tunneling
SBEs	Solid biopolymer electrolytes
SN-BMImBF$_4$	succinonitrile-1-butyl-3-methylimidazolium tetrafluoroborate
TiO$_2$	titanium oxide
TGA	Thermogravimetric analysis
TNM	Transference number measurement
XRD	X-ray diffractometer spectroscopy

CHAPTER 1

INTRODUCTION

1.1 Background of Research

Electrochemical energy devices play a main role in industry sectors that include material considerations and the history of changes in demand prospects, spanning fundamental mechanisms to engineering challenges. The first discovery of ionic conductivity by Wright in 1975 led to the development of solid polymer electrolytes (SPEs) where Armand in 1978 continued the study with the implementation of electrolytes in batteries (Isa & Samsudin, 2016; Sohaimy & Isa, 2016; Przyluski & Wieczorek, 1989). Polymer plays a role as the host in developing the migration of ion in SPEs.

Yet, today's industries are using materials in batteries that contain hazardous and toxic chemicals such as lithium, cadmium, mercury, and lead. These materials are unfriendly to the environment and humans. Most of the batteries are thrown away when they are broken or drained, which may cause environmental pollution. When the materials are burned, toxic chemicals will release hazardous gasses into the air, or known as air pollution (Verma et al., 2016). In addition, the polymer industry contributes to the pollution of the environment due to its poor disposal (Sakurai et al., 2003). A recent crisis involved the electronic device Samsung Galaxy Note 7, which exploded due to its battery and caused an adverse effect to the reputation of the company (Cheng & Dou, 2016).

In addition, it was reported in the previous studies that the usage of synthetic materials as polymer electrolytes (PEs) is harmful to the surrounding and costly. From the literature, there are many different types of PEs such as poly (ethylene oxide), poly (vinyl pyrrolidone), poly (vinyl alcohol), poly (acrylonitrile), poly (methyl methacrylate), poly (vinyl chloride), and other synthetic polymers (Maitz, 2015). The synthetic polymer

1

is costly and not environmentally friendly. The consideration to switch to a new system of electrolytes is an excellent step toward building green technology without the use of dangerous materials.

Solid polymer electrolytes (SPEs) are a promising substitute to liquid electrolytes (Itoh et al., 2009). SPEs are formed by dissolution of salts in a polymer matrix. They have received much attention as solid electrolyte materials for advanced applications, such as high-energy density batteries, sensors, electrochromic devices, and fuel cells (Zang, Luo & Ru, 2010). Several advantages of SPEs have been discovered since their development, such as good contact between the electrode and electrolyte, simple preparation in different forms, good mechanical and adhesive properties, no leakage of electrolytes, higher energy density, and improved safety hazards.

In recent times, researchers have started to focus on proton conducting PEs for use as a power source. They are keen to develop biopolymer electrolytes due to the eco-friendly and biodegradable properties. The biopolymer provides renewable energy, as well as being cheap and eco-friendly. These advantages have made the solid biopolymer electrolytes (SBEs) a promising alternative to synthetic polymers in the electrolytes system. Nowadays, SBEs have gained remarkable attention among researchers due to their potential application in electrochemical devices such as in batteries, electrochromic displays, fuel cells, and supercapacitors (Gurunathan et al., 1999; Hafiza & Isa, 2014; Khiar & Arof, 2011; Shukur et al., 2014). Currently, electronic devices like cell phones, remote controllers, laptops, and tablets used batteries as their energy storage.

Natural polymers meet the criteria to be used as an electrolyte due to the high demand for a green environment (Monisha et al., 2017; Ramesh et al., 2013; Ramli & Isa, 2016). The materials used for the PEs are from natural polymers such as starch, cellulose derivatives like hydroxyethyl cellulose (HEC), methyl cellulose (MC), carboxyl methylcellulose (CMC), chitosan, agar-agar, pectin, gelatin, and alginate, which are suitable to be used as a host polymer in the SBEs. Polysaccharides are made of natural polymers, which are abundant in nature. Among all the materials, alginate is a possible candidate as a polymer host for natural polymers electrolytes. Alginate is a biological polymer (biopolymer), which is a new industrial polysaccharide extracted from seaweeds, and it has shown excellent performance in water solubility. It may be used in many applications such as in the food industry, biomedical science, engineering, and

pharmaceutical (Andrea et al., 2016; Lee & Mooney, 2012). Purified alginates have widespread industrial uses especially due to their ability to form hydrogels, beads, fibers, or films. In addition, alginate is used as a host polymer due to its superior characteristics such as biocompatibility, low toxicity, and relatively low cost (Lee & Mooney, 2012). Due to these favorable characteristics, alginate is suitable to be used as a host polymer in this research.

However, the use of natural polymer in SBEs results in low ionic conductivity, which limits its use as energy sources (Awadhia & Agrawal, 2007). Therefore, the ionic dopant can overcome the ionic conductivity limitations. Ammonium salt is a good proton donor as it provides ions that can help the polymer host to increase its ionic conductivity (Hafiza & Isa, 2017). Thus, the SBEs system based on natural polymer, alginate doped with salt, ammonium nitrate (NH_4NO_3), will be studied in this research to find a replacement for the current electrolytes system. To the best of our knowledge, other researchers have never studied this material.

1.2   Problem Statement

Nowadays, most researchers demand for long cycle, reliable, and rechargeable devices especially in the application of electronic devices such as batteries, supercapacitors, and fuel cells. When it was first reported in 1973, researchers believed that SBEs could be used to replace synthetic polymers. SBEs are the negatively charged groups attached to the polymer backbone (Ng & Mohamad, 2008) and are the dominant charge carriers, while the positively charged ions are essentially harmonized to the host (Onishi et al., 1980). Indeed, the addition of salt ensures that the polymer is amorphous in nature above the glass-transition temperature, which is our aim of interest.

Synthetic polymers or referred to as "plastics" are derived from petroleum. The use of synthetic polymers such as poly (vinyl alcohol) (PVA), poly(vinylpyrrolidinone) (PVP), poly(ethylene oxide) (PEO), and poly(vinylidene fluoride) (PVDF) (Kulshrestha, et al., 2014; Ramya et al., 2007; Vijaya et al., 2012) in the making of SBEs has been increasing, but these polymers are costly and not environmentally friendly as compared to the natural polymer. Thus, many alternatives have been considered to replace the electrolytes by using the biopolymer electrolytes system to overcome the drawbacks of using un-renewable resources.

Biopolymer-based polymer-salt complex electrolytes are a relatively new class of material and being environmentally friendly, it can replace the usage of synthetic polymer (Basu et al., 2012; Singh et al., 2012). Many researchers are studying the biopolymer-based polymer-salt complexes. A review of natural polysaccharides as polymeric materials by Finkenstadt investigated the basics and importance of using nature-based electrolytes (Finkedstadt, 2005). Many green materials of SBEs have been discovered and used as a host polymer as they are the most abundant natural polymers on earth. A study on the suitable electrolytes made from alginate-based biopolymer has been conducted on the SBEs system. One of the efforts to preserve the environment is by learning about biopolymers as a host polymer. It is essential to replace synthetic polymers with a new system based on biopolymer that can produce green technology.

1.3   Significance of research

A few types of energies are continuously being used in our daily activities, such as oil, nuclear, and fossil fuels. To reduce the usage of these energies due to environmental concerns, environmentally friendly power sources need to be considered such as batteries, supercapacitors, and dye-sensitized solar cells. The concept of SBEs is very specific and involves multidisciplinary fields that include the disciplines of electrochemistry, polymer science, organic chemistry, and inorganic chemistry (Aziz, 2013). SBEs become the center of attention among researchers due to its interesting properties as compared to other systems such as liquid and gel electrolytes.

Recent studies have focused on electrolytes based on natural polymer due to the low cost of production, storage, and distribution of energy (Varshney & Gupta, 2011). Hence, the development of different electrolytes using natural products is vital to overcome the drawbacks of non-biodegradable products. Biodegradable natural electrolytes are already used to synthesize electrolytes for many applications, such as cosmetics (Al-Hetar et al., 2011; Jyothi, 2010), pharmaceutical (Andrade et al., 2009; Raphael et al., 2010), food industry (Osman et al., 2001; Vieira et al., 2007), and also in the preparation of new SBEs.

SBEs have gained attention due to its properties such as versatility of use, biocompatibility, biodegradability, abundance in nature, and lower cost. The natural

polymer, namely alginate, an anionic polymer derivative is chosen as a host polymer to discover the potential of alginate as a SBEs system for application in electrochemical devices. In the present work, alginate is used to discover its potential as a biopolymer matrix. Alginate molecules are a natural polymer of polysaccharides (natural carbohydrate) that have the cell structure of seaweeds. It is regarded as biocompatible, nontoxic, and biodegradable, which explains its extensive use in modern industry sites. In recent times, alginate has been tested with chemical modifications to enhance its hydrophilic property. The dispersion of free hydroxyl and carboxyl groups along the backbone makes it the best candidate for chemical testing (Braccini & Perez, 2001).

1.4   Objectives

The objectives of this research are as follow:

1.   To prepare alginate doped with ammonium nitrate (NH_4NO_3) as a solid biopolymer electrolytes (SBEs) system.
2.   To identify the structural and thermal properties of the alginate doped with NH_4NO_3 SBEs system.
3.   To determine the ionic conduction and transport properties of the alginate doped with NH_4NO_3 SBEs system.

1.5   Thesis Outline

This thesis contains five chapters with each chapter describing an aspect of the research. Chapter 1 gives an introduction to the research including the background of the study, problem statement, objectives, and scope of the thesis.

Chapter 2 contains the literature review, which gives an exhaustive overview of previous and current research on the SBEs system. The enhancement of biopolymer conductivity also are discussed.

Chapter 3 focuses on the research methodology used in the present research. The detail explanation in preparation of the thin films using casting method is presented. This chapter describes the details of sample preparation and characterization using Fourier transform infrared (FTIR) spectroscopy, X-ray diffraction (XRD) spectroscopy, and

thermogravimetric analysis (TGA), electrical impedance spectroscopy (EIS), and transference number measurement (TNM).

Chapter 4 elaborates the analysis and explains the results including structural properties, thermal properties, ionic conduction properties, and transport properties. Lastly, Chapter 5 explains the conclusion of the thesis that is reflected to the objectives in this research and explanation with several recommendations for future studies is presented.
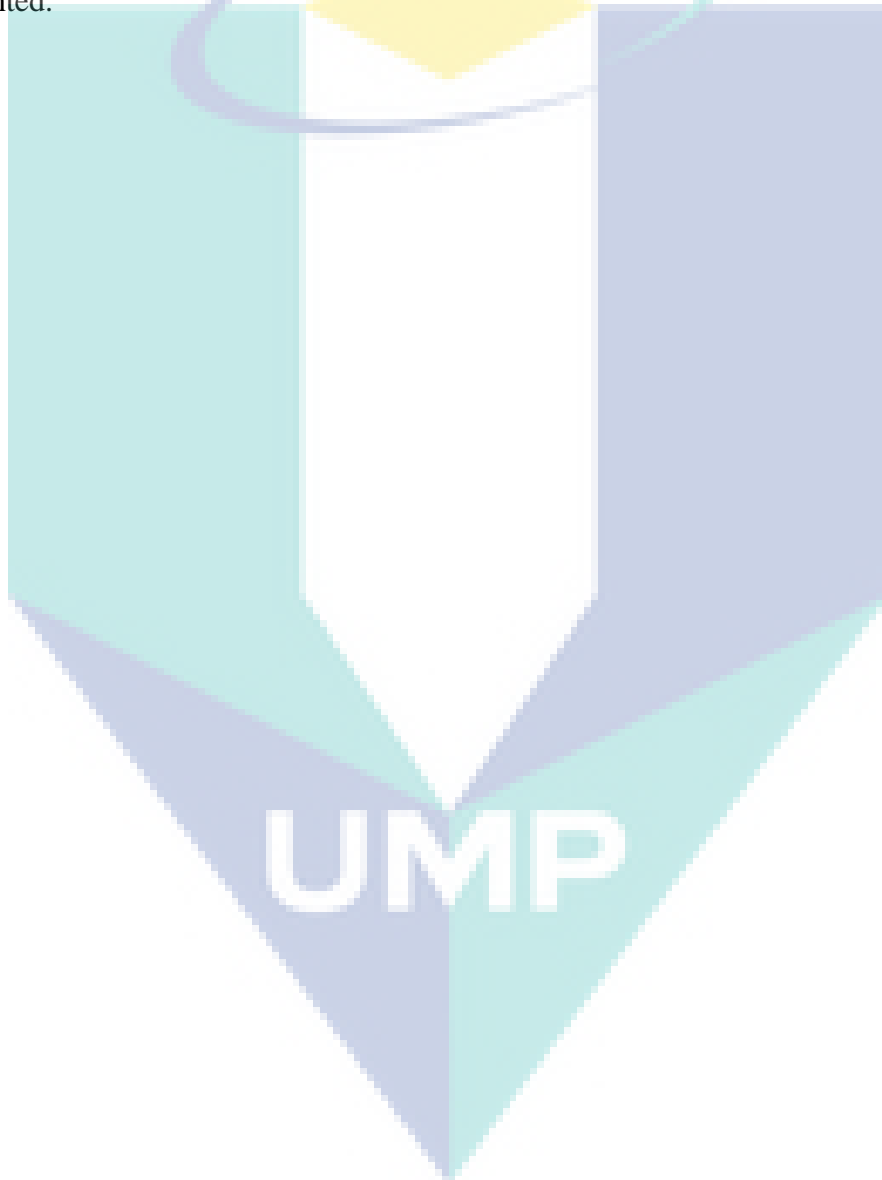
CHAPTER 2

LITERATURE REVIEW

2.1   Polymer electrolytes (PEs)

Electrolyte is the substance that conducts electricity, which occurs between the anode and cathode (Saikia et al., 2008). Ionic conductors or electrolytes are one of the main major components in energy sources as ionic conduction gives high impact to the durability of devices (Hofmann et al., 2013; Rao et al., 2012). In the past three decades, electrochemical devices have been extensively used in our daily lives with liquid electrolytes (LEs) because of their excellent ionic conductivity. Yet, there are problems in using LEs include leakage, low stability, and corrosion reactions with the electrode (Kim et al., 2013). The possibility of electronic conduction also leads to its drawbacks. These limitations of LEs make it less appropriate for use in electrochemical devices. New electrolytes materials need to be developed to replace the LEs to overcome the limitations and subsequently become the new energy sources in the electrolytes system (Goriparti et al., 2014).

The evolution of solid-state materials such as ceramic, glass, crystalline, and PEs as electrolytes were discovered in the early 1970s (Ngai et al., 2016; Ramesh & Liew, 2010). Other developments in PEs are amorphous polymers, hybrid composite materials polymers, and crystalline polymers (Armand et al., 2011). PEs was introduced by Fenton et al. in 1973, and the importance of its technological application was acknowledged in the early 1980s (Shriver, 1995). PE is a membrane made from the dissolution of salts in a polymer matrix with high molecular weight (Ramesh & Lu, 2012). This solid solvent-free system owns ionic conduction properties and therefore, is extensively used in electrochemical devices such as solid-state batteries and rechargeable batteries, especially lithium-ion batteries. In recent years, PEs have other medium applications in progressive

electrochemical, electrochromic, and electronic devices such as supercapacitors, fuel cells, dye-sensitized solar cells, rechargeable batteries, electrochemical sensors, analogue memory devices, and electrochromic windows (Kim et al., 2004; Scrosati, 1993; Vincent, 1987). It can also be used as a separator in batteries as a replacement for the ionic solution (Ahmad & Isa, 2012).

PEs consist of mutual characteristics, which are crystalline and amorphous phases. Some research works have shown that the transportation of ions happens in the amorphous phase rather than the crystalline phase; however, the PE host polymer is usually semi-crystalline (Aziz & Abidin, 2013; Aziz & Abidin, 2015). Therefore, to overcome the shortcomings and enhance PEs' conductivity, one of the most commonly applied techniques is to recover the ambient ionic conductivity. Ionic conductivity usually refers to the crystallinity phase and the viscosity of the PEs (Liew et al., 2014). Crystalline-based PEs are related to the sample with high crystallinity. It has lower ion mobility, which leads to low conductivity (Kam et al., 2014; Liew et al., 2014). The lower viscosity in PEs contributes to more holes and hence results in higher ionic conductivity (Liew et al., 2014).

In 1975, Wright introduced ionic conductivity based on polyethylene oxide (PEO) of PEs. In the same year, Feuillade and Perche reported the plasticization of polymer with an aprotic solution containing alkali metal salts. More than one type of polymers have been used as the host PE. If the mixture of the structurally different polymers interacts without covalent bond formation, it is known as blend electrolyte. Some polymer blends that have been studied include PEO (Devendrappa et al., 2006), PMMA (Rho & Kanamura, 2006), PVDF (Hwang et al., 2008), PVA (Rajendran et al., 2003), PVC (Reddy et al. 2006), CMC (Saadiah & Samsudin, 2018), and carrageenan (Zainuddin & Samsudin, 2018). In polymer blend electrolytes, inorganic salts usually cooperate to become charge carriers.

PEO is popular as a polymer host and has been widely investigated. PEO-based PE offers great potential for high energy density and high power lithium-ion batteries because of its ease of formation of a complex with lithium salt, flexibility, mechanical strength, comparatively high mobility of charge carriers, etc. Pure PEO shows both crystalline and amorphous phases at room temperature and has lower conductivity at

about ~10^{-7} Scm^{-1} (Zhao et al., 2012). However, PEO has some shortcomings, which limit its performances. The poor conductivity of PEO at room temperature is due to the high crystallite peak present in pure PEO; the conductivity is not high enough for industrial applications (Itoh et al., 2003).

PEs can be classified into two different types based on their physical properties and structures, namely gel polymer electrolytes (GPE) and solid polymer electrolytes (SPE). These types will be discussed in the next sub-section.

2.1.1 Gel polymer electrolytes (GPE) system

In 1975, gel polymer electrolytes (GPE) system was popular as gelionics (Appetecchi et al., 1994). It was first proposed by Feuillade and Perche (1975). GPE is formed by heating a combination of a suitable polymer matrix such as poly(ethylene oxide) (PEO), an alkali metal salt such as a lithium salt, and a solvent. GPE incorporates both the diffusive property of liquids and cohesive property of solids (Saaid, Rodi, & Winie, 2017).

GPE system has its own advantages such as high ionic conductivity, low volatility, low reactivity, good operation safety, and also good chemical, mechanical, photochemical, electrochemical, and structural stabilities (Ramesh & Wen, 2010; Saikia et al., 2011). It is also light in weight, solvent-free, possesses a wide electrochemical window, high-energy density, good volumetric stability, and is easily configured into a desired size and shape (Adebahr et al., 2003; Nicotera et al., 2006; Stephan, 2006; Uma et al., 2005). The interesting behavior of GPE increases its safety and applicability in modern electronics. The usage of GPE in battery avoids leakage and internal shorting and therefore lengthens shelf life (Kim et al., 2003). The unique behavior of GPE makes it a choice of electrolyte to replace the LEs.

GPE system has several shortcomings, which deters its usage in wider practical applications. The impregnation with liquid electrolytes leads to poor mechanical strength (Kim et al., 2008; Zhang et al., 2011). Insufficient mechanical strength refers to the inability to prevent the stress between the electrodes (Kim et al., 2003), the release of volatiles, and the increased reactivity to the metal electrodes (Jacob, Hackett, &

Giannelis, 2002). Nevertheless, this unexpected outcome can be reduced with the addition of fillers or nanomaterials to the samples (Zhang et al., 2011). Table 2.1 shows the GPEs from previous studies.

Table 2.1   Gel polymer electrolyte (GPE) and its conductivity from previous studies

Gel polymer electrolytes system	Conductivity $(S\ cm^{-1})$	References
poly(methyl methacrylate)-grafted/ lithium triflate/ ethylene carbonate MG30:LiTf:EC	8.95×10^{-3}	(Ali et al., 2013)
PVDF-HFP/SN-BMImBF$_4$	5.00×10^{-4}	(Pandey et al., 2016)
PVDF/PMMA/TiO$_2$	3.90×10^{-3}	(Zhou et al., 2013)
HNT-PEI	5.30×10^{-3}	(Wang et al., 2018)
LC/PEG	3.22×10^{-3}	(Song et al., 2017)
guar gum (GG)+ LiClO$_4$+glycerol	2.22×10^{-3}	(Sudhakar et al., 2014)

2.1.2   Solid polymer electrolytes (SPEs)

Wright (1975) launched the research on SPEs system and spread it extensively among the researchers. Armand et. al (1979) had verified the technological application of SPEs in electrochemical devices. A "dry solid" polymer electrolyte based on PEO was the first SPEs investigated (Fenton et al. 1973). This is a solvent-free system that does not use organic liquid. The performance of this PEO-based SPEs system was unsatisfactory due to the poor ionic conductivity at room temperature (Ramesh & Liew, 2012).

The realization of utilizing SPEs system in power sources is mainly due to certain advantageous features such as the feasibility of high ionic conductivity, non-volatility, no decomposition at the electrodes, no possibility of leaks, shape flexibility, wide electrochemical stability window, higher temperatures of operation, superior structural stability and so on. SPEs possess many interesting features such as solvent-free, leak-proof, low volatility, and also high thermal, electrical, mechanical, volumetric, and electrochemical stabilities. Other promising properties are light in weight, high ionic conductivity, high automation process, superior mechanical strength, high energy density, flexibility, and easy to process or fabricate and configure into various geometries.

Previous studies reported that there are different forms of SPEs, namely solid or gel ion-conducting membranes consisting of an ionic salt dispersed in a polymer matrix forming ionically conducting solid solutions. SPEs are solid ionic conductors that are formed by dissolving salt in host polymers with high molecular weight. They are usually prepared through an economic and reliable process in the form of semi-solid or solid state (Hsu et al., 2014; Kaneko et al., 2004; Majid & Arof, 2007; Sequeira & Santos, 2010; Singh et al., 2014; Singh et al., 2015). Like GPEs, SPEs system eliminate the occurrence of hazardous gas or corrosive solvent liquid leakage and offer a longer shelf life and wider operating temperature range.

The main disadvantages of GPEs are increased reactivity with lithium metal electrode, solvent volatility, and poor mechanical stability at a high degree of plasticization due to its gel type nature (Jacob et al., 2003). To preserve the desired mechanical characteristics of GPEs, these films have to be hardened either by chemical or physical curing process (high energy radiation), which results in high processing costs (Stephan & Nahm, 2006). Due to these reasons, SPEs system become the preferred choice among researchers for the electrolytes system.

However, SPEs system have some shortcomings, such as low conductivity at ambient temperature and high interfacial resistance. The use of SPEs system is limited by their propensity to crystallize whereas the high ionic conductivity is related to the amorphous phases. Some of the basic considerations to be a host polymer include features such as amorphous or low crystalline phases, involve polar groups such as O, N, S, and F, the molecular chain has a high molecular weight, and sufficient electron pair donors to coordinate with cations. The polymer is predicted to have a very small in glass transition temperature (T_g), i.e., higher flexibility of the polymer chain, which facilitates fast ion conduction and provides dissociation of salt that enhances only whenever the lattice energy of the selected salt and cohesive energy of the polymer are lower. Other than that, the fabricated material of the electrolytes needs to be stiff in order to form a device (Suthanthiraraj & Johnsi, 2017). Table 2.2 shows the SPEs system from previous studies.

Table 2.2   Solid polymer electrolytes (SPEs) from previous studies.

Solid polymer electrolytes	Conductivity, σ (S cm^{-1})	References
Dextan-chitosan- ammonium thiocyanate (NH$_4$SCN)	1.28×10^{-4}	(Kadir & Hamsan 2018)
polyethylene oxide (PEO)-LiClO$_4$	6.64×10^{-5}	(Gurusiddappa et al., 2016)
PEO-PVP-NaPO$_3$	1.07×10^{-5}	(Chandra, 2013)
Polyacrylonitrile (PAN)-ammonium hexafluorophosphate (NH$_4$PF$_6$)	3.90×10^{-3}	(Karthikeyan et al., 2016)
starch-chitosan- LiCF$_3$SO$_3$ $_+$ glycerol	1.32×10^{-3}	(Amran et al., (016)
PVP-NH$_4$SCN	1.70×10^{-4}	(Ramya & Selvasekarapandian 2014)

SPEs have emerged as the key in ionic conducting materials due to its interesting characteristics as discussed before. The aim of this research is to find a new type of biopolymer electrolytes that can be used as an alternative material for application as current industrial materials. With various types of biomaterial selections in the market, the product cost can be reduced. Typically, ionic conduction in PEs is governed by the salt concentration as well as the interaction of the polymer host with salt.

2.2   Solid bio-polymer electrolytes (SBEs) system

PEs based on petrochemicals have been widely investigated and are well known for causing environmental problems and expensive costs. It is possible to solve these problems by applying bio-polymers electrolyte as a host (Campo, Kawano, da Silva Jr, & Carvalho, 2009; Kumar, Tiwari, & Srivastava, 2012; Samsudin, Khairul, & Isa, 2012). The bio-based polymers are also promising candidates to be used as an electrolyte that meets different requirements especially to address the main issue of the synthetic polymer, which is insoluble in solution (Ma et al., 2007). SBEs system are believed to function as thin films due to their desirable size, good mechanical properties, and good contact with electrode materials (Winie et al., 2009). Thus, extensive work has been done to welcome the biopolymer electrolytes by using natural polymer.

Some biodegradable polysaccharides are appropriate to be used as the polymer matrix in the SBEs, such as alginates, cellulose, starch, cellulose, chitosan, kappa-

carrageenan, pectin, chitin, lignocellulosic materials, hyaluronic acid, agarose, polylactides, polyhydroxyalkanoates (bacterial polyesters), and soy-based plastics (Ma et al., 2007; Ma, Yu, & Zhao, 2006). This is due to their popular characteristics, which are richness and abundance in nature. As a comparison, Li^+ exhibits higher energy capacities than the proton conducting SBEs system, but in contrast, SBEs system have no safety issues and use cheap electrode and electrolytes materials, which can reduce the cost of production of the electrolyte system (Shukur et al., 2015). As mentioned earlier, polymer originally is an insulator and has very low conductivity value at room temperature. The conducting polymer is produced by doping the polymer with acids or ammonium salts. This is due to the mobile ion, proton (H^+) originating from acid or salt, which loosely bonds, and proton exchange occurs under the influence of an electric field. Thus, the polymer-acid or salt system becomes a proton conductor. Conduction takes place when protons from the acid/salt hop via each coordinating site of the polymer host. The development of new electrolyte materials for PEs and their application create an opportunity for new types of electrochemical devices, which may themselves, in turn, revolutionize many industrial areas. Many studies have been conducted by using natural polymer as biopolymer electrolytes, as listed in Table 2.3.

Table 2.3   Solid bio-polymer electrolytes (SBEs) from previous studies

SBEs	Conductivity without dopant, σ ($S\ cm^{-1}$)	Conductivity with dopant, σ ($S\ cm^{-1}$)	References
CMC-AC	1.00×10^{-7}	1.43×10^{-3}	(Ahmad & Isa, 2015)
MC-NH$_4$I	2.00×10^{-10}	5.08×10^{-4}	(Salleh et al., 2016)
CMC-DTAB	0.38×10^{-5}	7.72×10^{-4}	(Samsudin & Isa, 2012)
Alginate-NH$_4$Br	4.67×10^{-7}	4.41×10^{-5}	(Fuzlin et al.,(2018)
K-carrageen - NH$_4$SCN	4.81×10^{-6}	6.83×10^{-4}	(Selvin et al., 2018)
CMC-NH$_4$SCN	1.00×10^{-7}	6.48×10^{-5}	(Noor & Isa, 2016)
I-Carrageenan-NH$_4$Br	1.46×10^{-5}	1.08×10^{-3}	(Karthikeyan et al., 2017)

Among these well-known biodegradable natural polysaccharides, alginate as a polymer host is highlighted in this present work for the SBEs system. Alginate or known as algin, a natural anionic polymer extracted from brown seaweeds types, such as kelp, is a principal component of the cell membrane with other substances. Surprisingly, alginate can produce an "egg-box" form that can have complexed metal ions (Chtchigrovsky et

al., 2012; Davis et al., 2003; Fourest & Volesky, 1997; William & Edyvean, 1997). Alginate possesses some superior properties such as being biocompatible, non-immunogenic, non-toxic, and most importantly, biodegradable. It is attracting the attention of researchers in their quest to reduce the load on the environment (Fuzlin et al., 2018). Alginate is widely used in the pharmaceutical and food industries (Downs et al., 1992; Liu et al., 1997). Alginate is believed to speed up the process of wound healing as it can control the moisture of the microenvironment (Lee & Mooney, 2012). It is used as an energy storage material (Liu et al., 2016; Lv et al., 2016; Sun et al., 2017). The derivation of seaweed-based alginate is believed to give high performance in electrochemical materials, which can enhance energy conversion and storage (Li et al., 2015; Yang et al., 2014).

Alginate is a relatively economical biopolymer with compositions of α-1, 4-L-glucuronic acid (G units), and poly-β-1, 4-D-mannuronic acid (M units) which can provide rich ester groups (COO⁻) for adsorbing cation with the empirical formula, $NaC_6H_7O_7$ (Yang et al., 2014). Alginate can be dissolved in water, but it is not completely soluble in some organic solvents. Chemical components of alginate belong to carbohydrate. It only contains free carboxylate (COO⁻), and it is a macromolecule heteropolymer brought by copolymerization between mannuronic acid and guluronic acid.

Thus, the natural polymer material in SBEs system is chosen as the polymer host even though very few studies have reported of using alginate with ammonium salts, and polymer has shown relatively low ionic conductivity. Several methods will be focusing on to enhance the ionic conductivity because alginate is believed to have a good potential as a host polymer in the electrolytes system.

2.3   Enhancement of SBEs system conductivity

In recent years, some methods have been proposed to enhance ionic conductivity in the electrolytes system. Ionic conductivity can be enhanced with the addition of salt as ionic dopant, copolymerization, polymer blending, plasticization, and also by incorporating ceramic fillers (Amaral et al., 2015; Han et al., 2002; Ng & Mohamad, 2006; Rajendran & Sivakumar, 2008). Previous studies have shown that ionic dopant

presents the cheapest and simplest technique (Monisha et al., 2017; Sohaimy & Isa, 2016; Voigt & van Wüllen, 2012). The addition of a suitable ionic dopant is a common and favorable method, and the product of this process is called biopolymer salt complexes.

In the study of SBEs system, the main aspect that gains attention is its ionic conductivity at ambient temperature. As mentioned earlier, the ionic conductivity of polymer electrolyte is lower at room temperature (Schaefer et al., 2012) due to its dual features, which is partially amorphous and crystalline (Samsudin & Isa, 2012). The ionic dopant method is the best way for enhancing ionic conductivity because it is the easiest and the cheapest. This conductivity enhancement can be explained by the diffusion of free mobile ions, which can trigger conduction and hence, improve the ionic conductivity of the host polymer (Karthikeyan et al., 2016; Ma et al., 2016). The role of ionic dopant is to provide more ionic conducting species inside the polymeric matrix, for example, lithium-based electrolyte where Li^+ functions as the conducting species. Beside, H^+ acts as the conducting species in the proton-based electrolyte system.

The polymer-salt complexation system or salt-in-polymer electrolytes were studied in depth by (Armand et al., 1978). Recently, PEs that have sodium salts have gained some attention. The incorporation of sodium salts in PEs has a few benefits over their lithium medium. The softness of sodium resources makes them easy to use and handle with other components in the device (Reddy et al., 2006). Research on the development of sodium ions has received great attention from researchers (Vignarooban et al., 2016) as it is cheaper than lithium (Li). The similarities in chemical properties between sodium and lithium make them suitable to be used as an electrolyte. In addition, sodium has several advantages to be used in the battery such as environmentally friendly, non-toxic, and low cost (Li et al., 2016).

(Samsudin et al., 2012) stated that in polymer salt complexation, proton conduction could occur by lone pair migration or proton-carried migration mechanisms. According to (Ahmad & Isa, 2016), their study of SBEs system on CMC doped with NH_4CI found that lone proton migration of H^+ is more possible. With the addition of an ionic dopant, the amorphousness of the sample becomes higher. Similar behavior was also reported by other researchers (Chai & Isa, 2013; Kamarudin & Isa, 2013; Sit et al., 2012) where they believed that the amorphousness of the samples is important to obtain

good conductivity. Hema et al. (2009) stated that there are interactions between ammonium ions with the polymer host, CMC. A similar work by Kamarudin and Isa (2013) found that the addition of salt in the electrolytes system increased the dissociation of H^+. Furthermore, the enhancement of ionic conductivity can be related to the Arrhenius law of various polymer salt electrolytes at different temperatures. (Fuzlin et al., 2018) have studied alginate-NH_4Br of SBEs and found that the SBEs system behavior was in line with the Arrhenius behavior since ionic conductivity was found to increase from 303 K to 353 K. They assumed that the regression value of R^2 was close to unity, indicating that with the addition of NH_4Br, the sample's conductivity was a thermally activated process. The process of transportation of ions occurred when the ions jumped into neighbouring vacant sites, thus the ionic conductivity increased (Buraidah et al., 2009; Sit et al., 2012).

2.3.1 Ammonium salt dopant

Ammonium salt as an ionic dopant acts as a proton conductor of H^+ as it provides ions for the SBEs to enhance the ionic conductivity value (Radha et al., 2013; Salleh et al., 2016). It is the source of the charge carrier (conducting species) in PEs, which is vital in ionic conductivity that gives effects to the miscibility of polymer pairs and morphology of electrolytes through the interaction of ions. The Incorporation of ammonium salt has many benefits, including increasing the ionic conductivity from ~10^{-7} Scm^{-1} to ~10^{-3} Scm^{-1} (Ahmad & Isa, 2015).

In this research, ammonium nitrate (NH_4NO_3) has been used as a salt dopant in the development of alginate complexes-based SBEs system. Previous studies revealed that chitosan–NH_4NO_3 based electrolytes had shown complexation between the nitrogen of the amine functional group in chitosan with the cation of the salt (Majid & Arof, 2005; Majid & Arof, 2008). (Khiar & Arof, 2011) stated that the complexation of starch/chitosan with NH_4NO_3 has a conductivity of $3.89 \pm 0.79 \times 10^{-5}$ Scm^{-1}. The work done by (Ng & Mohamad, 2006) showed proton conductivity of 9.93×10^{-3} Scm^{-1} for plasticized chitosan with NH_4NO_3. (Kamarudin & Isa 2013) reported that their system gave the conductivity value of 7.71×10^{-3} Scm^{-1} for CMC with NH_4NO_3. (Monisha et al., 2017) presented the proton conductivity value of 1.02×10^{-3} Scm^{-1} for cellulose acetate doped with NH_4NO_3. Proton conductivity value of 1.03×10^{-3} Scm^{-1} for agar-

agar with NH$_4$SCN was reported by (Selvalakshmi et al., 2017). (Premalatha et al., 2016) reported proton conductivity value of 2.85×10^{-4} Scm^{-1} for tamarind seed doped with NH$_4$SCN. (Boopathi et al., 2016) claimed the value of conductivity for agar-agar doped with NH$_4$NO$_3$ was 1.09×10^{-3} Scm^{-1}. The natural polymer has anionic polysaccharide in its backbone, which has high affinity to proton ions (Monisha et al., 2017). Normally, the differential of the host polymer and ionic dopant can be explained in term of its motion of ions in electrolytes system which governed by the degree of crystallinity (Kumar et al., 2011), salt content (Idris et al., 2009; Sit et al., 2012) as well as the nature of polymer and ionic dopant. Table 2.4 shows some information on solid biopolymer electrolytes (SBEs) using NH$_4$NO$_3$ used from previous study with its ionic conductivity.

Table 2.4   Solid biolymer electrolytes (SBEs) using NH$_4$NO$_3$ from previous studies.

Solid polymer- electrolyte	Conductivity, σ (S cm^{-1})	References
MC -NH$_4$NO$_3$	2.10×10^{-6}	(Shuhaimi et al., 2010)
Agar-NH$_4$NO$_3$	1.09×10^{-3}	(Boopathi et al., 2017)
CMC-NH$_4$NO$_3$	7.71×10^{-3}	(Kamarudin & Isa, 2013)
Cellulose acetate-NH$_4$NO$_3$	1.02×10^{-3}	(Monisha et al., 2017)
2-HEC-NH$_4$NO$_3$- EC	1.17×10^{-3}	(Hafiza & Isa, 2018)

Ammonium salt is considered a good dopant where the H$^+$ ions from ammonium become a possible proton donor when doped in polymer/biopolymer. Ammonium salt is selected as it is proven to be a good proton donor to the electrolytes system (Buraidah et al., 2009; Chandra et al., 1990; Kumar & Sekhon, 2002; Samsudin et al., 2012). The previous work done by Aziz et al. (2010) was based on methyl cellulose (MC) and ammonium fluoride (AF) as one of the potential polymer-salt systems in electrolytes. The proton-conducting SBEs system has the highest conductivity of 6.4 x 10^{-7} Scm^{-1}, obtained at room temperature upon the addition of 18wt. % of AF. The ionic mobility and diffusion coefficient obtained for the system were in good agreement with the increment of the weight percentage (wt. %) of ammonium salt content. The cellulose-based system was successfully formulated with another polymer-salt system consisting of hydroxyethyl cellulose (HEC) by (Sit et al., 2012). By doping NH$_4$Br in polymer-salt complexes, they managed to get the optimum value of ionic conductivity and good electrochemical properties with conductivity of ~10^{-4} Scm^{-1}, and the increase in ionic conductivity was

due to the migration of proton H^+ ions from ammonium salts. Other ammonium salts studied include NH_4I (Maurya et al., 1992), $NH_4SO_3CF_3$ (Ali, Mohamed, & Arof, 1998), and $(NH_4)SCN$ (Vahini & Muthuvinayagam, 2018), which were used as doping salts. These results proved that ammonium salts are good candidates to be used as a dopant in polymer-salts complexes system and are also a proton conductor in the electrolytes system.

Based on this background, the present work was carried out using alginate-based SBEs doped with ammonium nitrate. To the best of our knowledge, the alginate doped with ammonium nitrate SBEs system has never been studied and reported by others. The alginate–NH_4NO_3 SBEs produced were explored in terms of its potential to be used as proton conducting electrolytes using electrical impedance spectroscopy (EIS), transference number measurement (TNM), Fourier transform infrared spectroscopy (FTIR), and X-ray diffraction (XRD). In addition, an ion-movement model and free ions mobile observation were studied for the doped SBEs system to gain new knowledge and understanding of the complexation within the components affecting the changes in conductivity in this system. Table 2.5 shows some information on ammonium salt used from previous study with its ionic conductivity.

Table 2.5   Types of ammonium salt used in electrolyte system

Polymer-salt electrolyte	Conductivity, σ (S cm^{-1})	References
CMC-NH$_4$F	2.68×10^{-7}	(Ramli & Isa, 2015)
PVA-CH$_3$COONH$_4$	9.29×10^{-3}	(Wen Liew et al., 2015)
MC- NH$_4$F	6.40×10^{-7}	(Aziz et al., 2010)
Alginate-NH$_4$Br	4.41×10^{-5}	(Fuzlin et al., 2018)
MC/potato starch-NH$_4$NO$_3$	4.37×10^{-5}	(Hamsan et al., 2017)
Chitosan/PVA- NH$_4$NO$_3$	2.07×10^{-5}	(Kadir et al., 2010)

CHAPTER 3

RESEARCH METHODOLOGY

3.1   Introduction

This chapter discusses the methodology of the present research that is divided into two parts, which are the first part is the preparation of solid biopolymer electrolytes (SBEs) and are the second part is the characterization of solid biopolymer electrolytes (SBEs) to achieve the objectives of this research. The entire experimental work in this research was carried out as presented in the flowchart in Figure 3.1.

3.2   Phase 1: Preparation of SBEs

In this present research, the SBEs system was prepared via the solution casting technique in ambient temperature. The alginate was prepared with various content of NH_4NO_3 from 5 *wt.* % until 35 *wt.* %. The alginate acts as electron donor to interact with cations from NH_4NO_3 to contribute the ion conduction of the SBEs system.

3.2.1   Materials

The SBEs films consisted of alginate, which was obtained from Shaxii Orient Co. with molecular weight (M.W.) ~10,000 acting as the bio-polymer host. In this research, ammonium nitrate (NH_4NO_3) (M.W.) of 80.043 g/mol from Merck KGaA was used as the ionic dopant, and distilled water was used as the solvent to prepare the sample. In this work, the alginate and NH_4NO_3 are based on powder form and mix with water to form a solution.

FLOW CHART OF THE RESEARCH
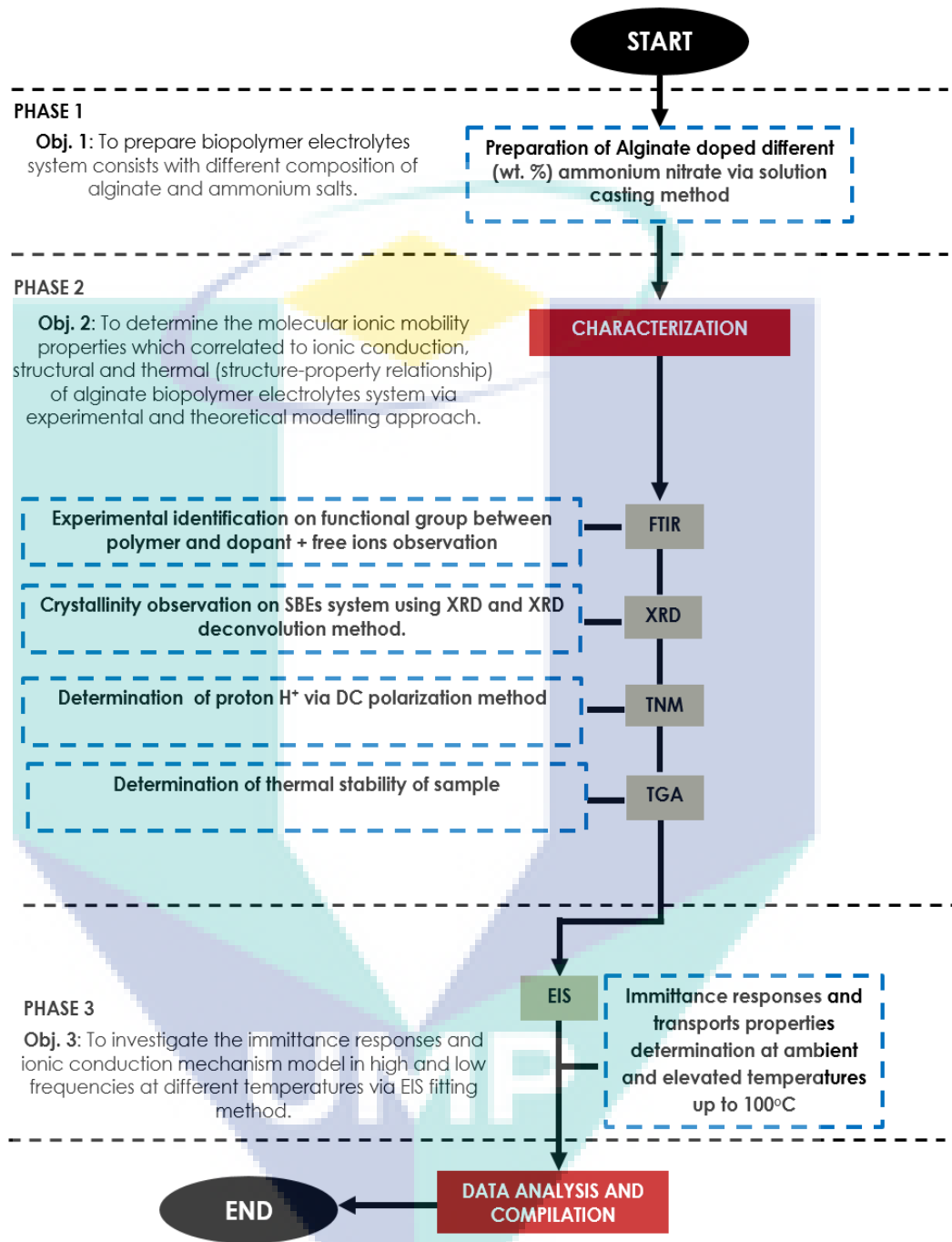
Figure 3.1   Overall view of experimental work in this research

3.2.2   Preparation of SBEs system films

Alginate was weighed 2.00 g with different contents in weight percent (wt.%) of NH$_4$NO$_3$ as calculated using equation 3.1. Then, distilled water was added and stirred

continuously until the solution appeared completely homogeneous. After a homogeneous solution was obtained, the mixture was cast into different glass Petri dishes and left to dry in the oven (55 °C) until alginate-NH_4NO_3 SBEs system films were formed. Lastly, the SBEs films were kept in the desiccator for further drying. Table 3.1 shows the list of sample content and their designation for the SBEs system.

Table 3.1   List of sample with their content respectively

Designation	Weight percentage (*wt. %*)	Ammonium **nitrate** (g)
S0	0	0.000
S1	5	0.1053
S2	10	0.2222
S3	15	0.3529
S4	20	0.5000
S5	25	0.6666
S6	30	0.8571
S7	35	1.0769

The amount of NH_4NO_3 used was calculated using equation 3.1 below:

$$wt.\ \% = \frac{x}{x+y} \times\ 100\%$$

3.1

where, x is the weight of NH_4NO_3 in gram, g

y is the weight of alginate in gram, g

wt. % is the weight percentage of NH_4NO_3

3.3   Phase 2: Characterization of SBEs system

Four different types of instruments were used to characterize the prepared alginate-NH_4NO_3 SBEs system, including Fourier transform infrared (FTIR) spectroscopy, X-ray diffraction (XRD) spectroscopy, thermogravimetric analysis (TGA), electrical impedance spectroscopy (EIS), and transference number measurement (TNM).

3.3.1   Fourier Transforms Infrared Spectroscopy (FTIR)

FTIR is the best tool for identifying the type of materials. FTIR spectroscopy has been used to explore molecular interactions occurring between the polymer host and salt system. The sample was tested whether using attenuated total reflectance infrared (ATR-

IR) for films sample and using solid materials with potassium bromide (KBr) for sample pure alginate in powder and ammonium nitrate powder. Besides, FTIR can detect the presence of impurities and confirm the pure compound through a collection of absorption bands. In this present research, the prepared samples were characterized via Perkin Elmer FTIR to obtain IR spectrum of the samples, as shown in Figure 3.2. The Fourier transform has an absorption or transmittance spectrum as a function of wavenumber (cm^{-1}). Some of the samples had been cut and put on a solenoid crystal; then the infrared light went through the prepared samples from wavenumber of 700 to 4000 cm^{-1} with a resolution of 2 cm^{-1}. While for the sample using (KBr) procedure, the prepared powder materials (alginate and NH_4NO_3) were subjected to high pressure to obtain (KBr) pellet. In general, the FTIR converts the collected spectra data from an interface pattern to a spectrum. The pattern of this analysis shows complexation between the materials, whether it shifts or has differences in term of intensity.

Figure 3.2   Perkin Elmer FTIR spectroscopy

3.3.2 X-ray Diffraction (XRD)

XRD was performed to determine the nature of the alginate and ammonium nitrate complexes whether crystal or amorphous. The chaos in the crystalline peaks can be valued by measuring the crystallite sizes according to the radial widths $\Delta(2\theta)$ of the reflections at a scattering angle 2θ by the Scherrer equation (Murthy, 2004). The broad peaks observed in the XRD pattern indicated the amorphous nature of materials (Jayalakshmi & Sivadevi, 2018). The XRD measurements were performed using MiniFlex II from Rigaku using monochromatic Cu-Kα radiation sources with 1.5406 Å wavelengths. The

sample was placed onto a glass slide and then placed in the sample holder of the diffractometer with a sample area of 1.5 cm × 1.5 cm. X-ray spectra were formed when electrons had abundant energy to remove inner-shell electrons of the materials. The intense reflected X-rays are produced when the wavelengths of the scattered X-rays interfere constructively due to a crystal is bombarded with X-rays of fixed wavelengths and at definite incident angles. The common relationship between the angle of incidence X-rays, the spacing between lattice planes of atoms, and the wavelength of incident X-rays is known as Bragg's Law, as shown in equation 3.2. In this present work, alginate and ammonium nitrate biopolymer electrolytes were scanned at 2θ angles between 5˚ and 80˚. The x-ray diffraction is shown in Figure 3.3.

$$n\lambda = 2d\ sin\ \theta \qquad\qquad 3.2$$

where, n = integer

λ   = is the wavelength of the incident X-ray beam

d = is the distance between atomic layers in a crystal

θ = Bragg angle

Figure 3.3   Rigaku Miniflex II Diffractometer

3.3.3   Thermogravimetric analysis (TGA)

The thermal stability of the obtained alginate-NH_4NO_3 polymer films was observed using NETZSCH TG- DTA 2010SA of TGA measurement as set up in Figure 3.4. The samples were placed into an aluminium pan and tested in various temperatures ranging from room temperature to 536 °C with a scan rate of 10 °C/min, with nitrogen

flow. The samples were carefully weighed at about ~4 mg and were subjected to TGA to determine the thermal stability range and decomposition characteristics of the SBEs. The TGA data of all SBEs samples were analyzed according to two possible aspects: (1) the content of alginate-NH_4NO_3 by temperature and (2) the thermal stability of each sample of the alginate-NH_4NO_3 SBEs system. This instrument can also verify the loss of water, loss of solvents, and weight percentage of ash. The TGA analysis can serve as a guideline to relate the results of the FTIR study where it provides the information of complexation between the alginate and NH_4NO_3 in the SBEs system.

Figure 3.4   TG/DTA 2010SA of TGA measurement

3.3.4   Electrical Impedance Spectroscopy (EIS)

The ionic conductivity, as well as electrical and conduction mechanism of the prepared samples were characterized via EIS using HIOKI 3532-50 LCR Hi-TESTER interfaced with a computer as shown in Figure 3.5. The EIS was similarly used in other works (Ahmad & Isa, 2016; Shukur et al., 2014; Taib & Idris, 2014). The measurements used the frequency range from 50 Hz to 1 MHz at ambient temperature. This analysis was carried out by sandwiching each sample of thin film between two stainless steel electrodes with a spring pressure on it. The SBEs system samples were cut into a suitable size and the thickness of each prepared SBEs system sample was measured using a digital micrometer screw gauge (Figure 3.6). The EIS machine recorded the real resistance and imaginary capacitance part of the response of the system. The imaginary impedance (Z_i) was plotted against real impedance (Z_r) while the bulk resistance (R_b) was taken from the

intercept of the semi-circle line and spike line. The ionic conductivity of each sample was calculated using the equation below:

$$\sigma = \frac{t}{R_b A} \qquad\qquad 3.3$$

where t is the thickness of the electrolytes, R_b is bulk resistance, and A is the electrode's electrolyte contact area (cm^2). The conductivity measurement was tested at different temperatures from 303 K to 343 K.

Based on the EIS measurement, the complex impedance data (Z^*) is represented by its real (Z_r) and imaginary (Z_i) through the equation:

$$Z^* = Z_r + Z_i \qquad\qquad 3.4$$

The plot of impedance analysis may not be exactly the same for all tested samples as the instrument itself depends on the behavior of the tested sample either wet or dry. To further study the conduction of ion among all the alginate- NH_4NO_3 SBEs system, frequency-dependent parameters were obtained using the impedance modulus |Z| and phase shift (θ) using the EIS technique. According to Macdonald (1987), the relationship between complex impedance, admittance, permittivity, and electrical modulus can be obtained. The formulation for the dielectric study is discussed in the next section.
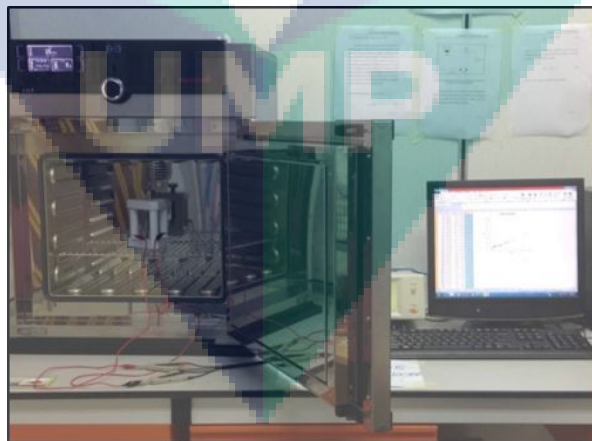
Figure 3.5   HIOKI 3532-50 LCR Hi-Tester interfaced to a computer

Figure 3.6   A digital micrometer screw gauge

For further study in electrical study, the dielectric constant, ε_r and dielectric loss, ε_i are determined and calculated with using the following equation:

$$\varepsilon_r = \frac{Z_i}{\omega C_o (Z_r^2 + Z_i^2)} \qquad 3.5$$

$$\varepsilon_i = \frac{Z_r}{\omega C_o (Z_r^2 + Z_i^2)} \qquad 3.6$$

where, $C_o = \varepsilon_o A/t$

$\omega = 2\pi f$

A = Electrode-electrode contact area

t = thickness of sample

f = frequency

The complex electric modulus (M*) is used to investigate the conductivity relaxation phenomena. It also needed to suppress the effects of electrode polarization and bulk dielectric properties of the SBEs system. The real modulus, M_r and imaginary modulus, M_i was calculated using the following equation:

$$M_r = \frac{\varepsilon_r}{(\varepsilon_r^2 + \varepsilon_i^2)} \qquad 3.7$$

$$M_i = \frac{\varepsilon_i}{(\varepsilon_r^2 + \varepsilon_i^2)} \qquad 3.8$$

3.3.5   Transference Number Measurement (TNM)

SBEs system are ionic conductors in electrolytes system. TNM was conducted to determine the mechanism of the transference ions for biopolymer electrolytes system by using the direct current (DC) Wagner's polarization technique (Monisha et al., 2017). Each sample was sandwiched between two stainless steel blocking electrodes and the current through the circuit was monitored with the time until it saturated at room temperature. The circuit was set up as shown in Figure 3.7 by using fixed dc voltage 1.5 V and the experimental arrangement for measuring ionic transference number shown in Figure 3.8.
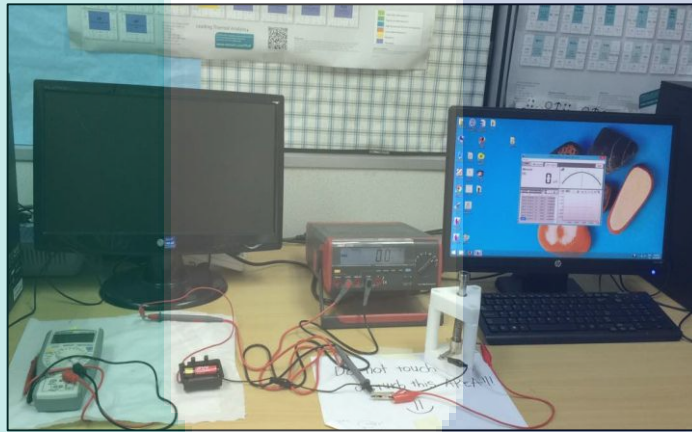
Figure 3.7   The Digital Auto-ranging True RMS Multimeter interfaced to computer
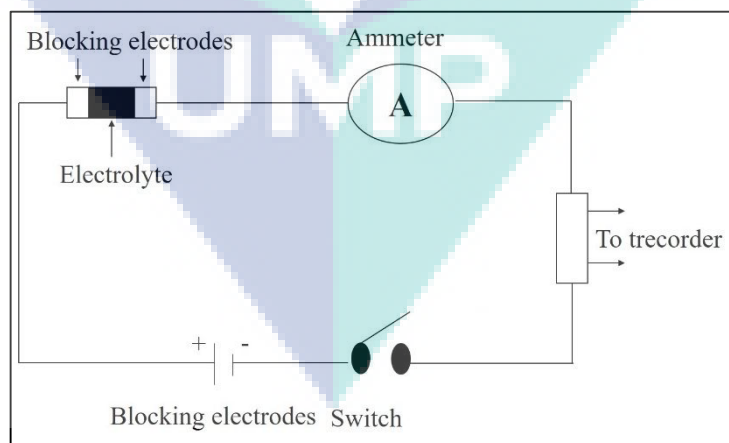
Figure 3.8   Experimental arrangement for measuring ionic transference number

According to Linford (1988), the cationic transference numbers of the SBEs system need to be determined using the dc polarization technique. The ionic proton

transference number (t_{ion}) and electron transference number (t_{ele}) are based on the equations below:

$$t_{ion} = \frac{I_s}{I_i}$$

3.9

$$t_{ele} = \frac{I_i - I_s}{I_i}$$

3.10

where, I_i = Initial current
I_s = Saturated current
t_{ion} = Transference number
t_{ele} = Electronic current

The current or charge carrier is purely ionic when $t_{ion} = 1$ (Aziz et al., 2010; Chai & Isa, 2013a). Once the transference number (t_{ion}) was measured and calculated, the contributing ionic species toward σ in this system was determined using equations (3.11) and (3.12) for diffusion coefficient, D, and mobility, μ, of conducting species.

$$t_{ion} = \frac{\mu_+}{\mu_+ + \mu_-} = \frac{\mu_+}{\mu}$$

3.11

$$t_{ion} = \frac{D_+}{D_+ + D_-} = \frac{D_+}{D}$$

3.12

where, μ_+ = Ionic mobility cation
μ_- = Ionic mobility anion
D_+ = Diffusion coefficients cation
D_- = Diffusion coefficients anion

CHAPTER 4

RESULT AND DISCUSSION

4.1 Introduction

In this chapter, the structural and physical properties of the SBEs system are analyzed using different techniques to achieve the objectives of this research.

4.1.1 Physical appearances of the samples

Figure 4.1 shows the SBEs films, which are transparent, clear, flexible, self-standing thin films with good appearance properties. In this work, the samples of alginate-NH_4NO_3 from S0 to S7 in solid forms which showed a solid property and good stability.
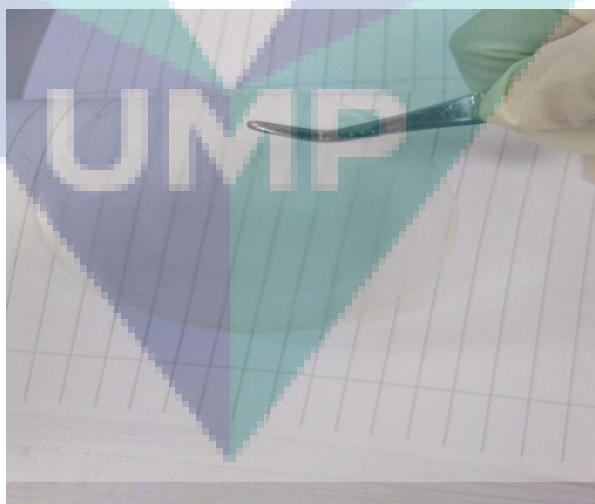
Figure 4.1   Clear and transparent solid film

4.2 ATR-FTIR spectra on Alginate

The structure of alginate by using Gaussian software is presented in Figure 4.2. Figure 4.3 presents the FTIR spectrum of alginate. The characteristic band at 3300 cm^{-1} corresponds to the -OH stretching band, 2890 cm^{-1} corresponds to -CH stretching, 1580 cm^{-1} and 1400 cm^{-1} correspond to COO^{-} stretching, and 1030 cm^{-1} corresponds to the C-O-C band. Table 4.1 shows the functional groups of alginate in the present system.

Figure 4.2   The structure of alginate
Source: Rasali & Samsudin, (2018)
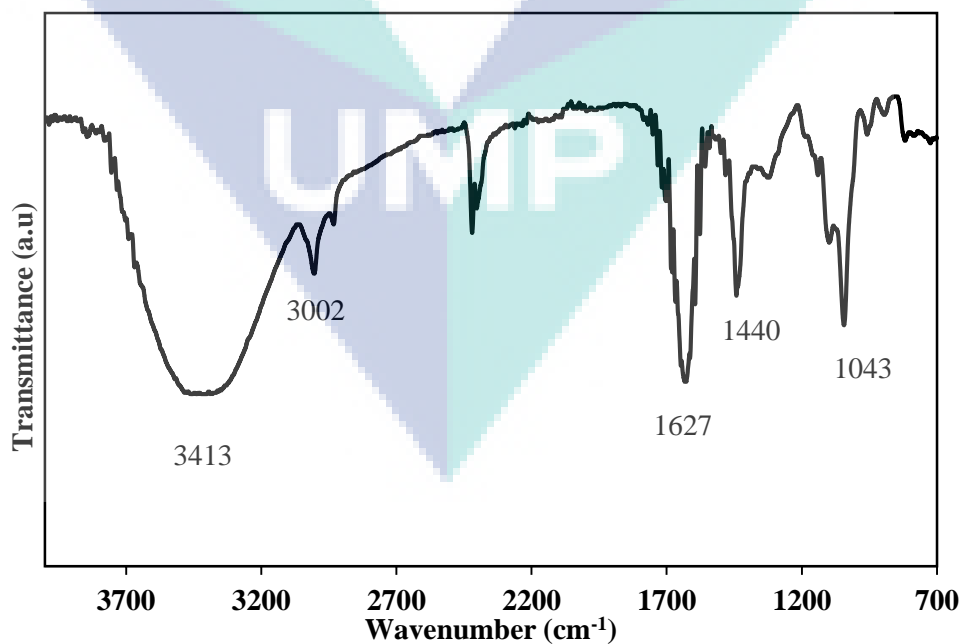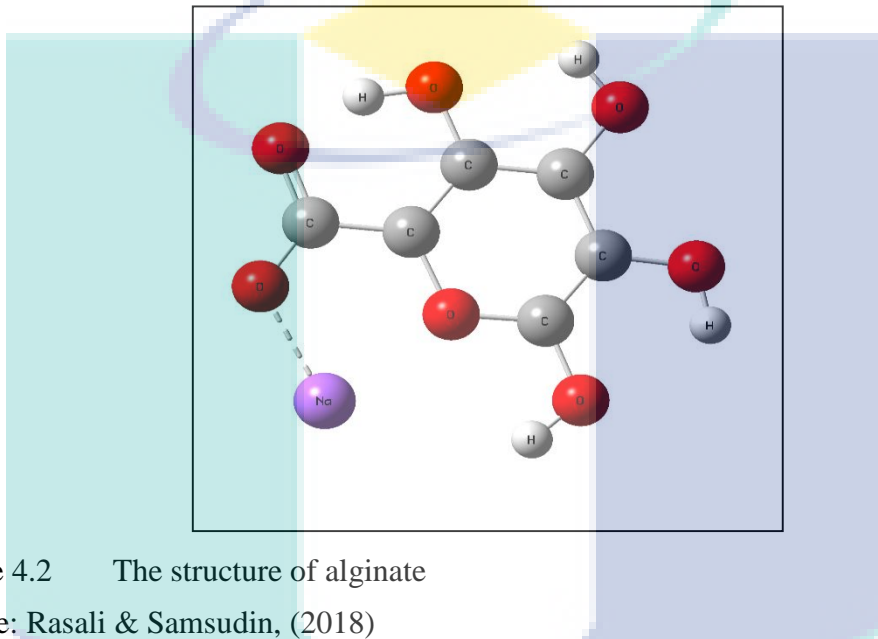
Figure 4.3   FTIR spectra of alginate powder

Table 4.1   The assignment of alginate with their references

Polymer	Wavenumber (cm^{-1})	Assignment	References
Alginate	1043	C-O-C stretching	(Chen et al., 2017; Helmiyati & Aprilliza 2017; Kanti et al., 2004)
	1627 and 1440	COO$^-$ stretching	(Solanki et al., 2016; Li et al., 2008; Helmiyati & Aprilliza, 2017)
	3002	C-H stretching	(Solanki et al., 2016; Li et al., 2008; Helmiyati & Aprilliza 2017)
	3413	O-H stretching	(Solanki et al., 2016; Li et al., 2008; Helmiyati & Aprilliza 2017)

4.2.1   ATR-FTIR spectra on NH$_4$NO$_3$

The structure of NH$_4$NO$_3$ is presented in Figure 4.4. Figure 4.5 presents the FTIR spectrum of NH$_4$NO$_3$. Figure 4.5 shows the ATR-IR spectra of pure NH$_4$NO$_3$ in the region of 700–40000 cm^{-1}. The band at 713 and 827 cm^{-1} corresponds to the symmetric bending (NO$_3^-$), 1041 and 1286 cm^{-1} for symmetric bending and stretching (NO$_3^-$) respectively. (N-H) band at 1408 cm^{-1} while 3057 and 3238 cm^{-1} were assigned to the asymmetric stretching (NH$_4^+$) band.
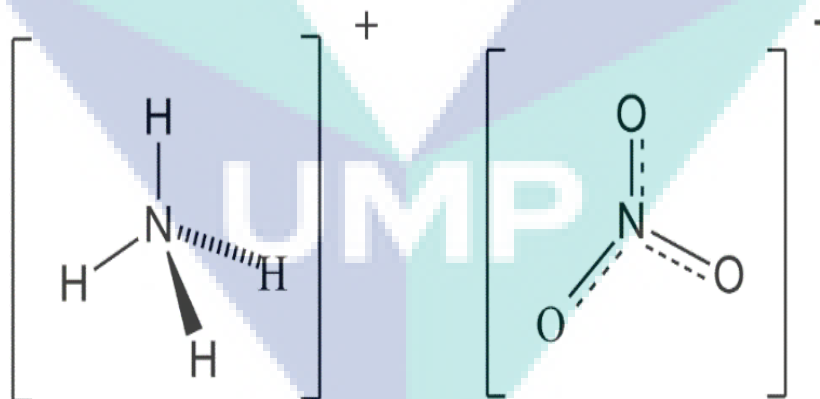
Figure 4.4   The structure of ammonium nitrate

31
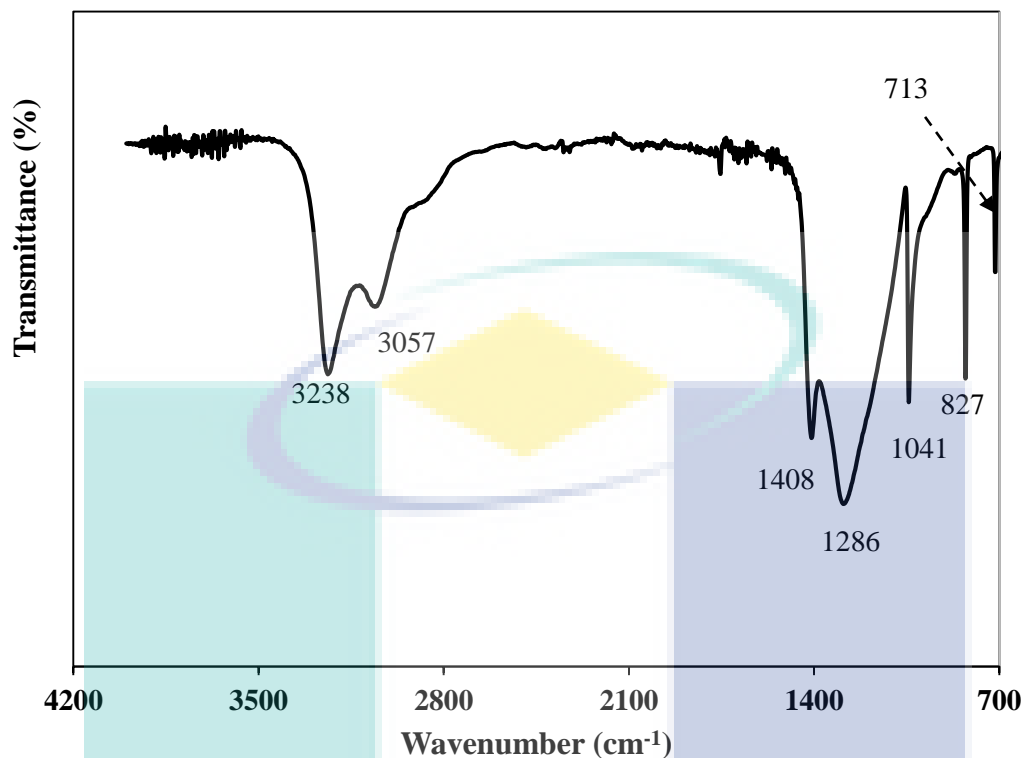
Figure 4.5   FTIR spectra of NH$_4$NO$_3$ powder

Table 4.2   The assignment of ammonium nitrate with their references

Material	Wavenumber (cm^{-1})	Assignment	References
	713	Symmetric bending (NO$_3^-$)	(Moniha et al., 2018; Rani et al., 2016)
	827	Symmetric bending (NO$_3^-$)	(Bourahla et al., 2014; Kamarudin & Isa, 2013; Shuhaimi et al., 2009; Wu et al., 2007)
	1040	Symmetric stretching (NO$_3^-$)	(Bourahla et al., 2014; Kamarudin & Isa, 2013; Shuhaimi et al., 2009; Wu et al., 2007)
Ammonium nitrate	1286	Asymmetric stretching (NO$_3^-$)	(Bourahla et al., 2014; Kamarudin & Isa, 2013; Shuhaimi et al., 2009; Wu et al., 2007)
	1408	N-H band	(Kamarudin & Isa 2013; Shuhaimi et al., 2009)
	3057 & 3238	Asymmetric stretching (NH$_4^+$)	(Bourahla et al., 2014; Shuhaimi et al., 2009; Wu et al., 2007)

4.2.2 ATR-FTIR of Alginate doped with NH₄NO₃

Some reports on IR spectrum studies on alginate can be obtained from the studies by (Chen et al., 2017) and (Aprilliza, 2017). The chemical structure of alginate is comparable to carboxymethyl cellulose (CMC) as the only difference between them is the presence of methyl carboxyl in CMC but absent in alginate, as reported by some researchers (Samsudin et al., 2012; Sohaimy & Isa 2017). The functional groups of interest for the alginate doped with NH_4NO_3 SBEs system which represent the complexes between the material are discussed below.

The FTIR spectra as shown in Figure 4.6 correspond to the present peak containing a functional group of carboxylate anion in alginate doped with NH_4NO_3. Figure 4.6 (a) and (b) shows the FTIR spectrum of sodium alginate/ammonium nitrate SBEs that is defined at peaks 1415 and 1598 cm^{-1} corresponding to the presence of COO^- stretching of C=O and $C-O^-$ in alginate (Li et. al., 2008; Ilie et al., 2016). As can be observed in Figure 4.6 (a) for pure alginate (0 wt.%), the peak intensity at 1598 cm^{-1} seemed to increase with the addition of NH_4NO_3. Besides, in Figure 4.6 (b), the peak at 1415 cm^{-1} has shifted to a lower wavenumber at 1406 cm^{-1} after adding 25 wt.% of NH_4NO_3 and disappeared when the addition of salt was more than 25 wt.% of NH_4NO_3.

These two obvious changes are expected and imply that interaction occurred between COO^- peak in the carboxylic group of alginate with proton H^+ from NH_4^+ that is a substructure in NH_4NO_3, which is considered as protonation interaction by COO^- group. According to the previous researcher (Hashmi et al., 1990), the H^+ acted as a conducting ion, which originated from the ammonium ion in the polymer-salt system. The conduction took place through the Grotthus mechanism when electric field was applied in relation to the exchange of ions between complexed sites, which caused complexation between the host polymer and ionic salt or can called by the conduction process (Ahmad & Isa, 2016; Hema et al., 2009; Sohaimy & Isa, 2016). Furthermore, in tetrahedral structure of ammonium ion (NH_4^+), one of four hydrogen atom was loosely bounded to the nitrogen atom and can be easily dissociated under influence of an electric field (Hafiza & Isa, 2017). The peak at ~1415 cm^{-1} started to disappear with the addition of more NH_4NO_3 might due to the ion association take place that lead to the founding of

neutral ion pairs (deprotonation). This would lead to the decrease in ionic conductivity and amorphousness of alginate– NH_4NO_3 system.

This result is similar with (Mason et al., 2010) and (Kadir et al., 2011) in their works. A new peak was observed at 1390 cm^{-1} due to the presence of NH_4^+ from NH_4NO_3. The interaction consequently caused an increase in intensity due to the addition of NH_4NO_3. These occurrences could be attributed to the coordination of NH_4^+ ions with the polar group's existence in the alginate group when NH_4NO_3 was incorporated into the system. The previous studies that used NH_4NO_3 as a dopant in their system also observed similar behaviour (Majid & Arof, 2008; Rajeswari et al., 2014). The authors assumed that the appearance of peaks at wavenumber ~1400 cm^{-1} corresponded to the NH_4^+ ions of the ammonium salts.
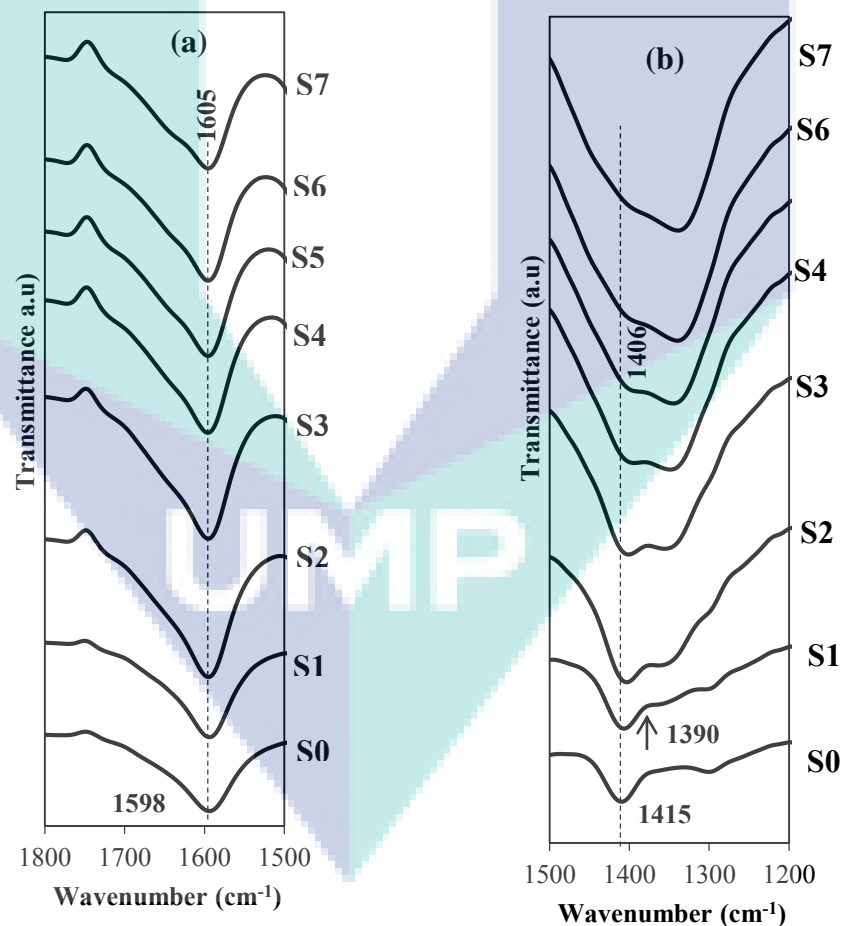
Figure 4.6   FTIR for a specific range of sodium alginate-ammonium nitrate correspond to carboxylic group between (a) 1500 – 1800 cm^{-1} and (b) 1200 – 1500 cm^{-1}

Furthermore, other evidence to prove the interaction can be seen in Figure 4.7, which shows that for the C–O–C group in alginate, the peak at wavenumber 1019 cm^{-1} shifted to a higher wavenumber at 1028 cm^{-1} when NH_4NO_3 was added in the system from S1 until S7. It can be assumed that the complexation occurred due to the migration of NH_4^+ toward C–O–C. There are strong contributions of hydrogen bonding and coordination interaction of H$^+$ to the C–O–C between alginate-NH_4NO_3 as found in other comparable work using ammonium salts (Samsudin & Isa, 2012). There are two possible charge carrier elements in the polymer–salt electrolytes system, namely cation and anion (Chai & Isa, 2013). Based on previous reports (Hema et al., 2008; Samsudin et al., 2012), it is believed that H$^+$ is the only cation contributing to the ionic transport properties, which would affect the ionic conductivity in the SBEs system. This proves that complexation had occurred at the coordinating site (oxygen) of the biopolymer (alginate), and thus conduction should take place by observing the change of peaks.
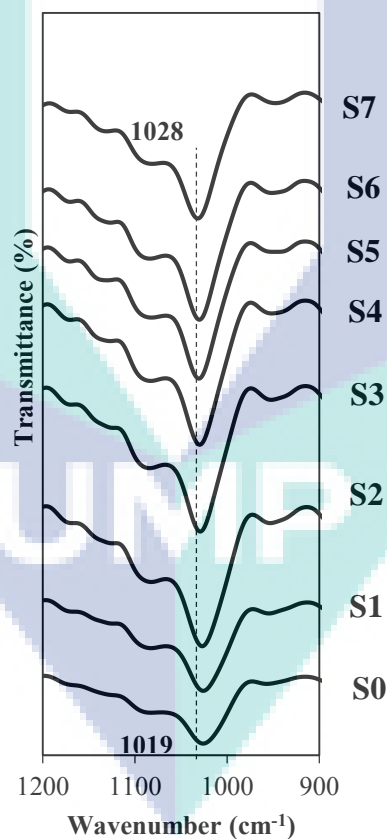
Figure 4.7   FTIR for a specific range of sodium alginate-ammonium nitrate correspond to C-O-C group between 900 – 1200 cm^{-1}

In Figure 4.8, the presence of the functional group, namely O-H stretching, can be observed, which corresponded to alginate at wavenumber 3393 cm^{-1} for sample S0.

The absorption peak of O-H stretching became more broadened with the addition of NH_4NO_3 in SBEs system where the wavenumber has shifted higher from 3393 cm^{-1} to 3452 cm^{-1}. A new peak can be seen at 3271 cm^{-1} with the addition of 15 wt.% of NH_4NO_3, which corresponded to the presence of asymmetrical N-H stretching from NH_4NO_3. The O-H band of alginate has obviously changed where overlapping of peaks is observed in the O-H region, which led to the shifting of the O-H group in alginate. This process is found in other similar works by other researchers that used NH_4NO_3 as an ionic dopant in the SBEs system (Shuhaimi, Majid, & Arof, 2009; Sohaimy & Isa, 2017).
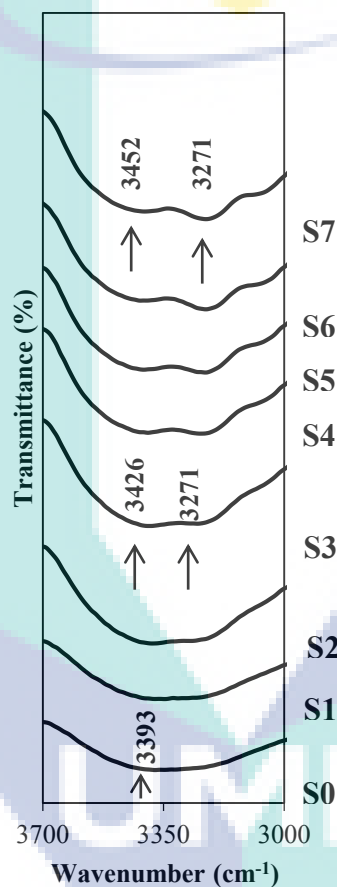
Figure 4.8   FTIR for a specific range of sodium alginate-ammonium nitrate correspond to O-H group between 3000 – 3700 cm^{-1}

The change in the O-H band of alginate confirmed the occurrence of complexation between salt and the polymer host. The shifting and change of intensity of the bands, absence of peaks, and appearance of new peaks can be due to the complexation of salt with the polymer matrix. The above result confirmed the interaction between the polymer and salt. Table 4.3 gives a summary of the changes in the wavenumber where it

is proven that complexation has occurred between alginate and NH_4NO_3 in the SBEs system. The schematic diagram of the proposed interactions occurred between alginate-NH_4NO_3 in SBEs system can be depicted in Figure 4.9.

Table 4.3   Summary of complexation between alginate and NH_4NO_3 for SBEs system

Sample	Functional group with wavenumber (cm^{-1})					
	C–O–C bending	COO$^-$ stretching	NH$_4^+$ stretching	COO$^-$ stretching	N-H stretching	O-H stretching
S0	1019	1415	-	1598	-	3393
S1	1019	1412	1390	1598	-	3403
S2	1021	1410	1390	1604	-	3414
S3	1025	1410	1390	1604	3271	3426
S4	1028	1408	1390	1604	3271	3433
S5	1028	1406	1390	1605	3271	3442
S6	1028	-	1390	1605	3271	3448
S7	1028	-	1390	1605	3271	3452
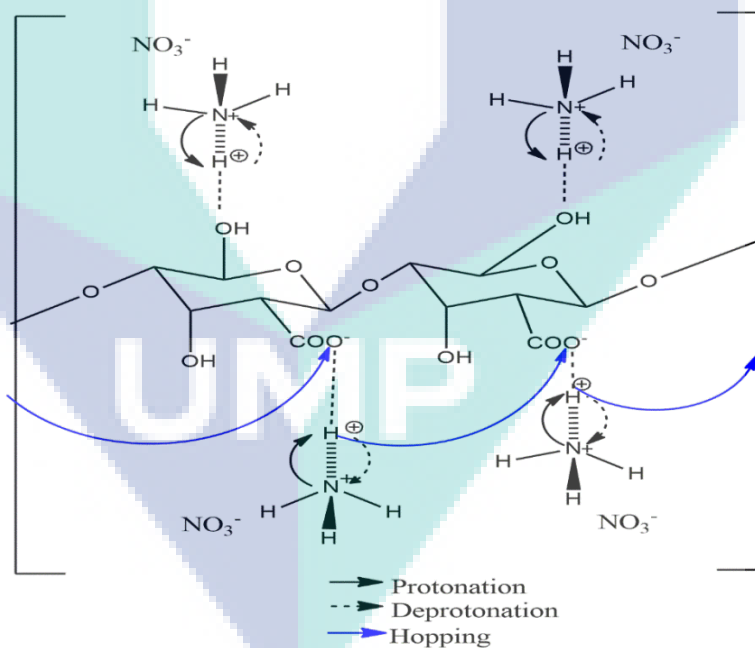
Figure 4.9   Proposed interaction alginate with NH_4NO_3 via $[N–H_4^+]$

From the findings, it is believed that there is obvious interaction of coordination interaction of H^+ of NH_4NO_3 between the COO^-, of carboxyl group of alginate and O-H hydroxyl group of alginate between alginate-NH_4NO_3 in SBEs system based on deprotonation, protonation and ion hopping process.

4.3   X-ray Diffraction (XRD) Spectroscopy Study

In the present research, XRD was used to reveal the nature of materials in the electrolytes system whether crystalline, amorphous, or semi-crystalline (Aravindran et al., 2009; Aziz et al., 2015; Aziz, 2016; Ramesh et al., 2011).

4.3.1   XRD spectra on Alginate and NH₄NO₃

The information on phases of the materials in this present work was examined by XRD analysis. Figures 4.10 and 4.11 show the XRD spectra of pure powder of ammonium nitrate and alginate, respectively. Based on the figure 4.10, the XRD pattern of NH_4NO_3 shows the presence of a peak at $2\theta = 17.18°$, $23.78°$, $29.94°$, $33.08°$, and $43.92°$, which correspond to the crystalline peaks of NH_4NO_3. From the literature by Shuhaimi et al., (2010) similarly assigned the peak at $\sim18°$, $22°$, $29°$, and $33°$ as the diffraction peaks of NH_4NO_3. Figure 4.11 shows the XRD pattern of alginate powder. Based on the figure, the peak intensity was seen at $2\theta = 13.16°$ and $21.78°$.
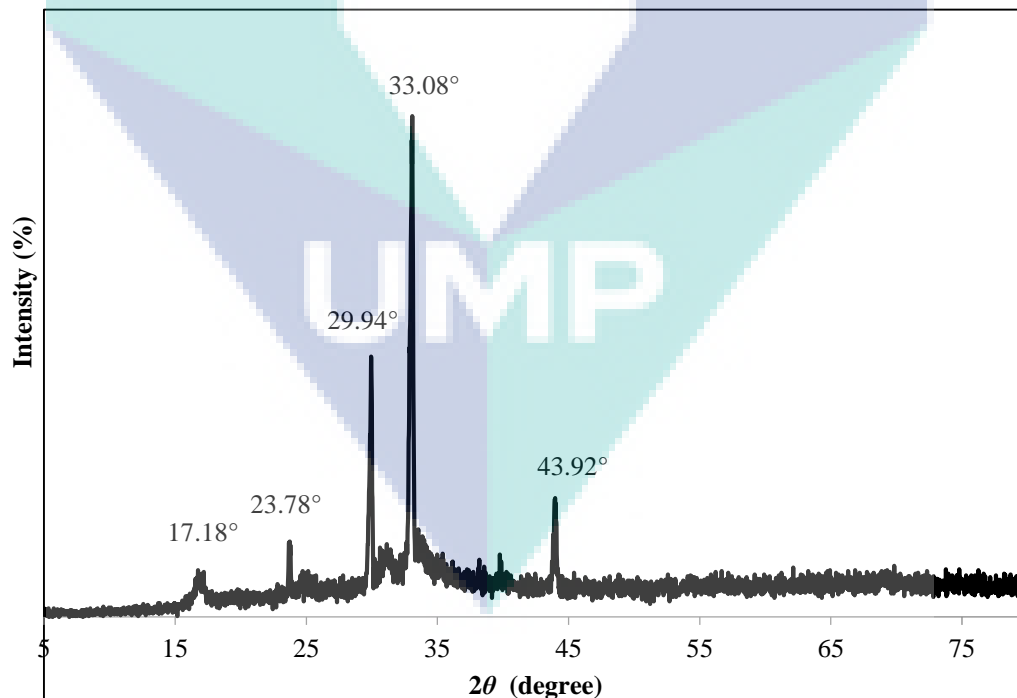
Figure 4.10   XRD analysis for ammonium nitrate.
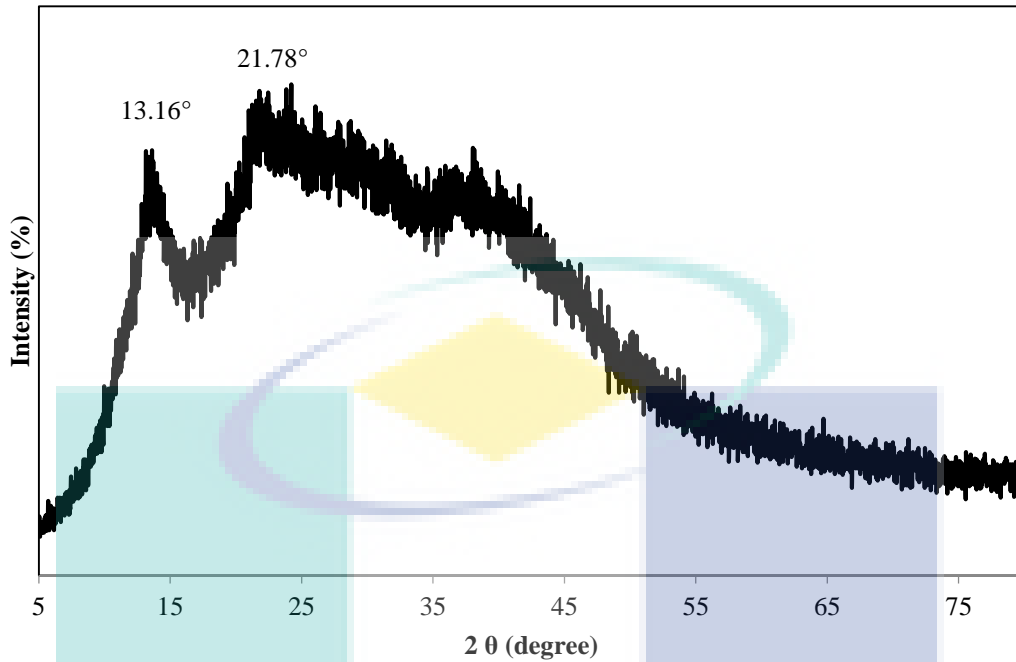
Figure 4.11   XRD analysis for alginate powder

4.3.2   XRD on Alginate doped with NH$_4$NO$_3$

The XRD patterns of SBEs of alginate doped with ammonium nitrate are shown in Figure 4.12. The previous researcher assigned alginate X-ray diffraction with two main semi-crystalline peaks at $2\theta = 13.7°$ and $23.0°$ (Wang, Hu & Du, 2014; Yang et al., 2000). Their work is similar to this present work. On the other hand, the peak become more amorphous due to the presence of NH$_4$NO$_3$ in the polymer host, and these regions increased after the addition of salt in the electrolyte system (Jafirin et al., 2013). From Figure 4.12, S0 gave a clear hump at 13° and 21°. These two peaks shifted to the higher intensity $2\theta = 14.42°$ and $22.06°$, respectively, with the addition of 5 wt. % NH$_4$NO$_3$. As the content of NH$_4$NO$_3$ increased, the hump became more broadened and shifted to the higher Bragg's angle implied that the microstructure of the host polymer became more homogeneous (Gao et al., 2017). Singh et al. (2017) proved that all the dopant system were well dissolved in the biopolymer matrix, which was confirmed by the disappearance of XRD peaks related to salts in the biopolymer-salt complex.

This XRD pattern implies that the samples became more amorphous due to the decrement in crystalline peaks with the addition of more NH$_4$NO$_3$. It could be suggested that the most amorphous sample is S5 where the peak shifted to lower Bragg's angle.
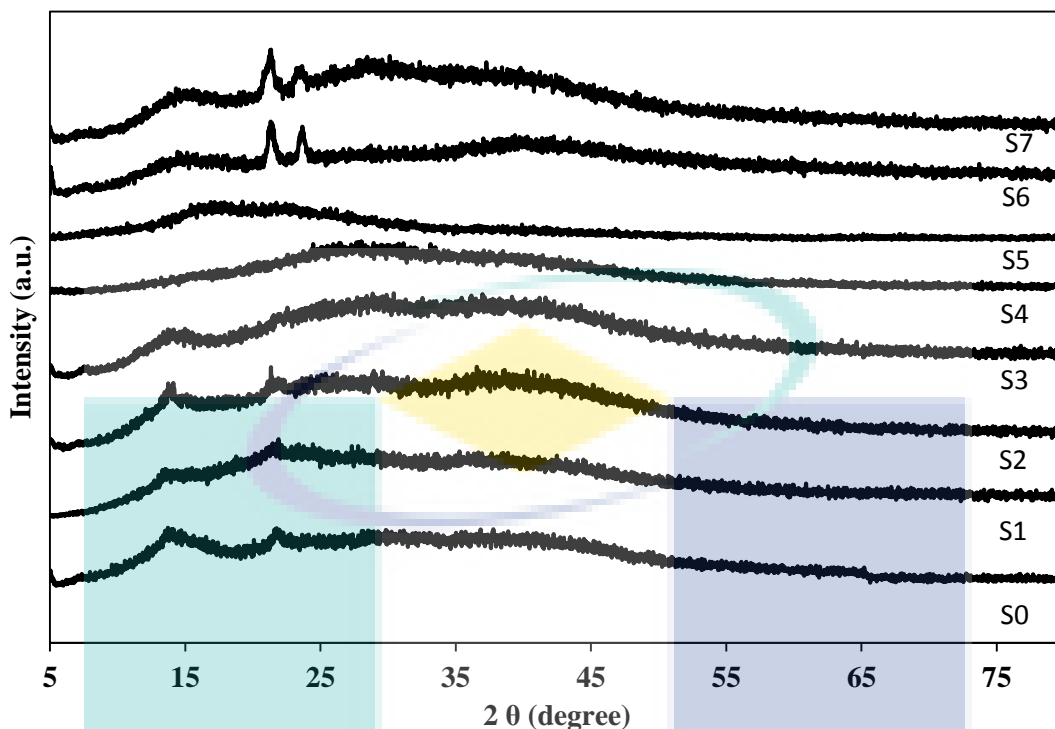
Figure 4.12   XRD analysis for entire content of alginate-ammonium nitrate

This might be attributed to the optimum complexation between alginate and ammonium nitrate which was discussed in FTIR analysis in previous section and this could lead to enhance the transport properties of SBEs system. This phenomena of the changes in Bragg's angle was supported by (Zainuddin et al., 2018) work. In their work, amorphous peak shifted to lower Bragg's angles while semicrystalline peak shifted to higher Bragg's angle due to the cross-linking of the host polymer, carboxymethyl cellulose/kappa carrageenan. Hence, upon the addition of more than 25 wt. % of NH_4NO_3, (samples S6 and S7), the samples became more crystalline.

The presence of two peaks at $2\theta \sim 21°$ and $23°$ corresponded to undissociated salt and reassociation of the ions into the aggregations of ion cluster in the SBEs. In addition, it indicates that the polymer could no longer dissolve the salt (Shuhaimi, Teo, & Arof, 2010). Therefore, the extra salt recrystallized out of the samples. The amorphous region contributed to the increment of protonation of H^+ in the alginate, thus leading to the enhancement of ionic conductivity among the samples.

Conductivity increased as the amorphousness of the sample increased (Rajendran & Sivakumar, 2008). Thus, the ionic conductivity increased by reducing the crystallinity

of the materials. This behavior confirmed that complexation has occurred in the amorphous sample. The amorphous phase obtained caused a reduction in the energy barrier to the segmental motion of the polymer electrolyte (Chu et al., 1999; Ibrahim et al., 2011). This amorphous nature resulted in high ionic conductivity, which can be observed in amorphous polymers having flexible backbones.

A study on crystallite size was carried out to examine the nature of alginate with the addition of NH_4NO_3. It involved an analysis using the information of full width at half maximum (FWHM) and calculated using the Debye-Scherrer equation (Aziz & Abidin, 2013; Mahakul et al., 2017; Mazuki et al., 2018; Samsudin et al., 2018) as shown in Equation 4.1 to examine the role of salt on the crystalline structure of alginate.

The FWHM values obtained for the samples are presented in Table 4.4, which lists down the summary of crystallite size, D. It can be found that the value of crystallite size is higher when alginate incorporate with NH_4NO_3 for sample S1 and S2. It might due to the salt undissolved well during the preparation and give the effect for the crystallite size as shown in region ~21 degree. The table shows that sample S5 exhibited the lowest crystallite size value. The addition of NH_4NO_3 managed to alter the crystallite size of the samples.

The increment in the amorphous phase of the polymer electrolyte was attributed to a delocalized complex system that affected the flexibility of the host polymer (Rasali & Samsudin, 2018). However, it is obvious that as more NH_4NO_3 was added, the samples S6 until S7 produced higher FWHM values, indicating a larger crystallite size. It suggested that the samples were in the crystallinity phase of the SBEs system and comparable with experimental result in XRD analysis.

$$D = \frac{K\lambda}{FWHM \cos \theta}$$
4.1

where K = 0.94, λ = 0.154 Å and θ = peak location

Table 4.4   Crystallite size of alginate-ammonium nitrate SBEs system

SAMPLE	2θ (degree)	FWHM (degree)	Crystallite size, D (Å)
S0	13.99	3.78	22.11
	21.75	0.83	101.76
	38.60	9.60	9.15
S1	14.46	4.09	20.44
	22.25	6.90	12.25
S2	13.64	1.90	43.96
	21.69	2.30	36.71
S3	13.72	3.02	27.66
	28.80	10.10	8.48
S4	28.13	8.10	10.56
S5	24.24	12.55	6.76
S6	14.46	5.01	16.68
	21.34	0.53	159.25
	23.61	0.48	176.53
	39.83	10.00	8.82
S7	15.21	2.96	28.27
	21.32	0.63	133.97
	28.20	5.60	15.27
	29.50	6.60	12.99

In addition, when a polymer host has complexation with salt, the crystallinity of that polymer could be disturbed by the presence of impurities (Armand, 1983; Kumar et al., 2007). It can clearly be seen that the crystallinity behavior started at the region between ~14° and 40° when the alginate was added with more than 25 wt.% of NH_4NO_3. The crystalline peaks observed corresponded to the appearance of NH_4NO_3 and alginate crystalline phase. This implies that the alginate could not solvate the NH_4NO_3 any longer as more free ions of H^+ concentration were supplied in the SBEs system that led to overcrowding and blocking of the pathway for migration, thus increasing the crystalline phase. This eventually led to the decrease in the transport properties and ionic conductivity in the present samples. The appearance of the crystalline peak also indicated that the de-protonation process has occurred, as proven in the FTIR analysis.

4.4   Thermogravimetric analysis (TGA)

Thermogravimetric analysis (TGA) was used to evaluate the thermal stability of the different samples. Thermal decomposition of alginate doped with ammonium nitrate for selected sample are presented in Figure 4.13 and the decomposition temperature value

are tabulated in Table 4.5. TGA thermogram of alginate undoped system exhibited two distinct stages. The first stage in the range of 30-108 °C where it showed that with increasing temperature the weight of sample decreases slowly up to 108 °C. This is mainly due to the diminished of water by the adsorption by hydrophilic polymer (Işıklan et al., 2009). In addition, based on pointed by Tripathy and Singh (2001), the first region of thermal decomposition of alginate (below 100 °C) is caused by the presence of moisture in alginate.

The second stage in the range of 208–330°C with a maximum decomposition temperature was found at 260.76 °C. At this stage, the phenomenon of dehydration of the saccharide rings, depolymerization with the formation of water, CO_2, and CH_4 are occurred in alginate backbone (Işıklan et al., 2009; Zhang et al., 2003). Previous report explained that the presence of COO^- groups in the alginate, which refers to the occurrence of decarboxylation where carbon atoms are removed from the carbon chains in the carboxylic acids in this temperature range (Tripathy & Singh, 2001).

With the addition of NH_4NO_3 in alginate, an improvement is observed in both the heat-resistivity and thermal stability of alginate pure film as indicated by the weight reduction of the TGA curve. For the different sample with addition of NH_4NO_3, there was three distinct regions of the decomposition SBEs system. The first region was between 30 until ~200 °C which corresponded to the loss of moisture from the presence of hydrophilic groups along the backbone chain of hydroxyl and carboxylic (Eldin et al., 2017). The second region's decomposition started at around 200 °C and continued above to 330 °C, which was attributed to the degradation of the alginate's backbone chain (Shaari et al., 2018).

Based on Table 4.5, the SBEs system with the content of 25% showed the highest maximum decompose temperature, T_d at 320.97 °C. Notably, the sample become more stable in term of its thermal stability as the temperature increased. This can be seen where the decomposed of sample is high and could be attributed to the interaction between alginate and NH_4NO_3 as explained in the FTIR analysis previously. Gao et al., (2017) and Azeredo et al., (2012) reported that the thermal decomposition of alginate based on their carboxylic groups was present at the second stage with temperature range of 216−312 °C, which supported this result.
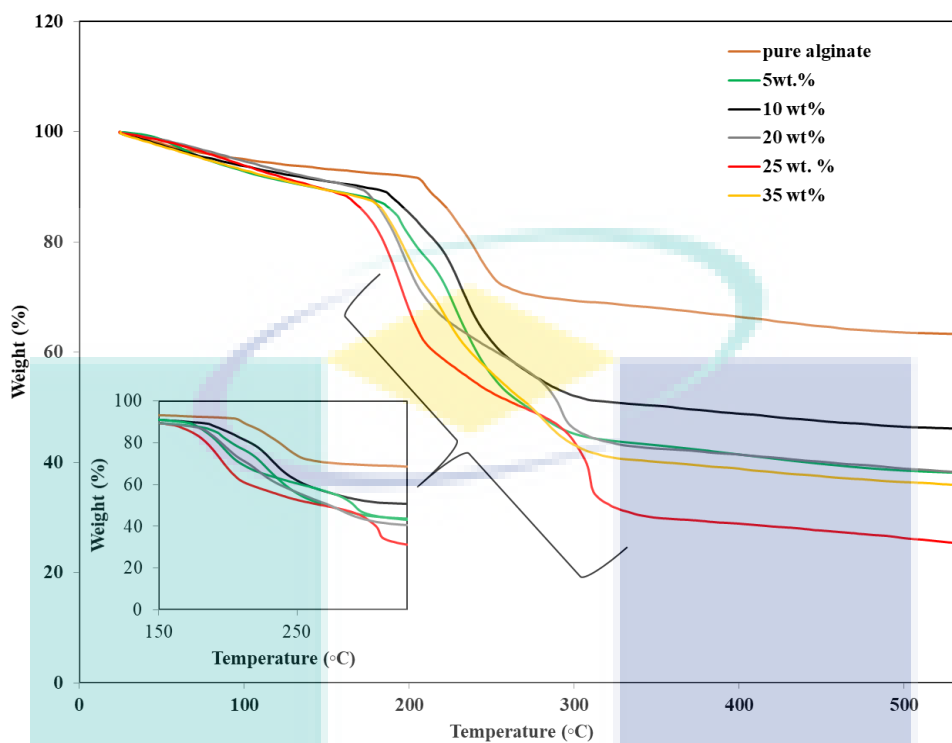
Figure 4.13   The comparison of thermal decomposition of the alginate-NH_4NO_3 SBEs system with different weight percentages.

In addition, this can be associated with the presence of greater amorphous phase in the SBEs system causing an increase in heat sensitivity. Since it is thermally stable, less monomer will be detached from the complex structure of alginate – NH_4NO_3 thus increased the decomposition temperature, T_d.

On the other hand, an increase in NH_4NO_3 content (above 25 wt. %) was found to lead to the reduction in heat resistivity and thermal stability. The displacement of the maximum decomposition temperature of samples with higher content to lower temperature reveals the decline in the samples heat resistivity. The diminishing heat-resistivity explains the possible structural disorderness in carboxylate anion (COO–) from alginate that leads to the existence of vast free volume between the connected molecules which results in deprotonation occurring which was supported by the FTIR results.

Similar pattern has been reported by (Samsudin et al., 2014) and (Mohamad & Arof, 2007), where the increased of ionic dopant in polymer electrolytes system would lead to the reduction in heat resistivity as more (+ve) ions was removed from the polymer

matrix in polymer electrolytes system through heating process. This observation demonstrates that the sample S5 containing with 25 wt. % NH_4NO_3 expected to exhibit highest ionic conductivity.

The third region at the temperature above ~320 °C elucidated the degradation process of the polymer backbone and ash formation (Freile et al., 2011; Liew et al., 2017). Accordingly, all the curves clearly demonstrated the different thermal behaviours of alginate, and from them, it is confirmed that the polymer is more thermally stable with the addition of ionic dopant.

Table 4.5   The maximum total decomposition of SBEs

Sample	Total maximum decomposition temperature, T_d ($\circ$C)
Alginate	260.76
S1	301.16
S2	304.37
S4	306.23
S5	320.97
S7	309.06

4.5   Ionic Conductivity Study

In this part, the result obtained from the experiment using Electrical Impedance Spectroscopy (EIS) is discussed in detail, as one of the objectives of this research is to determine the ionic conductivity of the samples.

4.5.1   Cole-Cole plot

Electrical properties of all the prepared alginate-NH_4NO_3 SBEs system have been analyzed using the EIS. From the EIS analysis, the Cole-Cole plot of imaginary impedance, Z_i, against real impedance, Z_r, for samples of alginate-NH_4NO_3 at room temperature was obtained, as shown in Figure 4.14. According to Havriliak and Negami (1996), almost all the polymer materials have an arcuated Cole–Cole plot at low-frequency and a linear Cole–Cole plot at high frequency. The compressed semicircle at higher frequency indicated the bulk conductivity process, and the spike line represented the migration of ions through the free volume of the polymer matrix in the SBEs system

(Reddy et al., 2006; Govindaraj, Baskaran, Shahi, & Monoravi, 1995; Samsudin & Isa, 2012).

Based on previous research, the impedance analysis showed that the Cole-Cole plot with an equivalent circuit having a semicircle was due to the parallel combination of bulk resistance, (R_b) and bulk capacitance, (C_b) or popularly known as the constant phase element (CPE) of the sample (Malathi et al., 2010). The value of bulk resistance is determined based on the intersection of the real impedance axis with the adjacent line (spike).

From the plot, samples S0, S1, S2, and S3 possessed the semicircle in the high frequency region and were inclined at the low frequency region. It implies that the line adjacent to the semicircle was caused by the effect of electrode polarization behavior in the diffusion part (Reddy et al., 2006). As the salt concentration of NH_4NO_3 increased, the bulk resistance of impedance seemed to lessen, and the highest conducting sample, namely the 25 wt.% of NH_4NO_3, gave the lowest frequency spike with the lowest bulk resistance.

It is noted that the semicircle observed at high frequencies completely disappeared in the SBEs with 25 wt.% of NH_4NO_3 (sample S5). This result suggests that only the resistive component of the SBEs prevailed when the amount of NH_4NO_3 was high. When the addition of salt increased up to 25 wt.%, the bulk resistance decreased due to the mobile charge carriers (Ramya et al., 2006; Shukur, Ithnin, & Kadir, 2014). It indicates that the current carriers were ions, and it can be concluded that the conduction was due to the ions (Jacob, Prabaharam & Radhakrishna, 1997; Kadir, Aspanut & Arof, 2009; Rajendran, Mahendran, & Krishnaveni, 2003). As a result, sample S5 exhibited the highest ionic conductivity at room temperature in the SBEs system.
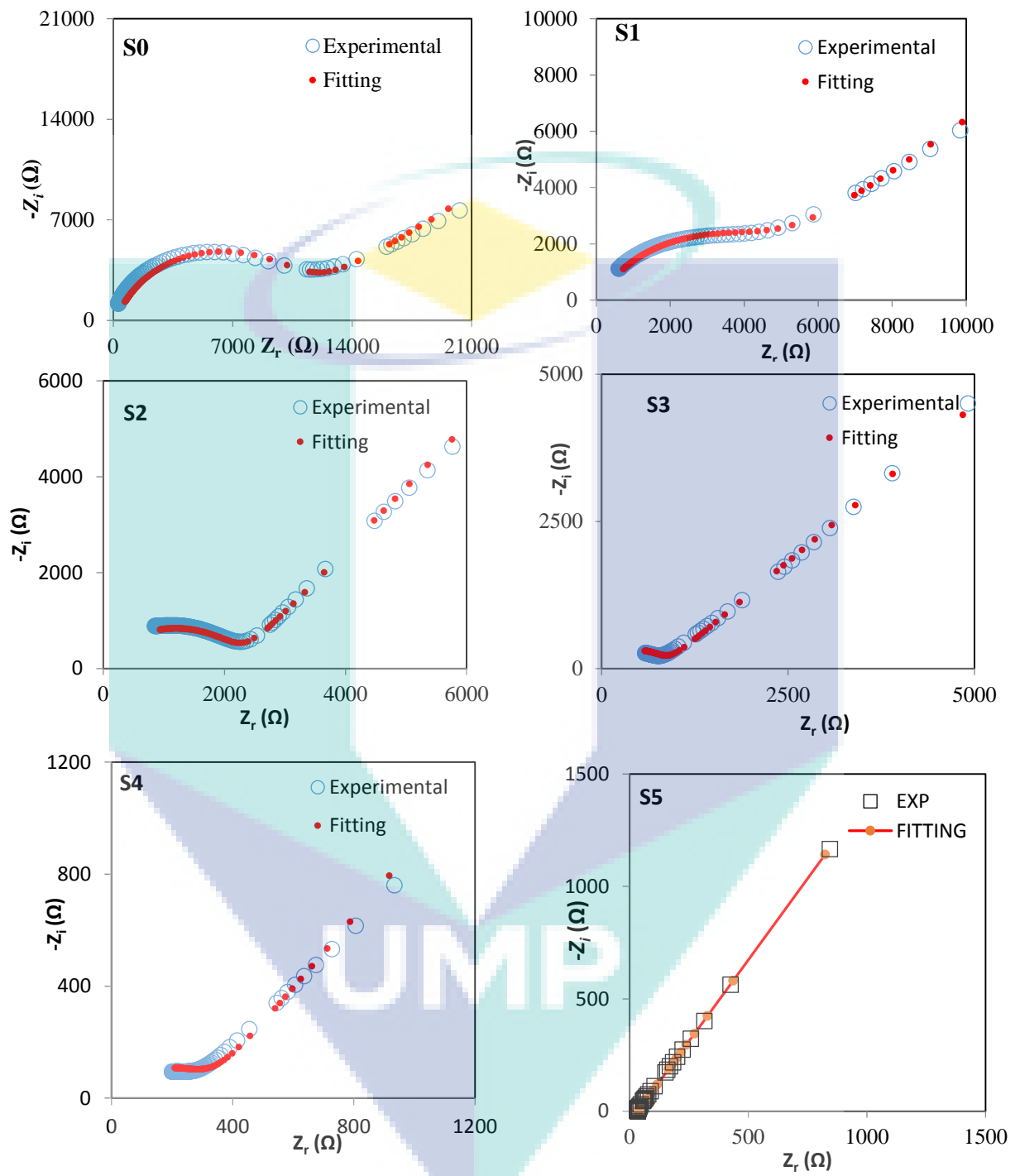
Figure 4.14   Cole – cole plot of alginate and ammonium nitrate SBEs system
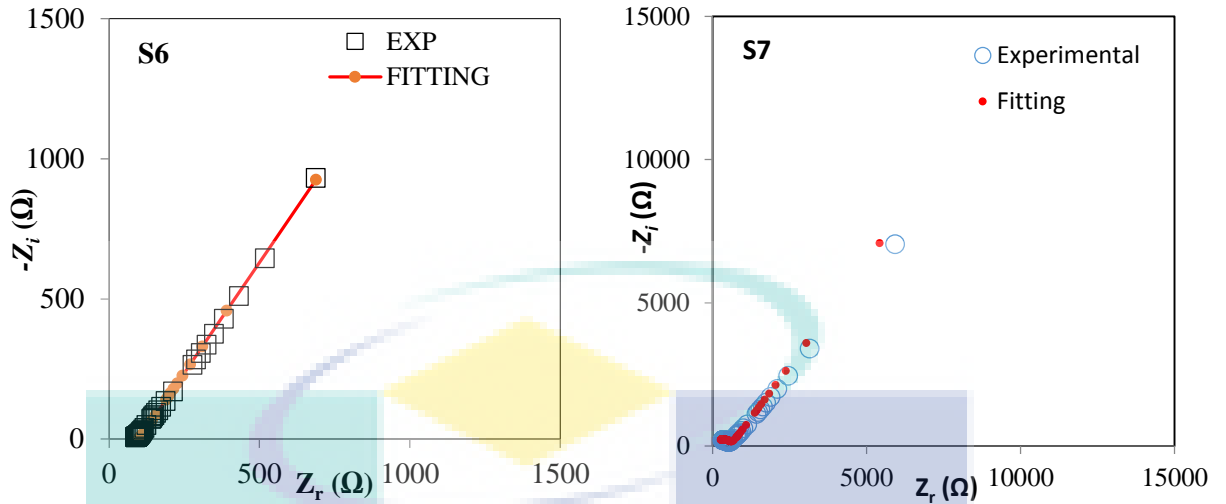
Figure 4.14   Continued

Table 4.6 lists down the calculated value of the circuit elements in the SBEs system samples. The result shows that capacitance was low when the frequency was in the high region, which is consistent with the equation:

$$C = \frac{\varepsilon_o \varepsilon_r A}{d}$$

4.2

where A is the area of the interface between electrode and electrolyte, d is the electrolyte's thickness, ε_o refers to the permittivity in vacuum, and ε_r refers to the dielectric constant. As the frequency increased, the value of ε_r decreased, which gave a low capacitance value (Hema et al., 2008). Details of ε_r for the present study will be explained further in the dielectric section.

Based on the table 4.6, the value of parameter in theoretical part is obtained from the substitution of the value with trial and error based on equation of 4.4 until 4.7 until achieved the suitable fitting pattern of the plot and reliable with the experimental result. In the present research, it shown the value of bulk resistance in theoretical and experimental is quite similar. The value of R_b decreased as NH_4NO_3 was added in the alginate SBEs system. The reduction of R_b's value is because of the enhancement of the polymer chain's segmental motion and salt's dissociation. As notice in table 4.6, the value of capacitance at lower frequency region higher than at higher frequency region which in line with equation 4.2. The value of p_1 and C_1 were missing for sample S5 and S6 due to the disappearance of semicircle that has been replaced by spike.

Table 4.6 The value of the circuit elements of the alginate-NH$_4$NO$_3$ SBEs system at room temperature

Sample (wt. %)	p_1 (rad)	C_1 (F)	p_2 (rad)	C_2 (F)	Theoretical R_b (Ω)	Experimental R_b (Ω)
S0	0.88	1.06×10^{-9}	0.41	3.33×10^{-6}	9.45×10^{3}	1.22×10^{4}
S1	0.86	1.76×10^{-9}	0.49	9.09×10^{-7}	3.41×10^{3}	9.42×10^{3}
S2	0.79	2.63×10^{-9}	0.59	1.56×10^{-6}	2.16×10^{3}	2.54×10^{3}
S3	0.77	4.90×10^{-9}	0.52	4.81×10^{-6}	8.00×10^{2}	8.86×10^{2}
S4	0.68	5.56×10^{-8}	0.58	4.26×10^{-6}	3.02×10^{2}	3.72×10^{2}
S5	-	-	0.63	2.00×10^{-5}	3.90×10^{1}	6.09×10^{1}
S6	-	-	0.63	2.39×10^{-5}	8.00×10^{1}	1.43×10^{2}
S7	0.76	1.43×10^{-8}	0.62	3.32×10^{-6}	6.00×10^{2}	6.77×10^{2}

In the impedance analysis, the electrical equivalent circuit was used due to its straightforwardness and ability to give the entire picture of the system (Teo et al., 2012) and can be determined from the result of Cole-Cole plot. Constant phase element (CPE) is a "leaky capacitor", which is due to inhomogeneity in the electrolyte and can be conveyed (Qian et al., 2001):

$$Z_{CPE} = \frac{1}{C\omega^p}\left[\cos\left(\frac{\pi p}{2}\right) - i\sin\left(\frac{\pi p}{2}\right)\right]$$

4.3

Here, Z_r and Z_i stand for the real and imaginary parts of impedance, respectively, p is correlated to the plot's deviation from the axis, ω stands for angular frequency, and C represents CPE's capacitance. If p is equal to 0, Z_{CPE} is frequency independent, and if p is equal to 1, $Z_{CPE} = R - i/C\omega$. CPE performs as the intermediary between a resistor and capacitor (Shuhaimi et al., 2012).

Scheme 4.1 represents an equivalent circuit for all the samples excluding for the highest conducting samples, S5 and S6. For impedance plot of this section, which is composed of a semicircle and a line adjacent to it, the equivalent circuit is a combination of constant phase elements (CPE) and R_b in parallel with another CPE in series. The deviations of impedance spectra from ideal behaviour can be explained as a new circuit parameter known as CPE. CPE alone gives impedance value which when plotted in the impedance plane looks like an inclined straight line.

The equivalent circuit is a combination of resistances and capacitances as well as a few electrochemical elements such as Warburg diffusion elements and CPE. CPE can be expressed in Scheme 4.1, the higher frequency semicircle refers to the dependent capacitor (CPE_1) in parallel with bulk resistance (R_b), and the low frequency spike corresponds to constant phase element (CPE_2) (Nath & Kumar, 2011).
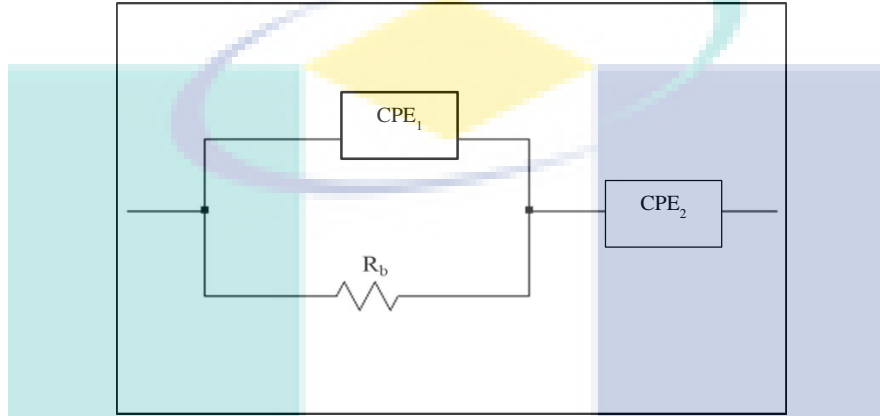
Scheme 4.1   Equivalent circuit of the SBEs system which correspond to plot of S0, S1, S2, S3, S4, and S7 of NH_4NO_3

The resistor refers to the ions migration through the polymer matrix, and the CPE_1 represents the polarized immobile polymer chains in the alternating field. Such plots are widely used for electrochemical measurement in other PEs (Ghelichi et al. 2013; Seanwa & Choundhary, 2014; Mohapatra et al., 2009). The Z_r and Z_i for this equivalent circuit are given as (Arof et al. 2014; Bandara & Mellander, 2011):

$$Z_r = \frac{R_b + R_b^2 C_1^{-1} \omega^{P_1} \cos(\frac{\pi p_1}{2})}{1 + 2R_b C_1^{-1} \omega^{p_1} \cos(\frac{\pi p_1}{2}) + R_b^2 C_1^{-2} \omega^{2p_1}} + \frac{\cos(\frac{\pi p_2}{2})}{C_2^{-1} \omega p_2} \qquad 4.4$$

$$Z_i = \frac{R_b^2 C_1^{-1} \omega^{P_1} \sin(\frac{\pi p_1}{2})}{1 + 2R_b C_1^{-1} \omega p_1 \cos(\frac{\pi p_1}{2}) + R_b^2 C_1^{-2} \omega^{2p_1}} + \frac{\sin(\frac{\pi p_2}{2})}{C_2^{-1} \omega p_2} \qquad 4.5$$

Here, p_1 stands for deviation of circle's radius from the imaginary axis while p_2 is the deviation of tilted adjacent line to the semicircle from the real axis. k_1 represents the high frequency capacitance, and k_2 stands for low frequency capacitance.

Scheme 4.2 shows that the bulk resistance, R_b, was in series with the CPE as the Cole-Cole plot gave the only spike results when the S5 and S6 of NH_4NO_3 were determined in electrical parts. The presence of a complex impedance plot with a spike at low frequency was due to the effect of the capacitive electrode performance.
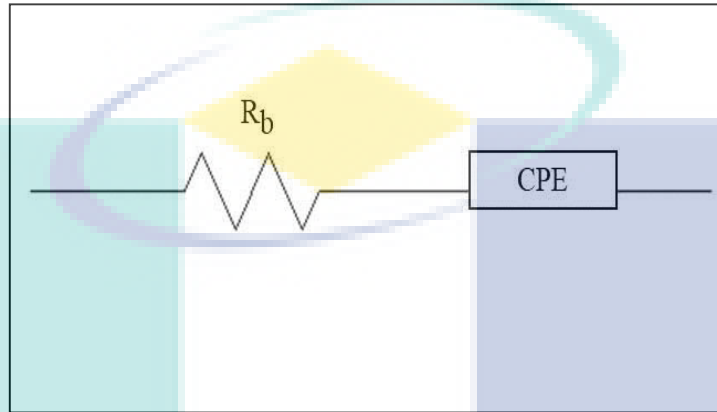
Scheme 4.2   Equivalent circuit of the plot S5 and S6 of NH_4NO_3 SBEs.

Further addition of more than 30 wt.% of NH_4NO_3 led to the forming of the semicircle in the high frequency range due to the effect of the blocking electrode (Muthupradeepa et al., 2017). This is due to the deprotonation and the formation of crystalline pattern of alginate–NH_4NO_3 SBEs system as proven in the FTIR and XRD analysis in the previous discussion.The Z_r and Z_i for this equivalent circuit are given as:

$$Z_r = R_b + \frac{\cos(\frac{\pi p_2}{2})}{C\omega^{p_2}}$$

4.6

$$Z_i = \frac{\sin(\frac{\pi p_2}{2})}{C\omega^{p_2}}$$

4.7

4.5.2   Ionic Conductivity of Alginate doped with NH_4NO_3 SBEs system

According to Samsudin et al. (2012) and Schantz and Torell (1993), the ionic conductivity of SBEs can be influenced by several factors, such as temperature, salt content, cationic or anionic type charge carrier, and the charge carrier's mobility. Other researchers opined that the ionic conductivity of SBEs system can be influenced by the amorphousness, thermal stability, cation and anion motions, and ion pair formation (Pradhan et al., 2007).

The variation of conductivity for alginate and ammonium nitrate SBEs system is presented in Figure 4.15. It is observed that the ionic conductivity of SBEs increased with the addition of NH_4NO_3, which can be related to the decrease in the value of R_b, indicating that lower R_b gives the higher conductivity. The dependence of ionic conductivity on the content of the ionic dopant gave specific information about the interaction that occurred between NH_4NO_3 and alginate in this SBEs system.
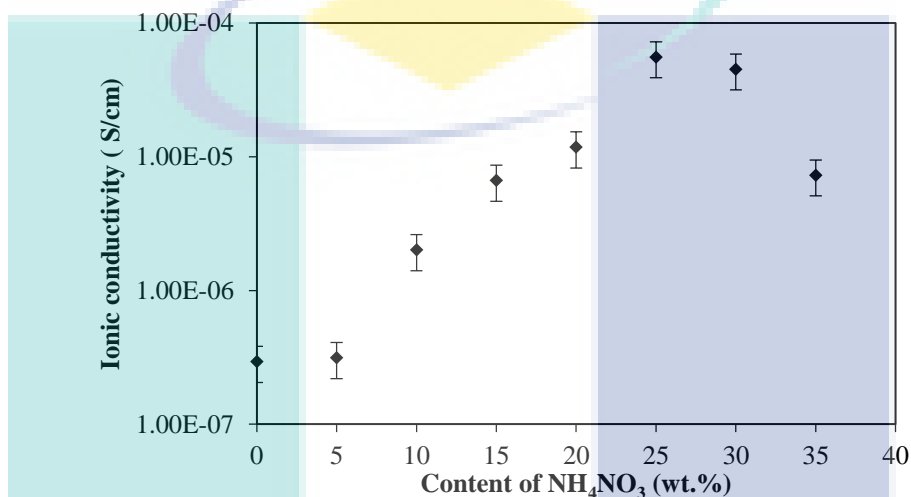
Figure 4.15   Ionic conductivity of alginate–NH_4NO_3 SBEs system at room temperature

Conductivity increased gradually with increasing NH_4NO_3 until it reached a maximum value at 25 wt.% of NH_4NO_3, which can be related to the dissociation of ion as proven in the FTIR analysis. In the complexation of entire samples of alginate-NH_4NO_3, the ammonium salt had interacted with the carboxyl group of the alginate host. More ions hopping were occurred, which enhanced the ionic conductivity.

As the content of salt increased, more free ions of H^+ were supplied due to dissociation of the salt (Sit et al., 2012). Hence, there was ion hopping and exchange among the ions occurring at vacant sites, which led to the increment in ionic conductivity. Moreover, XRD results suggested that the increasing amorphous phase in the SBEs system and from TGA analysis, the thermal stability increases with the addition of NH_4NO_3.

The preeminent ionic conductivity for this system is for the sample at 25 wt .% of NH$_4$NO$_3$ with 5.56×10^{-5} Scm^{-1} and for pure alginate, which reached 2.94×10^{-7} Scm^{-1} at room temperature. The most amorphous sample S5 (25 wt. % NH$_4$NO$_3$) as shown in XRD analysis showed the highest ionic conductivity where this sample has backbone flexibility due to the greater ion diffusion that caused a reduction in the energy barrier to the segmental motion in the SBEs (Othman, Samsudin, & Isa, 2012; Teeters, Neuman, & Tate, 1996).

Furthermore, TGA analysis proved that sample with 25 wt. % NH$_4$NO$_3$ will exhibit highest ionic conductivity as the decomposition temperature, T_d is higher and this would lead to greater protonation H$^+$ between alginate and NH$_4$NO$_3$. Beyond 25 wt.% of NH$_4$NO$_3$, the ionic conductivity decreased due to the re-association of the ions into the aggregations of ion cluster (Hodge et al. 1996; Schantz & Torell, 1993). The excess salt turned the sample into a recrystallized phase as figured out in the XRD analysis, which caused an increase in the energy barrier to the segmental motion in this system (Rasali et al., 2018). For further understanding of the ionic conductivity mechanism, the ionic conductivity of the alginate– NH$_4$NO$_3$ SBEs systems was tested at elevated temperatures from 303 to 343 K.

4.5.3   Temperature dependence

For further understanding of the mechanism of ionic conductivity, the entire samples of alginate– NH$_4$NO$_3$ SBEs system were tested at different temperatures within the range of 303 K to 343 K (5 K increment), as shown in Figure 4.16.

The plot in Figure 4.16 shows that the ionic conductivity for all samples increased with the increase in temperature from 303 K to 343 K where it was thermally assisted in the present system. In current work, no sudden drop or increase in conductivity value with temperature can be seen in each SBEs system. This indicates that the SBEs exhibit a completely amorphous structure (Ravi et al., 2011) and it proved that the ionic conductivity of SBEs is not affected by water content, but it is because of the existence of charge carrier from the salt or ionic dopant (Sim et al., 2016). The films seemed mechanically stable at higher temperatures, which contributed to the enhancement of

ionic conductivity due to the thermal movement of the polymer chain, indicating that the electrode-electrolyte interfaces acted as a capacitance (Hema et al., 2008).
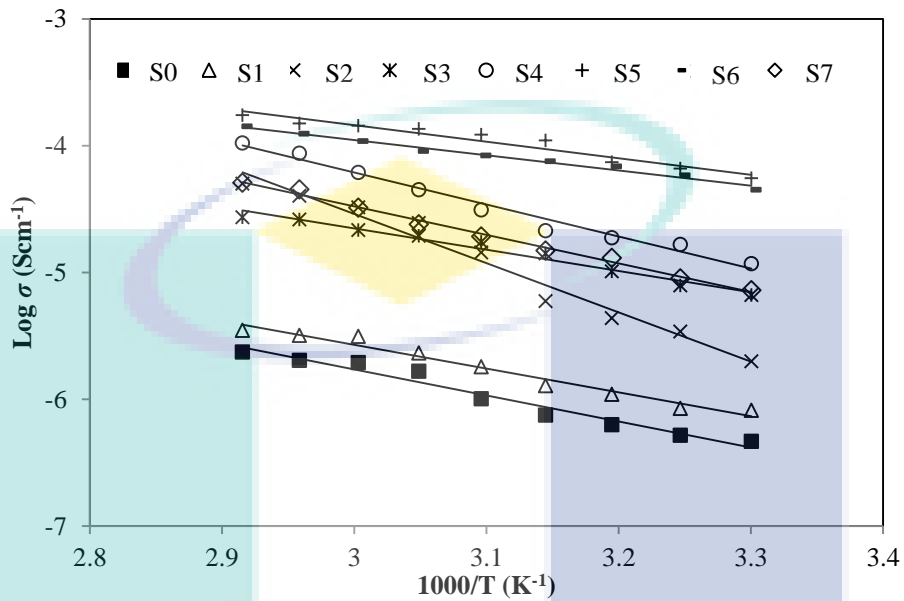
Figure 4.16   Temperature dependence of ionic conductivity for SBEs system at different temperatures

In addition, the increase in conductivity with temperature can be explained by the increase in free volume of SBEs in the ion movement. Consequently, ions and solvated molecules moved easily to the free volume, thus enhancing the ions and segmental mobility of polymer and ionic conductivity (Johan & Ting, 2011). This can also be explained by the segmental motion of the polymer facilitating the translational ionic motion (Buraidah et al., 2009). This event was also attributed to the decrease in viscosity of the electrolyte, thus increasing the chain flexibility (Michael et al., 1997; Yang et al., 2008). Thus, the ionic conductivity increased with increasing temperature.

The regression value, R^2, was found to be close to unity ($R^2 \sim 1$), suggesting that the plot was linear, and entire contents of the alginate–NH_4NO_3 SBEs system obeyed the Arrhenius rules (Teeter et al., 1999; Othman et al., 2012) as plotted in Table 4.7. Similar results were observed for different types of electrolytes (Rajendran & Uma 2000; Sit et al., 2012; Samsudin & Isa 2012; Hashmi et al., 1990; Shukur et al., 2014). Since the thermal stability of alginate was found to increase with the addition of NH_4NO_3, the increase in conductivity with temperature is assumed to be caused by the high free volume

of ions movement (Miyamoto et al., 1973) through the alginate backbone. This can be explained by the vibration of the energy of the segmental motion functions countering the hydrostatic pressure imposed by its neighboring atoms when the temperature increased.

Table 4.7   Regression value (R^2) of alginate–NH_4NO_3 SBEs system

Sample	Regression, R^2
S0	0.95
S1	0.99
S2	0.98
S3	0.99
S4	0.97
S5	0.98
S6	0.97
S7	0.96

As the plot obeyed the Arrhenius rules, the transportation of ions occurred that is the ions jumped into other sites, and hence the ionic conductivity in the system increased (Sauquet et al., 1994). This event of ion transportation also occurred in the ionic crystal. The increase in ionic conductivity with temperature can be related to the segmental motion where it led to the increment in the free volume in the system (Hema et al., 2008).

It can be assumed that with the segmental motion, the ions can jump to another site or provides a pathway for the motion among the ions. This interaction of ions movement led the ionic conductivity to increase with the increase in temperature (Buraidah et al., 2009). Other researchers with different types of SBEs also claimed the same behavior (Chai & Isa, 2013; Kadir et al., 2010).

The conductivity of alginate–NH_4NO_3 at elevated temperature was also determined. The activation, E_a of the samples can be calculated as it corresponds to the effect of temperature on conductivity by using the Arrhenius relation:

$$\sigma = \sigma_0 \exp^{(\frac{-E_a}{kT})} \qquad 4.8$$

Where

$$\sigma_o = \quad \text{pre-exponential factor}$$
$$k = \quad \text{Boltzmann constant}$$
$$E_a = \quad \text{Activation energy}$$
$$T = \quad \text{Absolute temperature in Kelvin}$$

From the temperature dependence plot, the activation energy, E_a, can be calculated from the slope of the graph by using equation (4.8). Activation energy is defined as the requirement of energy for an ion to start a movement. When the ion has enough energy, it can easily escape from a donor site and jump to another donor site (Ahmad, 2012; Ahmad & Isa, 2012).

Figure 4.17 shows the activation energy, E_a, for all samples of the alginate–NH_4NO_3 SBEs system. The value of E_a is inversely proportional with the value of ionic conductivity, where the sample with 25 wt.% of NH_4NO_3 has the lowest E_a, 0.11 eV, which indicated that less energy is required by the charge carriers in higher conducting electrolyte to make a motion of ions.

The activation energy value obtained in the work is similar as reported by Asmara et al. 2011. As can be observed in Figure 4.17, the value of E_a decreased as the conductivity of the samples increased, indicating that the ions in highly conducting samples need lower activation energy to have the migration of ions.

The decrement in E_a was due to the increasing density of ions in the sample with the increase in NH_4NO_3, hence the energy barrier of the ion transport decreased. Since the transportation of ions was affected by its segmental motion (Ramesh & Arof, 2000), the sample with a lower value of E_a applied rapid conduction of ions. This can be further explained with the presence of charge carriers that moved easily, leading to an increase in ionic conductivity (Sit et al, 2012). The value of E_a was low, which could be due to its amorphous nature that produced more free ions of H^+ in the SBEs system.
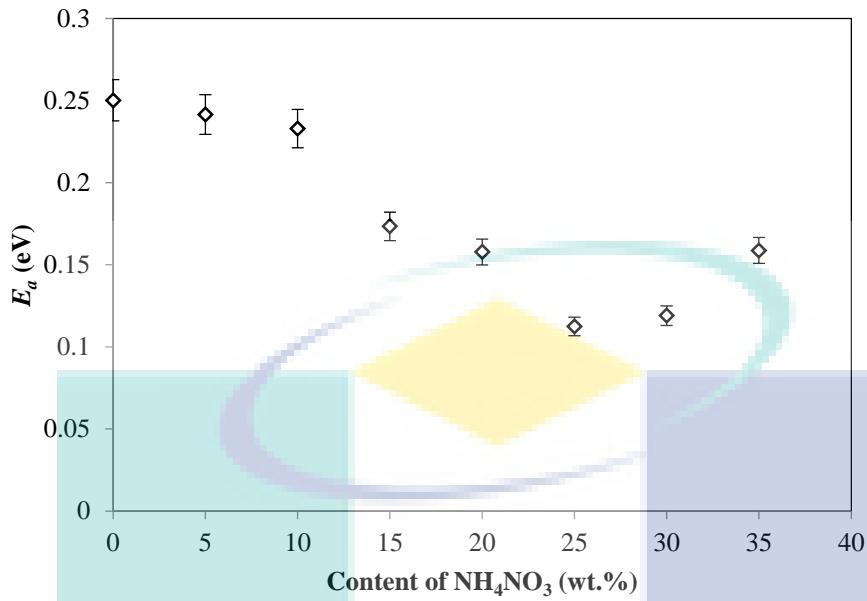
Figure 4.17   Activation energy (E_a) for SBEs system at different temperatures

4.5.4   Transport Properties Study

The transport parameter was determined by using the deconvolution of IR method using Origin Lab 8.0 analysis which can detect the free ions, contact ions, and what can influence the ionic conductivity (Kauppinen et al., 1981). The IR-spectra chosen in this work were between the range 1200–1500 cm^{-1} based on the obvious interaction occurring in this work as discussed in the FTIR analysis and were plotted as shown in Figure 4.18 (Aniskari & Isa, 2017; Hay & Myneni, 2007). This region was selected due to the appearance of functional group of carboxyl group as revealed from FTIR analysis. Based on this method, the determination of considerable peaks can be done, which may then be separated into free or contact ions. The peak consists of several overlapping bands that represent different ionic species, which are, free ions and contact ions. Thus, curve fitting is applied to separate or deconvolute envelope into individual component bands. The percentage of free ions, contact ions, ion pairs and ion aggregates are estimated from the area under the respective band. The free ions was calculated using equation as shown below:

$$\text{Percentage of free ions (\%)} = \left(\frac{A_f}{A_f + A_c} \right) \times 100\%$$ 4.9

where A_f is the area under the peak referring the free ions region, and A_c is the total area under the peak referring to the contact ions.
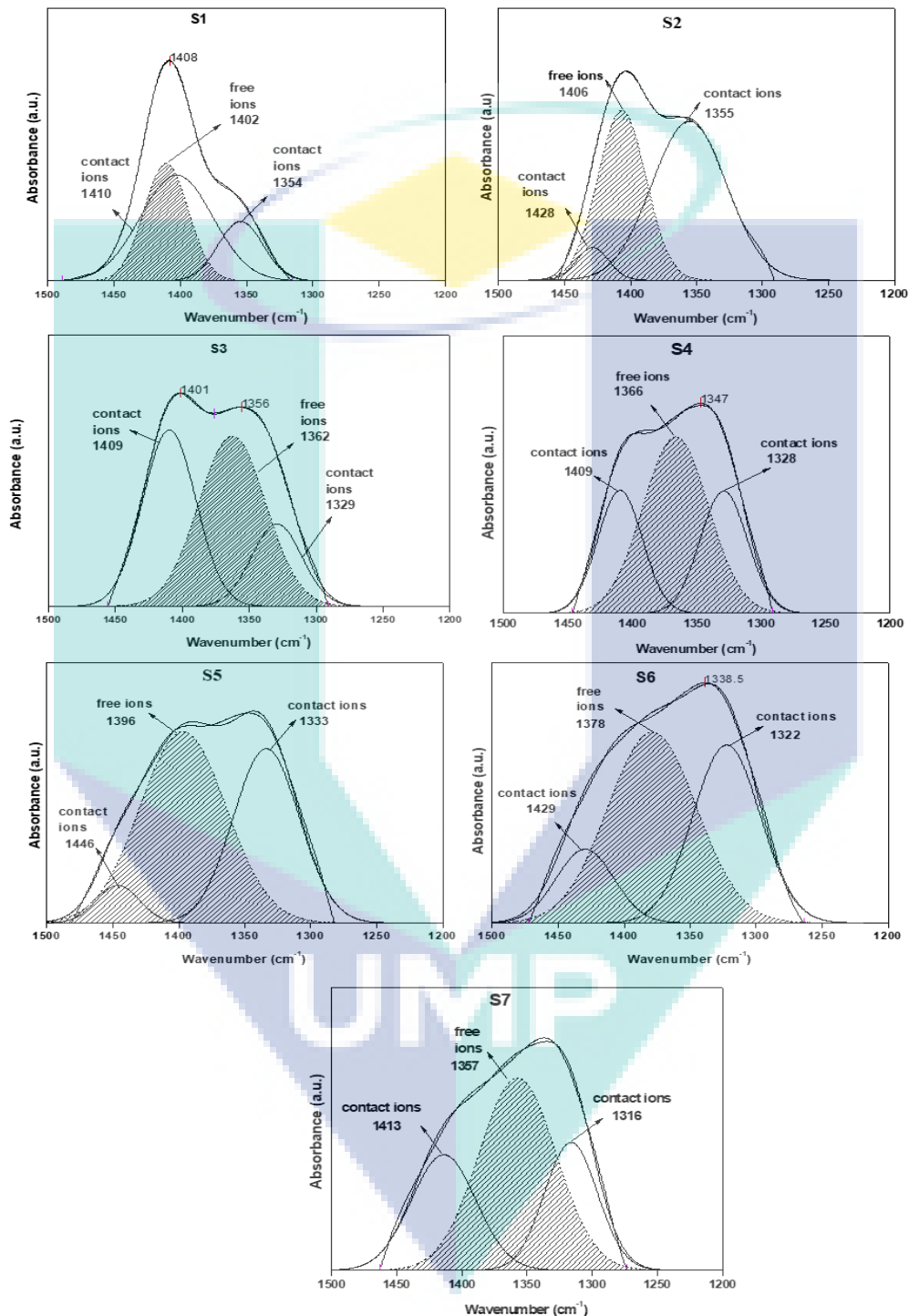
Figure 4.18   FTIR deconvolution of various sample of SBEs system

Based on Figure 4.18, the free ions indicated the free mobile ions ($\sim$1350 cm^{-1} to $\sim$1400 cm^{-1}), and the contact ion pairs ($\sim$1350 cm^{-1} to $\sim$1420 cm^{-1}) indicated the contact

ions and ion aggregates in the present system (Hafiza & Isa, 2017; Ramli & Isa, 2016; Rasali & Samsudin, 2018; Yap, 2012). The free and contact ions can be derived based on the total area from the deconvolution of the peaks, which is shown in Table 4.8. The table shows that the percentage of free ions increased as NH_4NO_3 was added until reached maximum value for sample S5. This occurrence was due to the increase of ion dissociation between H^+ substructures of NH_4^+, which caused more ion conduction that led to the improvement of the ionic conductivity in the SBEs system. According by (Hema et al., 2010), it is due to the increment in number of mobile charge carriers and also the increment in amorphous nature of the polymer electrolyte which decreases the energy barrier thereby facilitating the fast ion transport.

Table 4.8   Percentage of free ions and contact ions in SBEs system

Sample	Free ions (%)	Contact ions (%)
S1	33.39	66.61
S2	38.77	61.23
S3	45.78	54.22
S4	50.67	49.33
S5	55.68	44.32
S6	51.06	48.94
S7	50.95	49.05

It was observed in Table 4.8 that the percentage of free ions in this work increased until S5. This may be due to the dissociation of ions that led to an increase in the conduction of ions. For the addition of salt up to 25 wt.% of NH_4NO_3 (S6 and S7), the free ions were observed to decrease, which can be related to the result of ionic conductivity at room temperature, giving a decrement with content beyond 25 wt.% of NH_4NO_3. The value of free ions decreased due to the association of ions, similar to the work by Rahaman et al. (2014). Thus, it can be concluded that the free ions increased as ionic conductivity increased. . This may be due to the influence of ion pairs and ion aggregation leading to the formation of ion clusters, thus decreasing the number of mobile charge carriers and the overall mobility (Hema et al., 2010).

Since the area of the de-convoluted peaks was selected, the transport parameters in this system, namely the number of ions (η), the mobility of ions (μ), and diffusion coefficient (D), were determined and calculated using the following equations (Rahaman et al., 2014):

$$\eta = \left(\frac{M \times N_A}{V_{total}}\right) \times \text{free ions (\%)} \qquad 4.10$$

$$\mu = \frac{\sigma}{\eta e} \qquad 4.11$$

$$D = \left(\frac{kT\mu}{e}\right) \qquad 4.12$$

where M is the number of moles of salt used in the present work, $N_A = 6.02 \times 10^{23}$ mol^{-1}) is the Avogadro's number, V_{total} is the total volume of the SBEs sample, $e = 1.6 \times 10^{-19}$, C is the electric charge, $k = 1.38 \times 10^{-23}$m^2 kg s^{-2}, K^{-1}/JK^{-1} is the Boltzmann constant, and T is the absolute temperature in Kelvin.

Based on the data presented in Table 4.8, the transport parameter were calculated using equations 4.10 to 4.12 and presented in Figure 4.19. From the percentage of free ions obtained in the FTIR deconvolution, the number density (η), ionic mobility (μ), and diffusion coefficient (D), of charges carriers can be determined.

Based on the figure 4.19, the result of the transport properties shows that the number of ions (η) increased gradually with the addition in salt, while the mobility of ions (μ) and the diffusion coefficient (D) were aligned to the ionic conductivity pattern. The pattern of η values increased continuously with the increase in NH_4NO_3 and can be related to the gradual increment in the percentage of free ions in the system. When the sample became more amorphous, the free ions of H$^+$ moved easily and complexed with COO$^-$ of alginate more rapidly, hence increasing the ionic conductivity along with transport properties until the highest conductivity was achieved.

As the salt increased to more than 25 wt.% of NH_4NO_3, the value of η kept increasing. In contrast, μ and D were found to decrease. This phenomenon conveys that the SBEs system was overcrowded with the formation of more ions (H$^+$) and needed enormous amount of the activation energy, E_a, to migrate the ions and hence, the diffusion of ions decreased (Chai et al., 2013; Ramesh & Ng, 2009).
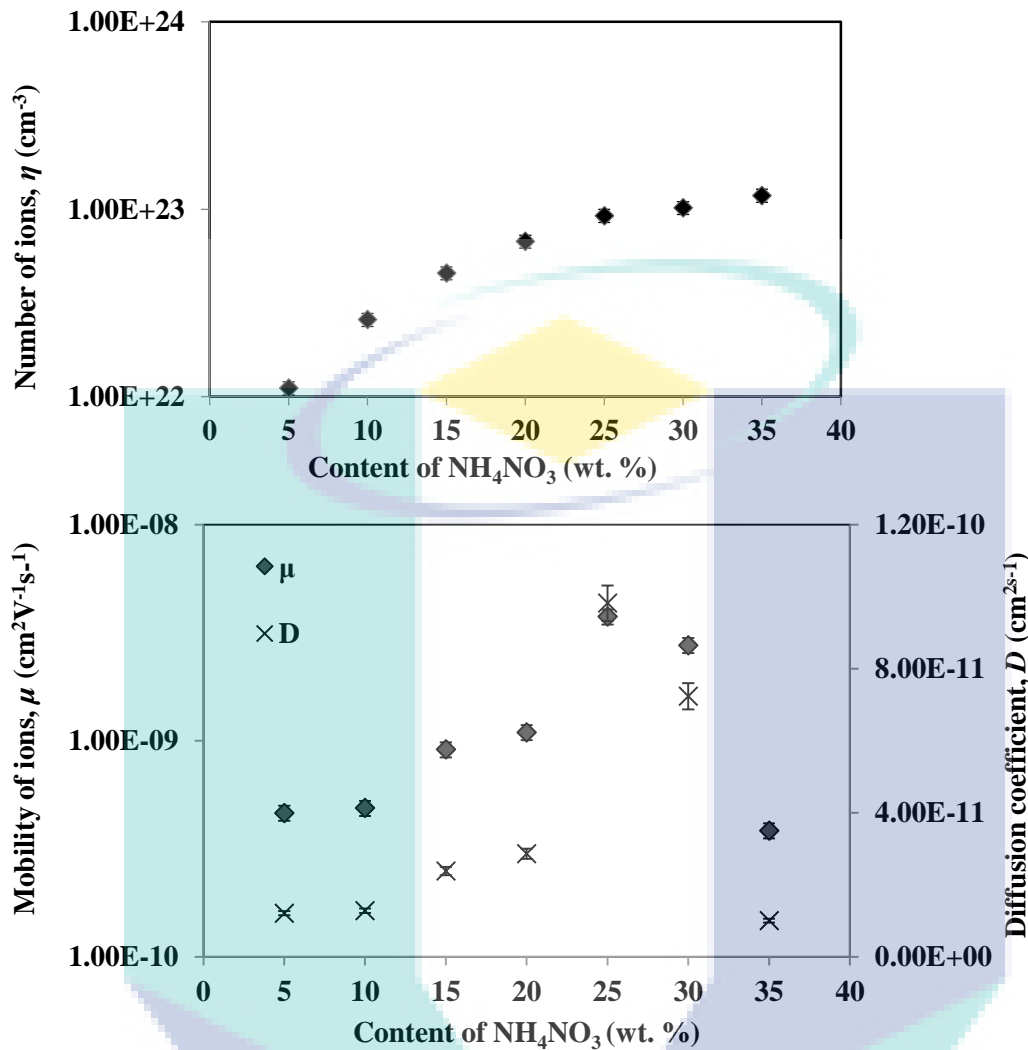
Figure 4.19   The transport parameters of the alginate–NH_4NO_3 SBEs system

Besides, the result of the XRD analysis suggests that the pathways for ions to jump into other vacant sites were difficult due to the presence of the crystal peak for samples S6. It can be explained by the blocking site for the transition of ions created by the crystalline phase in the SBEs system. Thus, it resulted in a decrement in three factors: mobility, diffusion, and ionic conductivity. This behaviour was found in other works of the SBEs system (Samsudin & Isa, 2012; Shuhaimi et al., 2010).

4.5.5   Electrical properties

The dielectric properties were studied to understand more about the conduction mechanism of the SBEs system (Ravi et al., 2015). The study also covers the electrical/dielectric behavior based on the frequency and temperature of the sample

(Halder et al., 2018). The electrical modulus formalism has been extensively used to study electrical relaxation behavior in ion conducting materials (Macedo et al., 1972). The advantage of this plot is that the electrode polarization effects are reduced in this formalism.

4.5.5.1 Dielectric constant ε_r and dielectric loss ε_i

The dielectric constant, ε_r, for the alginate–NH_4NO_3 SBEs system at room temperature is indicated in Figure 4.20. Figure 4.20 depicts ε_r at a lower frequency with the addition of up to 25 wt.% of NH_4NO_3, and this pattern was detected to follow the ionic conductivity pattern. As the NH_4NO_3 increased, the amount of stored charge also increased, implying that there was an increment in the number of mobile ions, which caused the asymptotic rise in ε_r. ε_r continued to show a decrement and became saturated at a higher frequency as witnessed in Figure 4.20 (Ganea, 2012; Woo et al., 2013; Majid & Arof, 2005; Saroj & Singh, 2012).
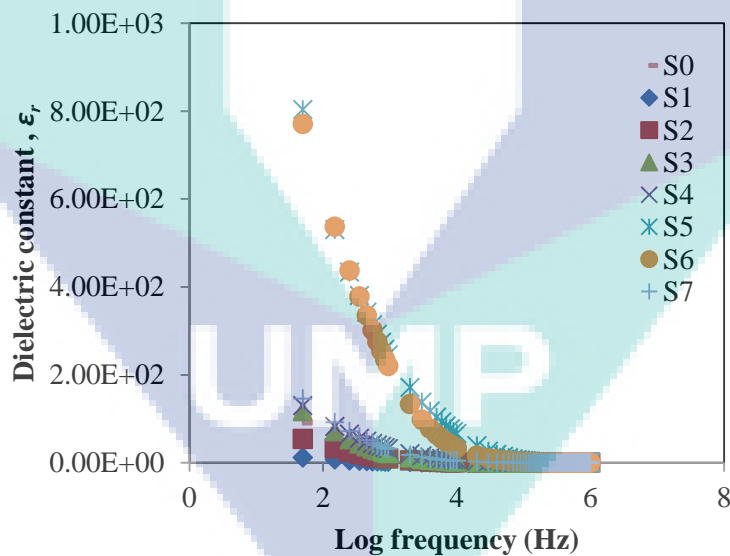
Figure 4.20   Dielectric constant of SBEs system at ambient temperature

Based on Figure 4.20, at higher frequency part, the electric field orientation, acting on the medium occurs so quickly and there is no time for ion diffusion thru the medium following the direction of the electric field. It can be noted that the polarization due to the charge accumulation decreases and so does the ε_r values.

Meanwhile, Figure 4.21 shows the plot of ε_r for entire contents at various temperatures. It can be observed that the value of ε_r increased as the temperature increased. As the temperature increased, the degree of salt dissociation and redissociation of ion aggregation also increased, resulting in the increasing number of free ions of H^+ or charge carrier density and thus leading to the increment in the ε_r value. Majid and Arof (2007) stated that charge build-up at the boundary would be suppressed at high frequency.
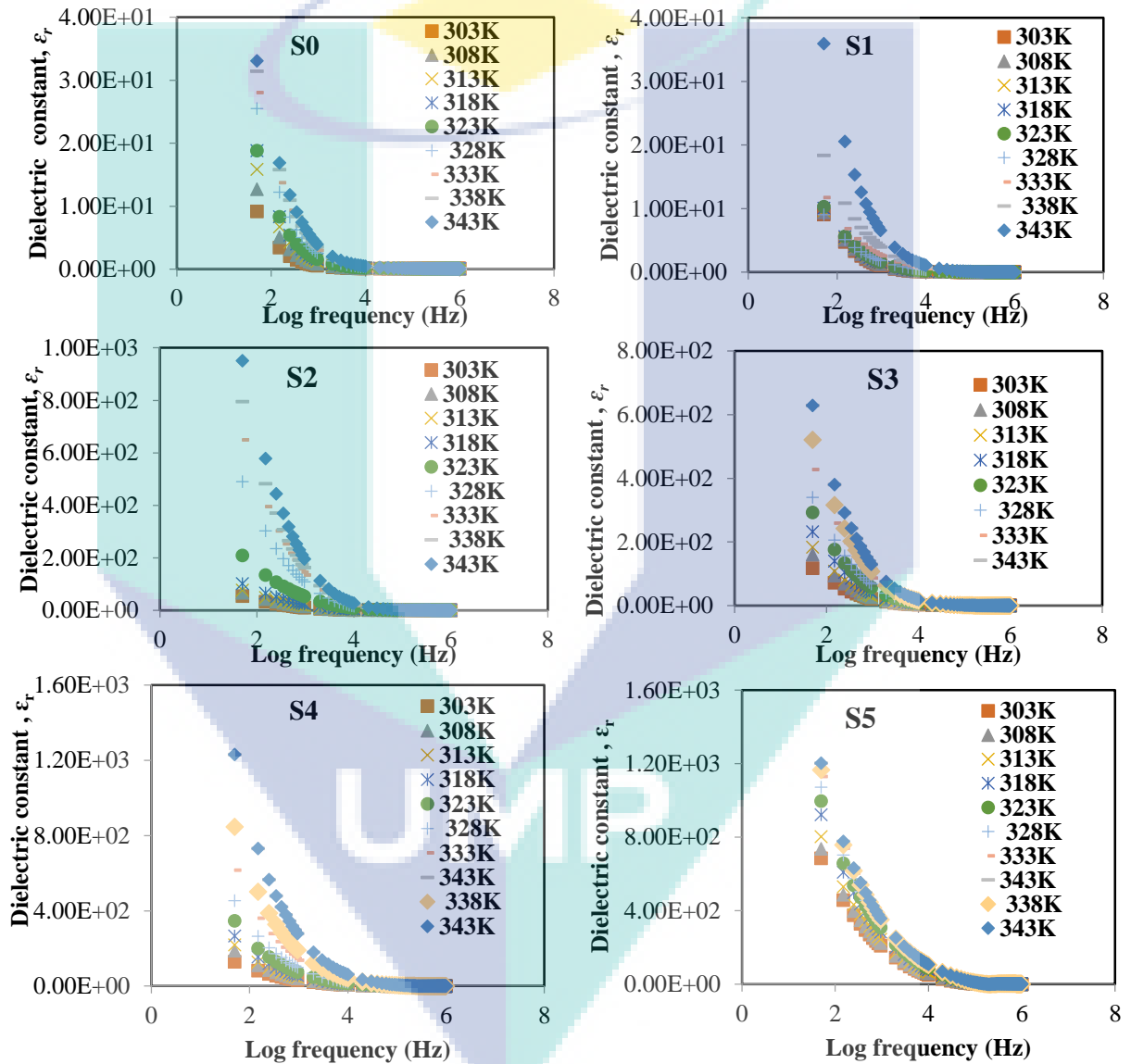
Figure 4.21   Dielectric constant of entire contents of SBEs system at various temperatures
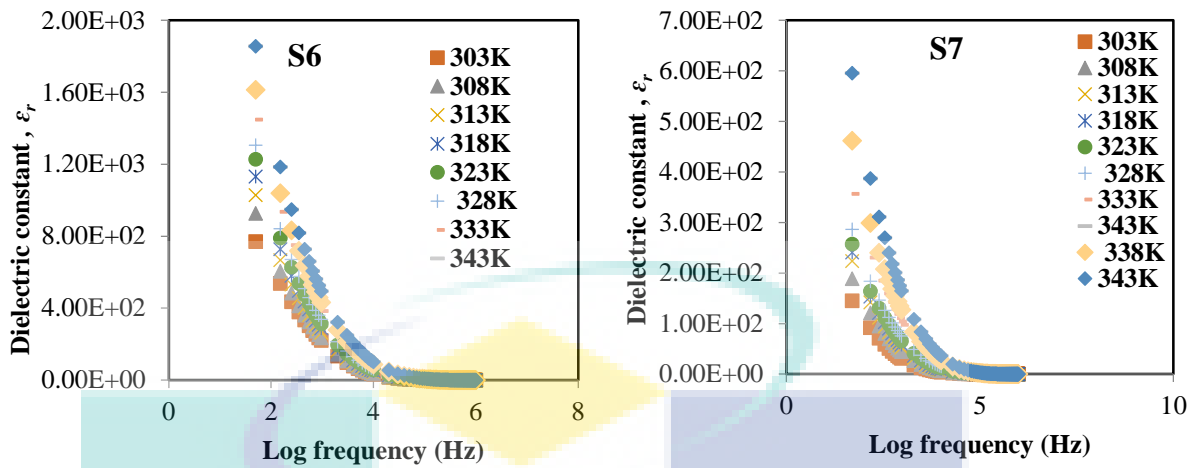
Figure 4.21   Continued

This led to the enhancement in ionic conductivity as the value of ε_r increased for all samples in this work. Moreover, the absence of the relaxation plot strengthened this work study. It could be due to the easy movement of ions because of the increment in the amorphous nature in this work and the flexibility of the backbones from alginate as confirmed in the XRD analysis (Kulshrestha et al., 2014).

Besides, with increasing frequency during the investigation, there was no time for charge build-up at the interface because of the increasing rate of reversal of the electric field. Thus, the polarization due to charge accumulation decreased because of the decrement in the value of ε_r (Molak et al., 2005; Shafee, 1996).

The plot in Figure 4.22 depicts the dielectric loss, ε_i for the all samples of the alginate– NH_4NO_3 SBEs system at room temperature. From the plot, it can be seen that ε_i increased with the increment of NH_4NO_3 content at lower frequency in room temperature. At lower frequency, the value of ε_i increased due to no charge movement through the samples and the increase in mobility of the charge carrier in the electrolytes system (Hasan & Nasir, 2015).

The value of ε_i decreased through the increment in frequency due to the fast rate occurring in the electric field that led to the decrement in ionic conductivity. On the other hand, Figure 4.23 presents ε_i for all contents of the SBEs system at various temperatures.
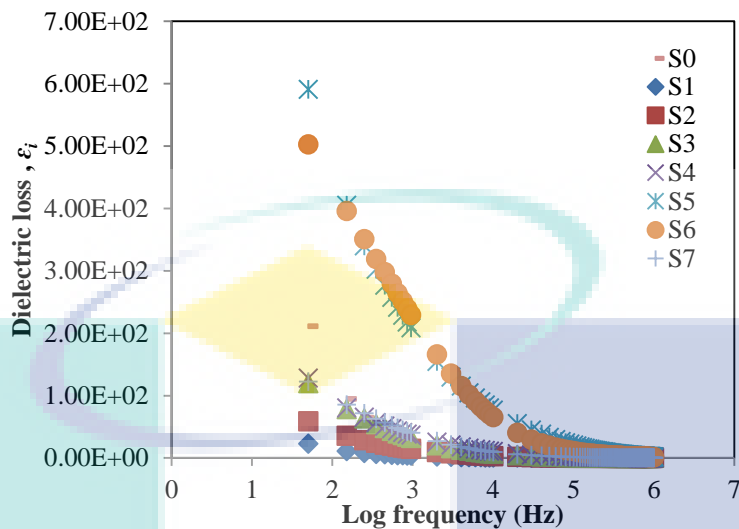
Figure 4.22   Dielectric loss of entire contents of SBEs system at room temperature

Based on the plot of ε_r and ε_i, it can be said that both of the plots gave the same characteristics for all samples. A sudden increase of ε_r and ε_i at low frequency and high temperature was observed, which can be attributed to the anode and cathode polarity effects (Shasty & Rao, 1991) in the SBEs system. At high frequency, the periodic reversal of the electric field occurred rapidly as there was no excess ion diffusion in the path of the field (Baskaran et al., 2006a; Ramesh et al., 2007). Baskaran et al. (2006a) stated that charge build-up at the boundary would be suppressed at high frequency. The polarization due to the charge accumulation decreased, which lowered the value of the real and imaginary parts of ε_r (Baskaran et al., 2006a). This characteristic indicates non-Debye characteristics with no single relaxation time.
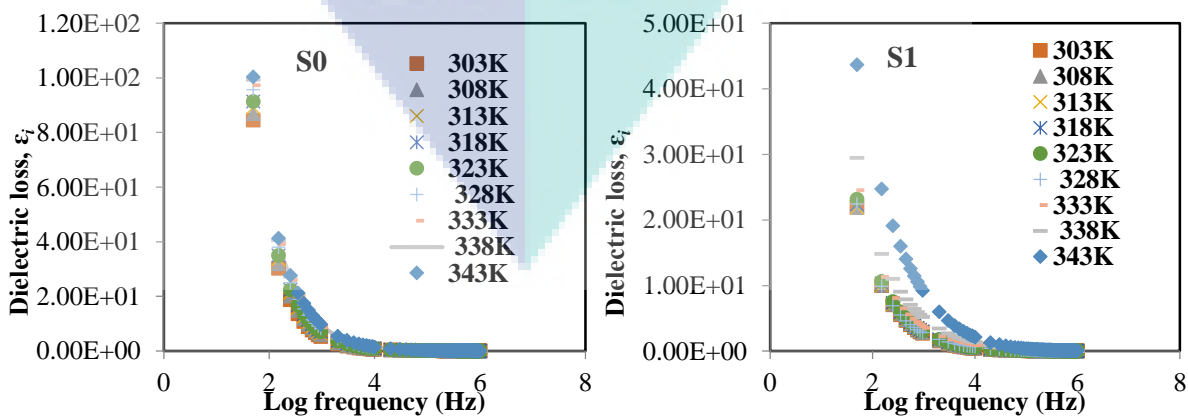
Figure 4.23   Dielectric loss of SBEs system at various temperature
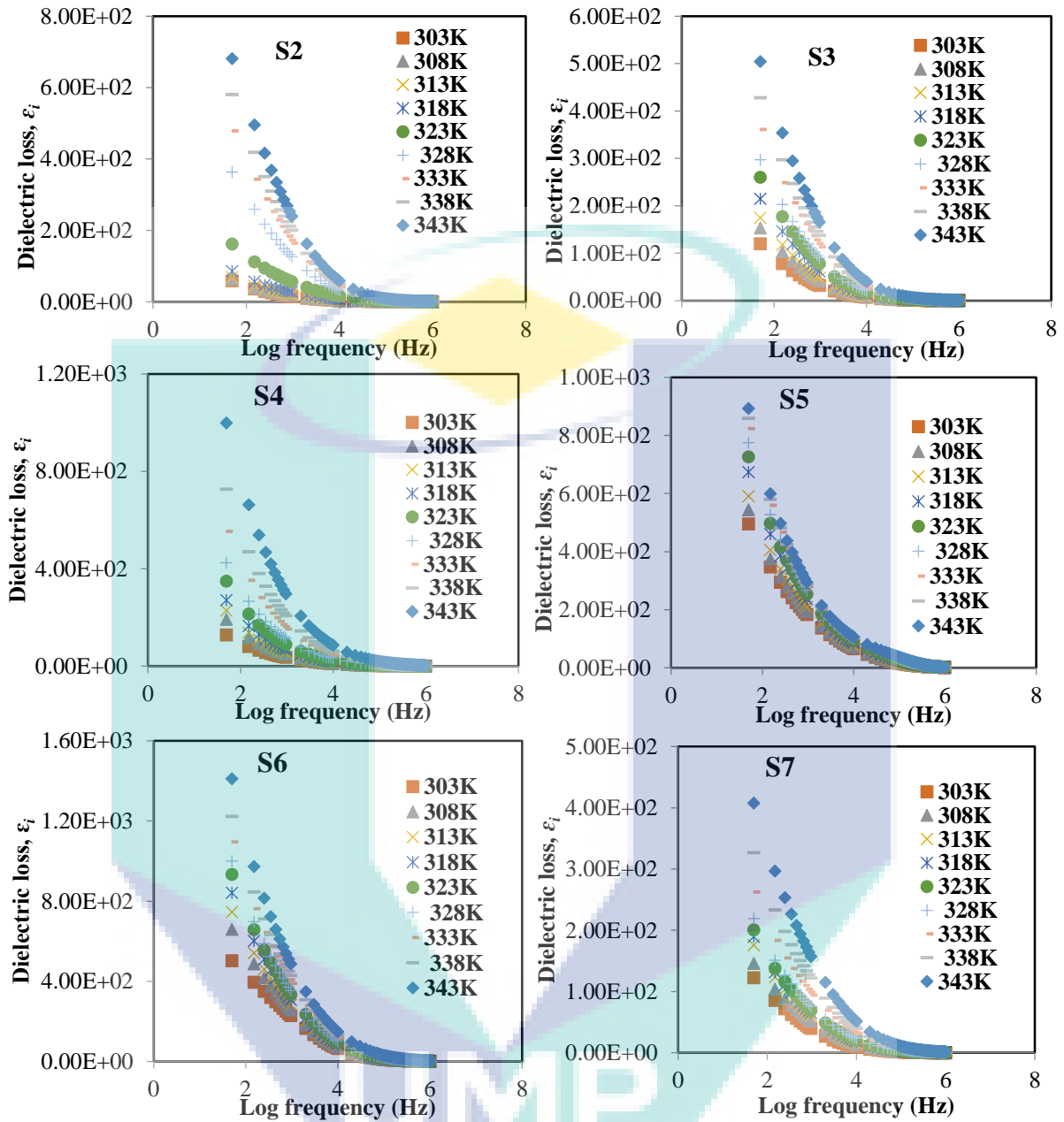
Figure 4.23   Continued

4.5.5.2   Real Modulus and Imaginary Modulus, M_i

The complex electric modulus (M*) is used to investigate the conductivity relaxation phenomenon. It is also needed to suppress the effects of electrode polarization and bulk dielectric properties of the SBEs system. Figure 4.24 presents the real part of $M*$ for the alginate–NH$_4$NO$_3$ SBEs system at room temperature. From Figure 4.24, it can be observed that the real modulus, M_r, increased as frequency increased. At a lower

frequency, the plot approached zero due to electrode polarization (Mishra & Rao, 1998; Pradhan et al., 2008).
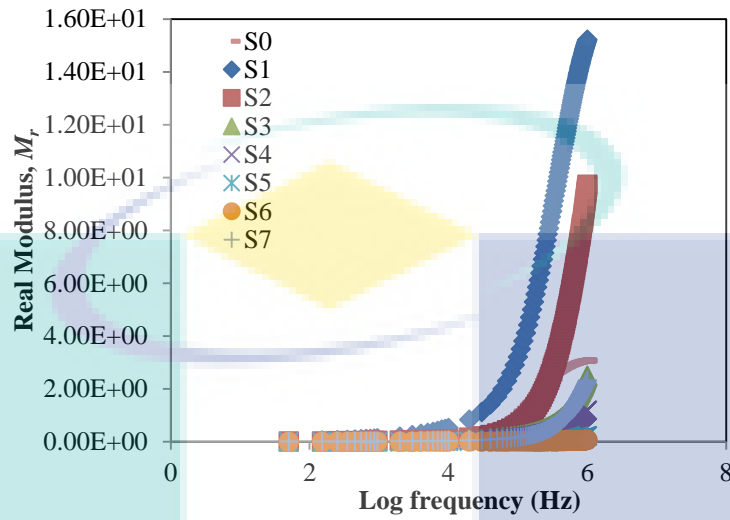
Figure 4.24   The real modulus of SBEs system at room temperature

As frequency increased, the value of M_r also increased until it reached the maximum constant value for all temperatures in the electrolyte system as shown in Figure 4.25.
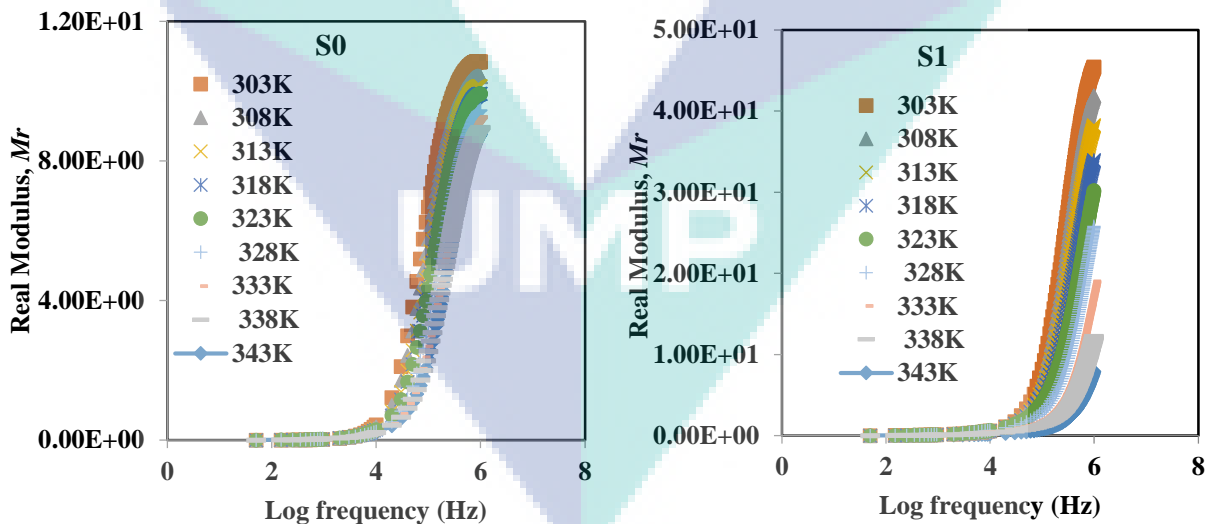
Figure 4.25   Real modulus study of entire contents in *wt*.% at various temperature
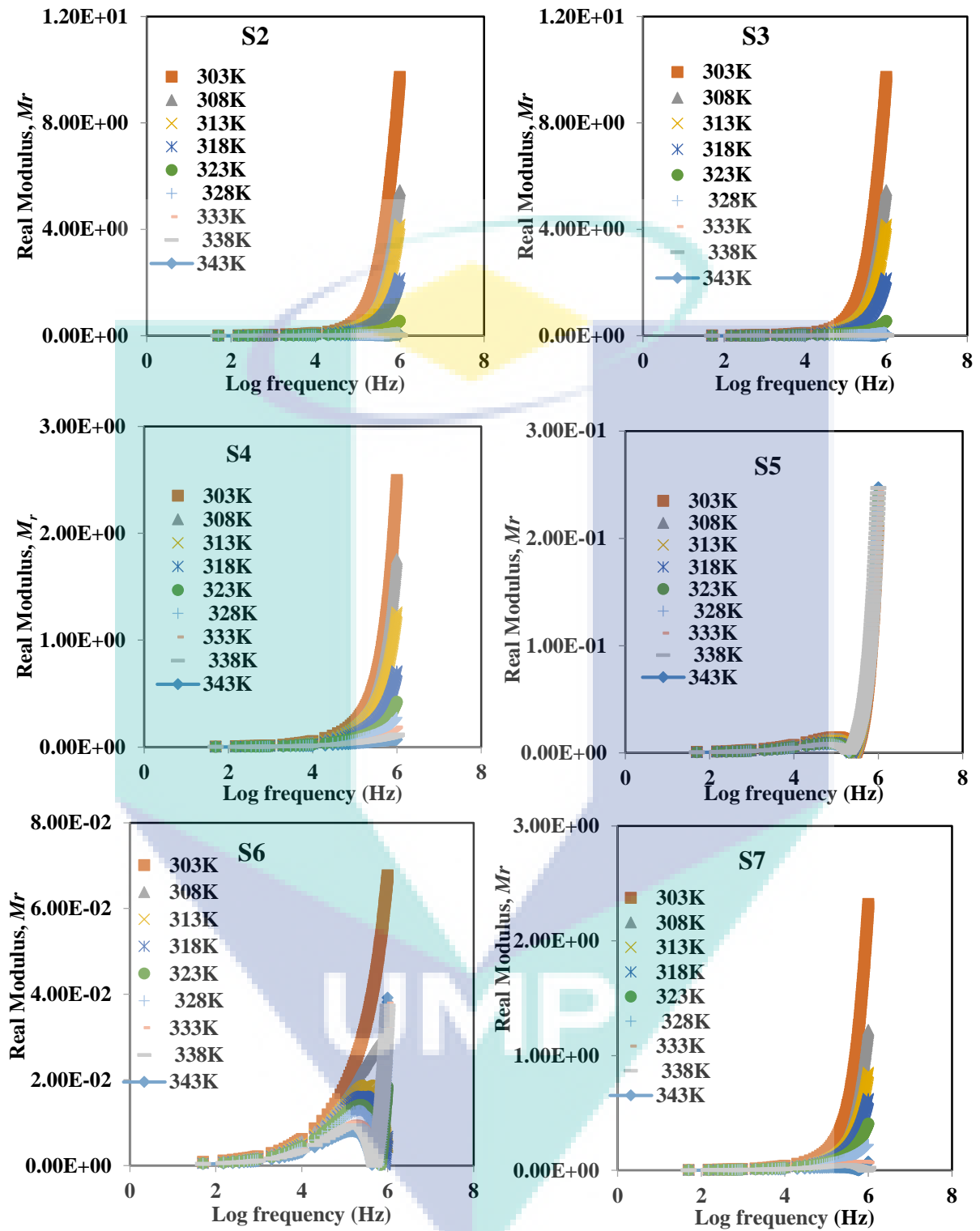
Figure 4.25   Continued

Based on Figure 4.25, the value of the real part modulus has reached a constant value at high frequencies, and it approached zero at low frequencies suggesting that the interfacial effect tends to be eliminated in modulus representation (Migahed et al., 1996).

Figure 4.26 presents the plot of the imaginary modulus, M_i, for entire contents of the SBEs system at various temperatures. From Figure 4.26, it can be observed that M_i increased proportionally to the increment in frequency. According to Ramesh et al., (2011), when M_i is approaching zero in the low frequency region, the anode and cathode polarity phenomena are negligible. The slope of each plot for the imaginary electrical modulus exhibited a long tail extending into the region of longer relaxation time
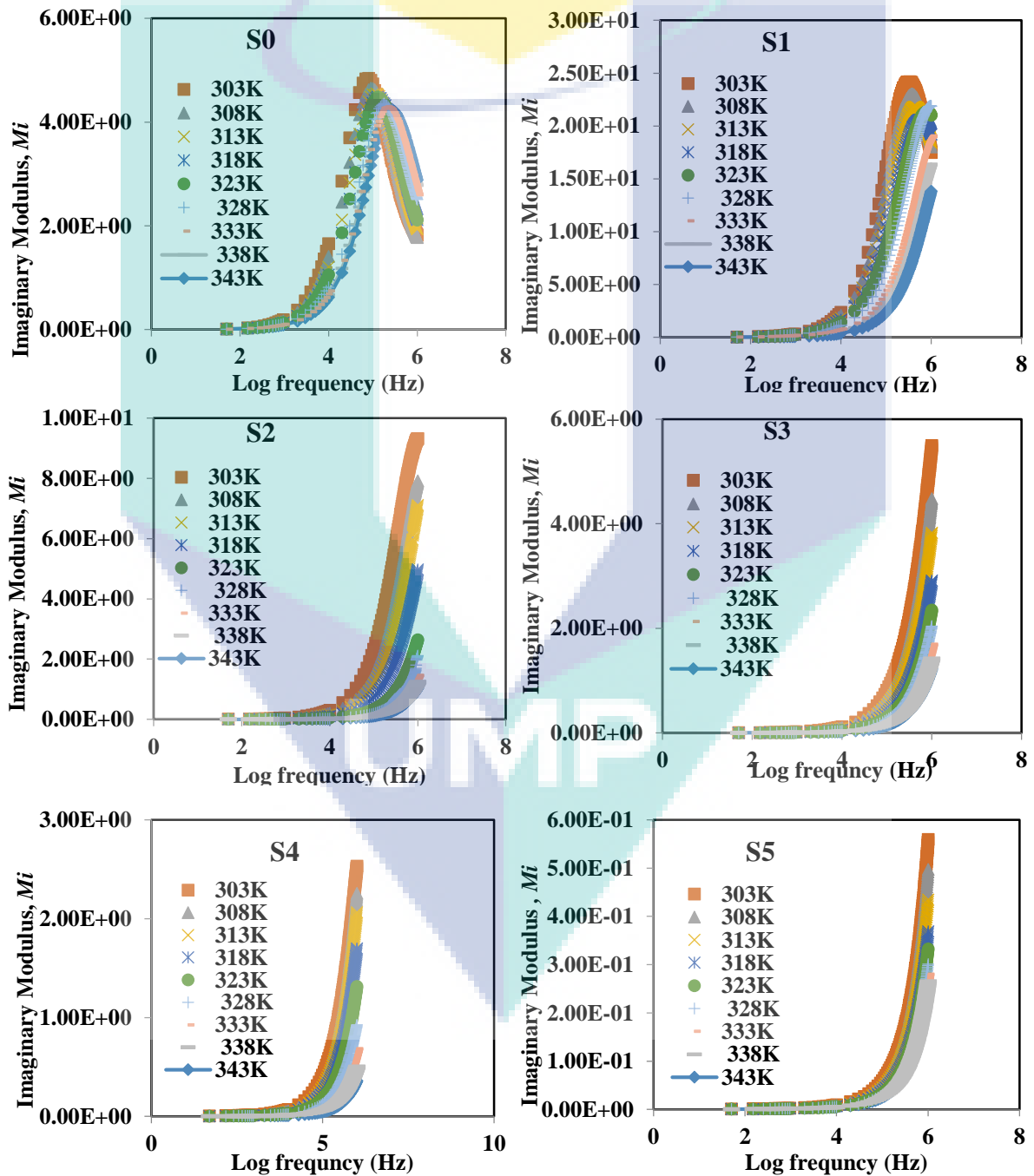
Figure 4.26   Imaginary Modulus study of entire contents in *wt*.% various temperature
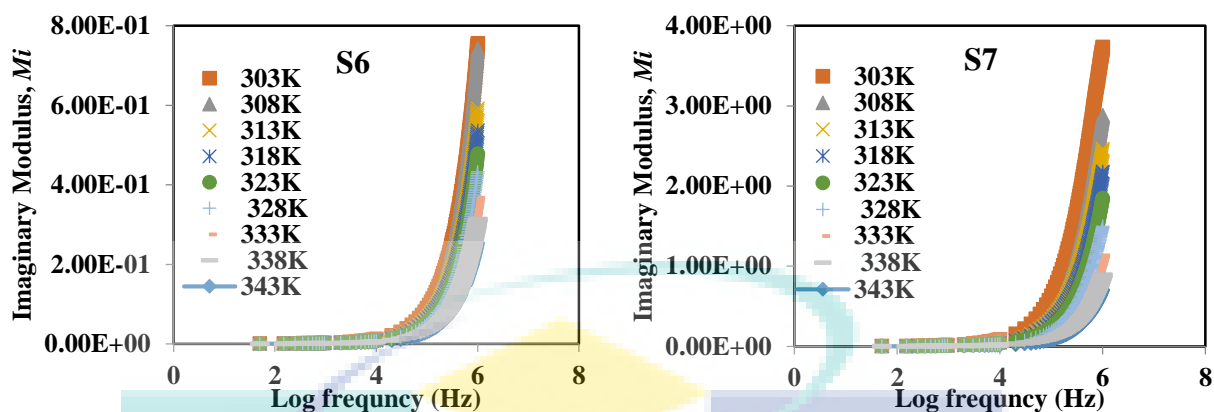
Figure 4.26   Continued

These plots imply that the asymptotic peak shifted to the higher frequency region as temperature increased. These show that the entire samples were highly capacitive and suggest excellent electrochemical stability (Suthanthiraraj et al., 2009). The relaxation peak did not appear in the plot, indicating that the plot was more intense at the high frequency region. The curve peaks imply the bulk effect in the SBEs and further conclude that the SBEs are an ionic conducting mechanism.

4.5.6   AC Conduction Properties of Alginate-NH₄NO₃ SBEs system

In this present research, the ion movements in the SBEs system need to be understood in order to identify the theoretical hopping mechanism or the physical conduction model for the interaction in the alginate-NH_4NO_3 SBEs system. The appropriate model for the conduction mechanism depends on the conduction mechanism of ac conductivity with s (T) characteristics. Besides, one material can be categorized by two or more different conduction mechanisms in different temperature ranges (Kahouli et al., 2012). The value of the exponent *s* can be achieved from the slope of ln ε against ln ω, where no or minimal space charge polarization occurred at this acceptable frequency range of $12.0 < \ln \omega < 14$ (Buraidah et al., 2009).

According to Buraidah et al. (2009), the lower electrode polarization nearest to zero in the higher frequency region was due to less time needed for the electric field to change at a fast rate. In the literature, the conduction models were developed to convey the characteristic of the conduction of model by exponent *s*, namely the quantum mechanical tunneling (QMT) model, the small polaron hopping (SPH), the correlated

barrier hopping (CBH) model, and the overlapping large-polaron tunneling (OLPT) model, which was determined using the logarithm rule in the following equation (Khiar & Arof, 2011; Rani et al. 2015).

Furthermore, the temperature dependence of *s* is very useful to confirm the AC conduction mechanism in various types of materials (Elliott & Philos, 1977; Pike, 1978). As reported in earlier studies, many theoretical models for ac conductivity have been developed to explain the temperature dependence of *s*. The electron tunneling model suggests that *s* is not influenced by temperature but depends on frequency. The value of *s* increases in the case of small polaron tunneling, whereas for the large polaron tunneling process, *s* decreases up to a certain temperature and then increases with a further increase in temperature (Elliott, 1978).

The ac conductivity can be found from dielectric loss, ε_i at every frequency with using equation:

$$\sigma_{ac} = \varepsilon_i \varepsilon_o \omega \qquad\qquad 4.13$$

The occurrence of ac conductivity can be determined using Jonscher's Universal Power Law (UPL) (Winie and Arof, 2004).

$$\sigma_\omega = \sigma_{dc} + A\omega^s \qquad\qquad 4.14$$

$$\sigma_{ac} = A\omega^s \qquad\qquad 4.15$$

Here, $\sigma(\omega)$ is the total dc and ac conductivity. The dc conductivity, σ_{dc} is the frequency independent component, *A* is a parameter dependent on temperature and *s* is the power law exponent with value in the range between 0 and 1. In the literature, the conduction models were developed to convey the characteristic of the conduction of model by exponent *s*, namely the quantum mechanical tunneling (QMT) model, the small polaron hopping (SPH), the correlated barrier hopping (CBH) model, and the overlapping large-polaron tunneling (OLPT) model. The value of *s* can be expressed by the relation of (Khiar & Arof, 2011; Misenan et al., 2018; Rani et al. 2015; Samsudin & Isa, 2012):

$$\ln \varepsilon_i = \ln \frac{A}{\varepsilon_o} + (s\text{-}1)\ln \omega \qquad\qquad 4.16$$

To determine precisely the predominant conduction process under the alternating current (AC) field for the studied device, different theoretical models have been proposed. One such model, the OLPT model, was proposed by Chakchouk et al., (2017), Rosli et al., (2012), and Navaratnam et al., (2015). In their work, the OLPT model implied that the exponent s decreased with increasing temperature to a minimum value at a certain temperature and then began to increase with increasing temperature. Therefore, the OLPT conduction mechanism is not applicable to the obtained results. In the non-overlapping small polaron hopping (SPH) conduction mechanism, the exponent s increases with increasing temperature. In the SPH model, a conduction electron localizes at a site in the system, and lattice distortion is present which can be stable at the localized electron (Khan et al., 2011). Due to thermal motion, this electron migrates from site to site via a hopping mechanism. The small polarons are produced when the strong electron–phonon reacts adequately in these structures. This model was used by Holstein to confirm whether the polaron is diabatic or non-diabatic.

According to Samsudin and Isa (2012), the SPH model can be explained by the difference of the index s with the temperature at the formation of the charge carrier, which results in the large degree of local lattice distortion. They believed that the small polarons are localized to ensure their distortion clouds do not infringe so that the jumping energy does not depend on intersite separation. This SPH model was also used by Jung (2002), Chai and Isa (2012), and Buraidah et al. (2009) for other electrolyte systems. In the QMT conduction mechanism, the exponent s is almost equal to 0.8 and increases slightly with increasing temperature or is independent of temperature (Mansor et al., 2010). According to Shukur et al. (2013), the ionic hopping between two points occurs not only by jumping over a barrier but can also be accompanied by QMT. Other similar works following the QMT model include Hafiza and Isa (2014), Isa and Samsuddin (2013), and Shukur et al. (2013). Therefore, the OLPT, SPH, and QMT conduction mechanism are also not applicable to the obtained results.

Figure 4.27 shows the plot of frequency against dielectric loss, ε_i, at an elevated temperature for the sample with the highest conductivity, 25 wt.% of NH_4NO_3 (S5). The sample of S5 was chosen to classify the theoretical hopping mechanism or physical conduction model of alginate–NH_4NO_3 SBEs system due to the sample is most conducting and good thermal stability sample compared to other samples. Furthermore, sample S5 was the most amorphous sample and it is considered being an almost disordered ionic conductor (Shujahadeen, 2012).
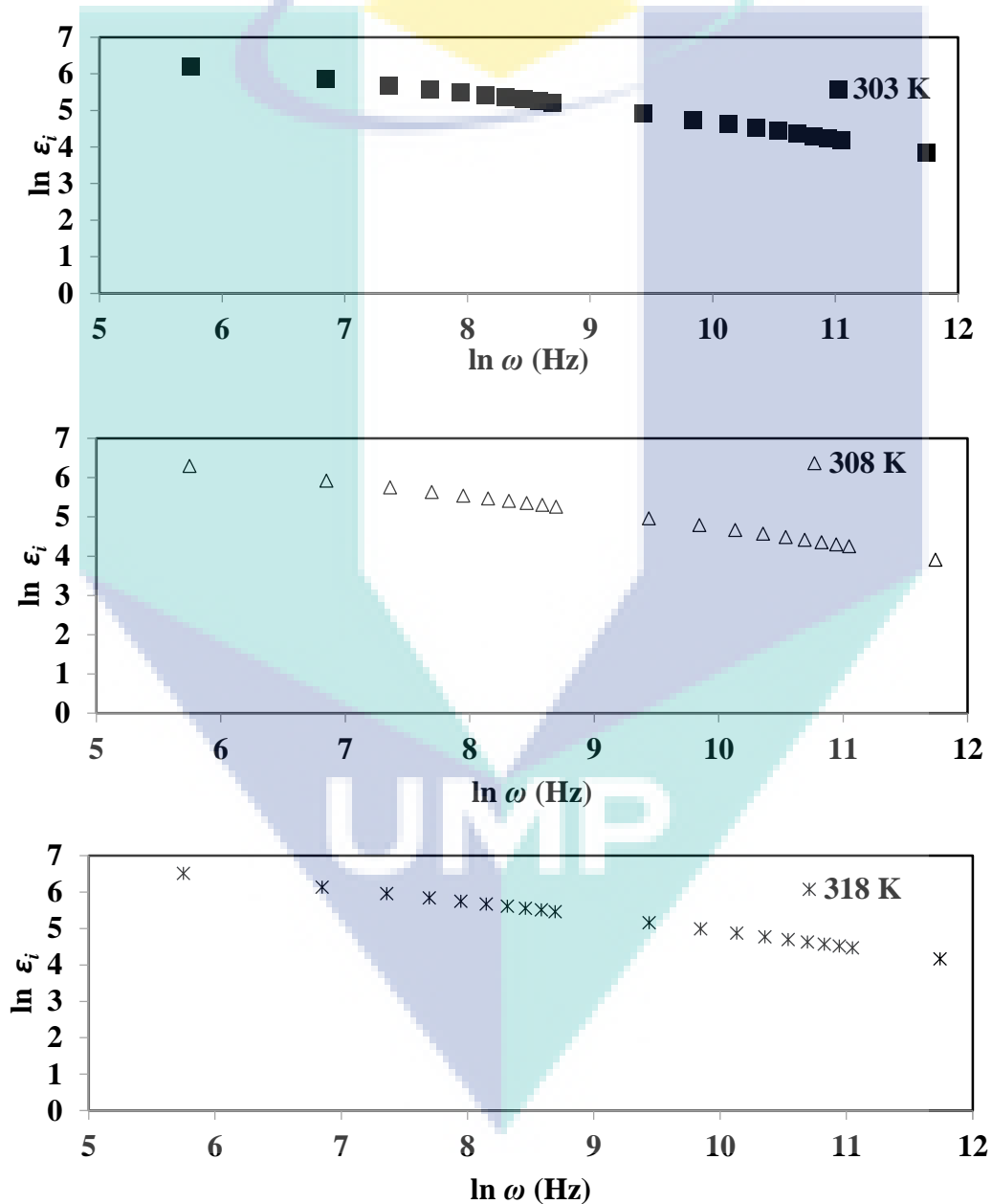
Figure 4.27   Plot of ln ε_i against ln ω for 25 wt.% of NH_4NO_3 at various temperatures (sample S5)
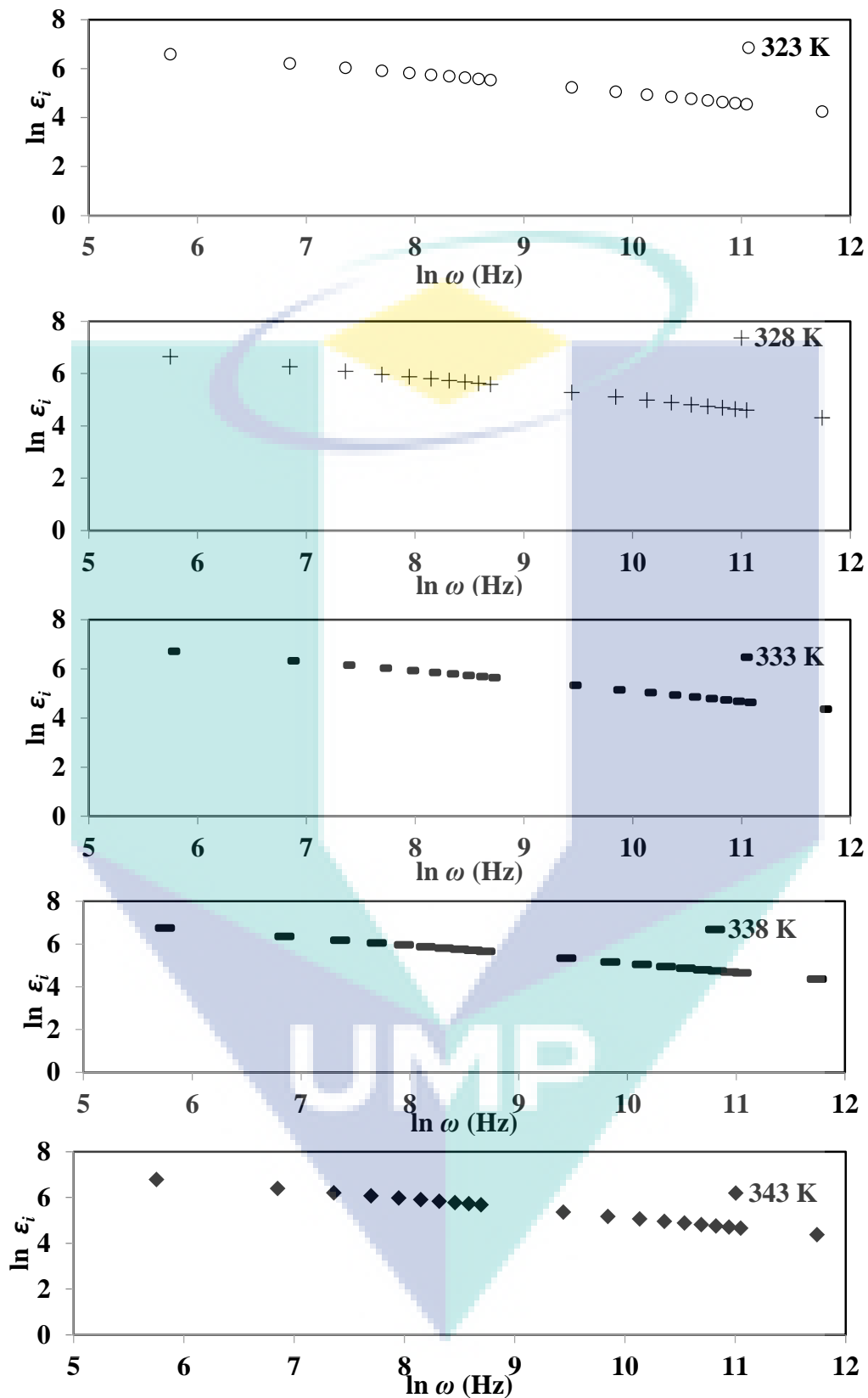
Figure 4. 27   Continued

It can be observed from Figure 4.27 that the value of *s* is independent of the

increase in temperature at selected frequency range is between (5 < ln ω < 12). The value of s can be determined at a higher frequency of the slope. Other researchers claimed that the value of s is obtained due to the negligible or less space charge polarization effect (Buraidah et al., 2009; Khiar & Arof, 2011).

The plot of s against temperature is shown in Figure 4.28. From the figure, it is clear that the value of s decreased as the temperature increased and can be best presented by the equation s = -0.0007T + 0.8451, shown a negative gradient in the plot. It suggesting that the correlated barrier-hopping (CBH) conduction mechanism model is applicable in this system. The exponent s has values between 0 and 1 (Dyre, 1988). In this present research, the results of the temperature dependence of s gave the range of values (0.59–0.63).

The CBH model is proposed by Pike (1972) and developed by Elliot (1977). According to (Farid et al., 2005), the concept of CBH is based on ion hopping between two charge-defect states over the barrier separating them. The correlated barrier-hopping (CBH) model has been widely used to semiconducting materials (Sahu et al., 2013). According to this mechanism, the conduction occurred via a bipolaron hopping process where ions were assumed to be surrounded by a Columbic interaction that occurred between many ions and a potential well. When the ions had enough energy, they jumped from one site to another. The hops were thermally activated (Buraidah et al., 2009). Other similar works following the CBH model include Ajili et al., (2018) and Kahouli et al., (2012).
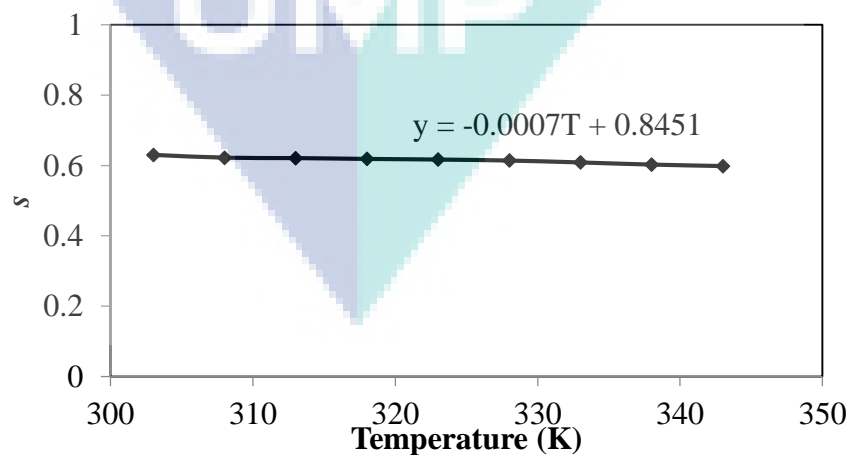
Figure 4.28   Plot of s against temperature for 25 wt.% of NH_4NO_3

4.6   Transference Number Measurement (TNM)

Transference number measurements (TNM) are presented to reveal a correlation between the diffusion of the ion and the conductivity behavior of alginate-NH_4NO_3 SBEs was calculated from DC polarize method (Pushpamalar et al., 2006; Samsudin et al., 2011). This technique defines the transmission mechanism of a sample whether cationic, anionic, or electronic in the electrolytes system. Figure 4.29 shows the plot of the normalized current against time, and Table 4.9 shows the list value of t_{ion}.
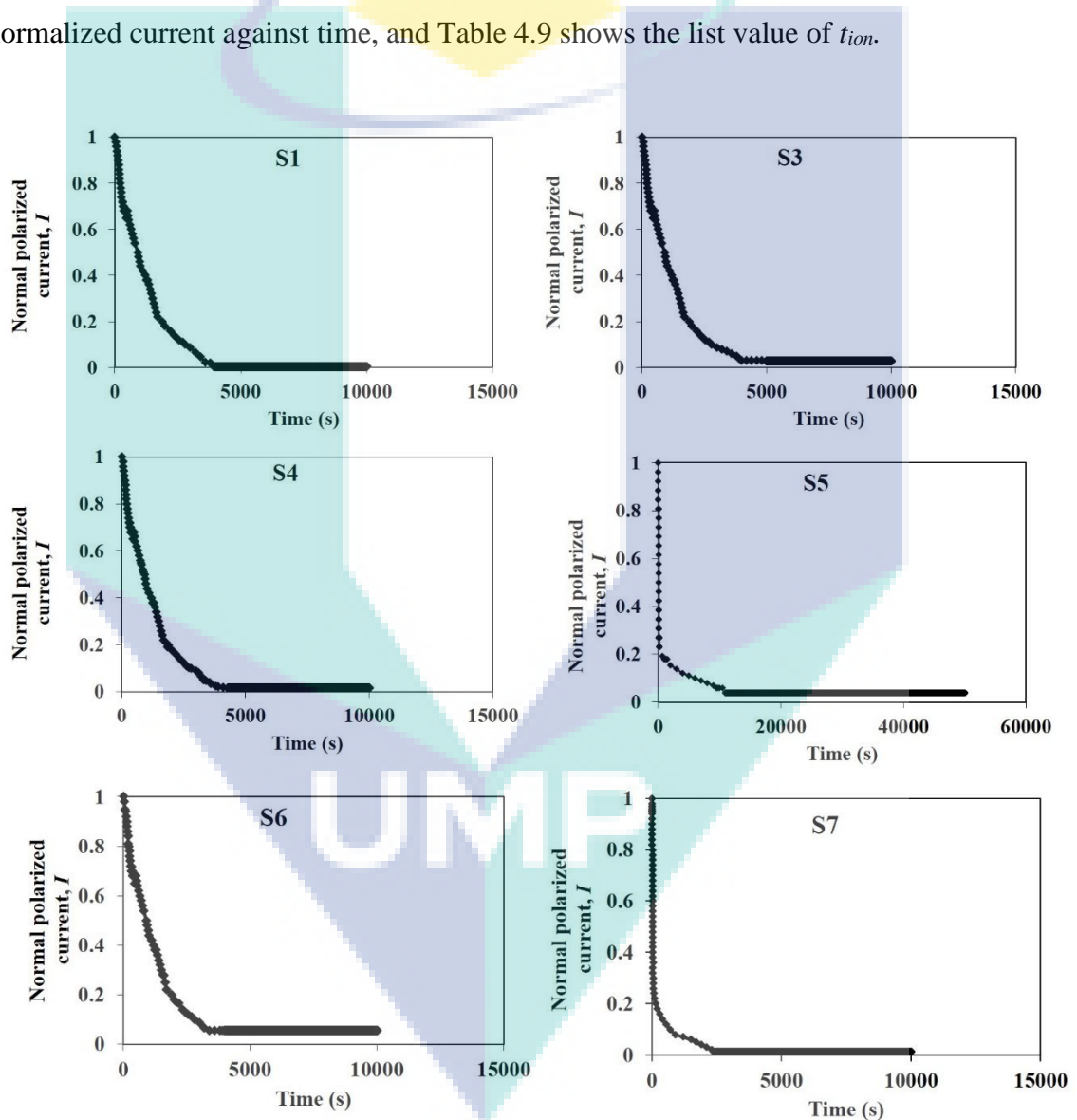
Figure 4.29   The plot of normalized current against time for alginate–NH_4NO_3

A steady state or constant current signifies that the electrolytes are ionic conductors (Woo, Majid, & Arof, 2012) where the cell is polarized and current flows due

to the electron movement between the electrolytes and surfaces (Monisha et al., 2017). The t_{ion} values were between 0.92 and 0.98, thus ions were the dominant conducting species. Other works on ammonium salt-based electrolytes reported the values of t_{ion} in the range of 0.91 to 0.98 (Shukur & Kadir, 2015; Vijaya et al., 2013).

As can be seen from Table 4.9, the highest conductivity sample, S5gave the t_{ion} value of 0.97. This result matched the conductivity result. This evidence shows that the conduction species for this present work were primarily cation. From the results, based on ionic mobility (μ) and diffusion coefficient (D) results, it showed that μ_+ and D_+ were higher than μ- and D-, implying that the samples were more cationic (+) than anionic (-), which confirmed the Grotthus-type mechanism of protonation conduction in this present work. It can be assumed that in an electrolytes system, the ionic transference number, t_{ion}, should be higher than the value of ionic conductivity. This is due to the increase in the concentration gradient of ions and decrease in working current in the lower transference number. Thus, this will finally lead to battery letdown (Lu et al., 2007; Tao & Fujinami, 2007).

Table 4.9   TNM parameters data of alginate-NH$_4$NO$_3$ for SBEs system

Sample	t_{ele}	t_{ion}	μ_+ (cm^{2}V^{-1}s^{-1})	μ_- (cm^{2}V^{-1}s^{-1})	D_+ (cm^{2}s^{-1})	D_- (cm^{2}s^{-1})
S1	0.01	0.99	4.58×10^{-10}	4.63×10^{-12}	1.19×10^{-11}	1.20×10^{-12}
S3	0.03	0.97	8.84×10^{-10}	2.73×10^{-11}	2.30×10^{-11}	7.14×10^{-13}
S4	0.02	0.98	1.07×10^{-09}	2.19×10^{-11}	2.80×10^{-11}	5.72×10^{-12}
S5	0.03	0.97	3.65×10^{-09}	1.13×10^{-11}	9.52×10^{-11}	2.94×10^{-12}
S6	0.06	0.94	2.60×10^{-09}	1.66×10^{-10}	6.80×10^{-11}	4.34×10^{-12}
S7	0.01	0.99	3.80×10^{-10}	3.83×10^{-11}	9.92×10^{-12}	1.00×10^{-13}

CHAPTER 5

CONCLUSION AND RECOMMENDATION

5.1 Conclusion

In this research, alginate and ammonium nitrate were selected due to their favorable characteristics such as low cost, non-toxic, renewable, and good solubility. Alginate and ammonium nitrate solid biopolymer electrolytes (SBEs) system is clear and transparent with no phase separation of thin films. As a conclusion, this work was well prepared by the solution casting method with salt content from 5 to 35 wt.% of NH_4NO_3. The highest ionic conductivity for this system was for the sample S5 containing 25 wt.% of NH_4NO_3 which achieved 5.56×10^{-5} Scm^{-1}.

The SBEs system was observed to follow the Arrhenius behavior with $R^2 \sim 1$, implying that the samples were thermally assisted with increasing temperature. The highest conducting sample had the lowest value of E_a (0.11 eV). X-ray diffraction analysis (XRD) showed that the sample with 25 wt.% of NH_4NO_3 was the most amorphous, and the complexation of the materials showed the change of state of the material from semi-crystalline to amorphous. FTIR analysis confirmed that interaction has occurred between the carboxylate group (COO^-) from alginate with H^+, where there were changes in wavenumbers 1415 cm^{-1} and 1598 cm^{-1} which were associated to C=O and C-O$^-$ in alginate, 1019 cm^{-1} corresponding to C–O–C, and 3393 cm^{-1} corresponding to the OH$^-$ group. This result also confirmed that more ions were produced and interacted with oxygen atoms in the C–O–C group as ammonium salt increased by weight percentage. Based on these interpretations, the H atom of the N–H_4^+ from NH_4NO_3 is believed to interact with the oxygen in alginate as proposed in Chapter 4. The mobility (μ) and diffusion coefficient (D) were found to influence the ionic conductivity of the SBEs system, as observed via the IR-deconvolution technique. The thermogravimetric analysis

(TGA) proved that the addition of alginate influenced the thermal stability of the system by increasing the temperature decomposition until get the highest maximum decompose with sample S5 at 320.97 $\circ$C. The transference number of 0.97 was reached for the most conducting sample, S5. Analysis of frequency exponent indicated that correlated barrier hopping (CBH) was the hopping mechanism in the alginate-NH_4NO_3 SBEs system.

5.2   Recommendations

From the result obtained in this study, it is recommended for future researchers to take precautionary steps during the laboratory research. The use of chemicals or equipment may be harmful or toxic. The preparation must be done properly as the solution casting method has many problems during the sample preparation, which can affect the behavior of the biopolymer electrolytes. Besides, during sample preparation, the accuracy of the amount of ammonium nitrate is very important because it will influence the properties of the SBEs system. Ammonium nitrate is very sensitive to the environment as it can melt easily. The experiments should be conducted in a suitable laboratory environment so that the actual amount of materials is not affected.

The structural study of the SBEs can be furthered by using Scanning Electron Microscopy (SEM), Atomic Force Microscopy (AFM), and Energy Dispersive Spectroscopy (EDS) to identify the surface structure of the materials to confirm the homogeneity of the system. Nuclear Magnetic Resonance (NMR) test can be conducted for verification of structure and elucidation. It can also verify the pureness of raw materials used in the system. Next, it is necessary to investigate the thermal properties and transition behavior pf the SBEs system with the differential scanning calorimetry (DSC) In addition, the density functional theory (DFT) can be examined using the Gaussian software that provides structural information of a molecule of the polymer, and this can be correlated to the ATR-FTIR characterization.

Lastly, the ionic conductivity of alginate doped with ammonium nitrate biopolymer electrolytes can be increased with the addition of a plasticizer. The plasticizer is expected to increase the ionic mobility in the material and increase the ionic conductivity of SBEs. For additional learning in this field, battery or supercapacitor

application can be produced by using the natural polymer electrolyte, which is environmentally friendly to be used in the electrolytes system.
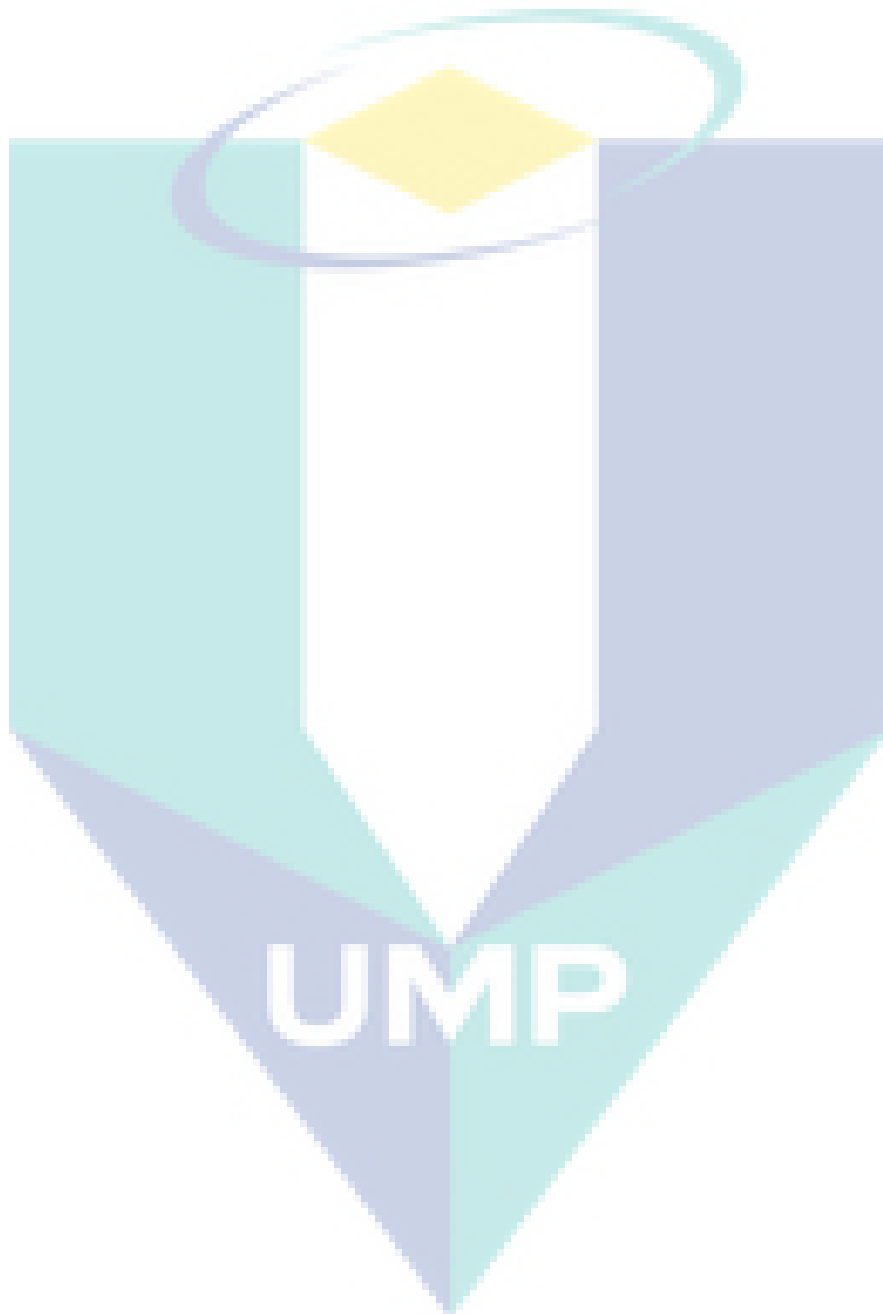
REFERENCES

Adebahr, J., Byrne, N., Forsyth, M., MacFarlane, D., & Jacobsson, P. (2003). Enhancement of ion dynamics in PMMA-based gels with addition of TiO_2 nano-particles. *Electrochimica Acta, 48*(14-16), 2099-2103.

Ahmad, Z., & Isa, M. (2012). Ionics conduction via correlated barrier hoping mechanism in CMC-SA solid biopolymer electrolytes. *Int J Latest Res Sci Technol, 1*(2), 70-75.

Ahmad, N. H. B., & Isa, M. I. N. B. M. (2015). Proton conducting solid polymer electrolytes based carboxymethyl cellulose doped ammonium chloride: ionic conductivity and transport studies. *International Journal of Plastics Technology*, *19*(1), 47-55.

Ahmad, N. H., & Isa, M. I. N. (2015). Structural and Ionic Conductivity Studies of CMC Based Polymerelectrolyte Doped with NH_4Cl. *Advanced Materials Research* 1107, 247-252. Trans Tech Publications.

Ahmad, N. H., & Isa, M. I. N. (2016). Characterization of un-plasticized and propylene carbonate plasticized carboxymethyl cellulose doped ammonium chloride solid biopolymer electrolytes. *Carbohydrate polymers*, *137*, 426-432.

Al- Hetar, M., Zainal Abidin, M., Sariah, M., & Wong, M. (2011). Antifungal activity of chitosan against Fusarium oxysporum f. sp. cubense. *Journal of Applied Polymer Science, 120*(4), 2434-2439.

Ali, A., Mohamed, N., & Arof, A. (1998). Polyethylene oxide (PEO)–ammonium sulfate $((NH_4)_2SO_4)$ complexes and electrochemical cell performance. *Journal of Power Sources, 74*(1), 135-141.

Ali, A. M. M., Subban, R. H. Y., Bahron, H., Yahya, M. Z. A., & Kamisan, A. S. (2013). Investigation on modified natural rubber gel polymer electrolytes for lithium polymer battery. *Journal of Power Sources*, 244, 636-640.

Ajili, O., Louati, B., & Guidara, K. (2018). Electrical properties and conduction mechanism by CBH model of $Na_2SrP_2O_7$. *Journal of Materials Science: Materials in Electronics*, *29*(10), 8649-8659.

Amaral, F. A., Sousa, R. M., Morais, L. C. T., Rocha, R. G., Campos, I. O., Fagundes, W. S., & Canobre, S. C. (2015). Preparation and characterization of the porous solid polymer electrolyte of PAN/PVA by phase inversion. *Journal of Applied Electrochemistry*, *45*(8), 809-820.

Amran, N. N. A., Manan, N. S. A., & Kadir, M. F. Z. (2016). The effect of $LiCF_3SO_3$ on the complexation with potato starch-chitosan blend polymer electrolytes. *Ionics*, *22*(9), 1647-1658.

Andrade, J. R., Raphael, E., & Pawlicka, A. (2009). Plasticized pectin-based gel electrolytes. *Electrochimica Acta, 54*(26), 6479-6483.

Andreev, Y. G., Seneviratne, V., Khan, M., Henderson, W. A., Frech, R. E., & Bruce, P. G. (2005). Crystal Structures of Poly (ethylene oxide) 3: $LiBF_4$ and (Diglyme) n: $LiBF_4$ (n= 1, 2). *Chemistry of materials*, *17*(4), 767-772.

Aniskari, N.A.B. & Mohd Isa, M.I.N.B.. (2017). The effect of ionic charge carriers in 2-hydroxyethyl cellulose solid biopolymer electrolytes doped glycolic acid via FTIR-deconvolution technique. *Journal of Sustainability Science and Management*. 2017. 71-79.

Appetecchi, G., Croce, F., Gerace, F., Panero, S., Passerini, S., Spila, E., & Scrosati, B. (1994). New concepts in primary and rechargeable solid state lithium polymer batteries. *MRS Online Proceedings Library Archive, 369*.

Aprilliza, M. (2017). Characterization and properties of sodium alginate from brown algae used as an ecofriendly superabsorbent. In *IOP Conference Series: Materials Science and Engineering* (Vol. 188, No. 1, p. 012019). IOP Publishing.

Aravindan, V., Lakshmi, C., & Vickraman, P. (2009). Investigations on Na^+ ion conducting polyvinylidenefluoride-co-hexafluoropropylene/poly ethylmethacrylate blend polymer electrolytes. *Current applied physics*, *9*(5), 1106-1111.

Armand, M., Chabagno, J., & Duclot, M. (1979). Fast ion transport in solids. *Eds. Vashishta, P., Mundy, JN & Shenoy, G. K, North Holland, Amsterdan, 52*.

Arof, A. K., Amirudin, S., Yusof, S. Z., & Noor, I. M. (2014). A method based on impedance spectroscopy to determine transport properties of polymer electrolytes. *Physical Chemistry Chemical Physics*, *16*(5), 1856-1867.

Asmara, S. N., Kufian, M. Z., Majid, S. R., & Arof, A. K. (2011). Preparation and characterization of magnesium ion gel polymer electrolytes for application in electrical double layer capacitors. *Electrochimica acta*, 57, 91-97.

Azeredo, H. M., Miranda, K. W., Rosa, M. F., Nascimento, D. M., & de Moura, M. R. (2012). Edible films from alginate-acerola puree reinforced with cellulose whiskers. *LWT-Food Science and Technology*, *46*(1), 294-297.

Aziz, N. N., Idris, N. K., & Isa, M. I. N. (2010). Proton conducting polymer electrolytes of methylcellulose doped ammonium fluoride: Conductivity and ionic transport studies. *International Journal of Physical Sciences*, *5*(6), 748-752.

Aziz, S. B. (2013). Li$^+$ ion conduction mechanism in poly (ε-caprolactone)-based polymer electrolyte. *Iranian Polymer Journal, 22*(12), 877-883.

Aziz, S. B., & Abidin, Z. H. Z. (2013). Electrical conduction mechanism in solid polymer electrolytes: new concepts to arrhenius equation. *Journal of Soft Matter, 2013*.

Aziz, S. B., Abidin, Z. H. Z., & Kadir, M. F. Z. (2015). Innovative method to avoid the reduction of silver ions to silver nanoparticles in silver ion conducting based polymer electrolytes. *Physica Scripta*, *90*(3), 035808.

Aziz, S. B., & Abidin, Z. H. Z. (2015). Ion- transport study in nanocomposite solid polymer electrolytes based on chitosan: Electrical and dielectric analysis. *Journal of Applied Polymer Science, 132*(15).

Aziz, S. B. (2016). Role of dielectric constant on ion transport: Reformulated Arrhenius equation. *Advances in Materials Science and Engineering*, *2016*.

Bandara, T. M. W. J., & Mellander, B. E. (2011). Evaluation of mobility, diffusion coefficient and density of charge carriers in ionic liquids and novel electrolytes based on a new model for dielectric response. In *Ionic Liquids: Theory, Properties, New Approaches*. InTech.

Basu, T., Goswami, M. M., Middya, T. R., & Tarafdar, S. (2012). Morphology and Ion-Conductivity of Gelatin–LiClO$_4$ Films: Fractional Diffusion Analysis. *The Journal of Physical Chemistry B*, *116*(36), 11362-11369.

Boopathi, G., Pugalendhi, S., Selvasekarapandian, S., Premalatha, M., Monisha, S., & Aristatil, G. (2017). Development of proton conducting biopolymer membrane based on agar–agar for fuel cell. *Ionics*, *23*(10), 2781-2790.

Bourahla, S., Ali Benamara, A., & Kouadri Moustefai, S. (2013). Infrared spectra of inorganic aerosols: ab initio study of $(NH_4)_2SO_4$, NH_4NO_3, and $NaNO_3$. *Canadian Journal of Physics*, *92*(3), 216-221.

Buraidah, M. H., Teo, L. P., Majid, S. R., & Arof, A. K. (2009). Ionic conductivity by correlated barrier hopping in NH_4I doped chitosan solid electrolyte. *Physica B: Condensed Matter*, *404*(8-11), 1373-1379.

Buraidah, M. H., & Arof, A. K. (2011). Characterization of chitosan/PVA blended electrolyte doped with NH$_4$I. *Journal of Non-Crystalline Solids*, *357*(16-17), 3261-3266.

Braccini, I., & Pérez, S. (2001). Molecular basis of Ca^{2+}-induced gelation in alginates and pectins: the egg-box model revisited. *Biomacromolecules*, *2*(4), 1089-1096.

Campo, V. L., Kawano, D. F., da Silva Jr, D. B., & Carvalho, I. (2009). Carrageenans: Biological properties, chemical modifications and structural analysis–A review. *Carbohydrate Polymers, 77*(2), 167-180.

Chai, M. N., & Isa, M. I. N. (2012). Investigation on the conduction mechanism of carboxyl methylcellulose-oleic acid natural solid polymer electrolyte. *International Journal of Advanced Technology & Engineering Research*, *2*(6), 36-39.

Chai, M. N., & Isa, M. I. N. (2013). The oleic acid composition effect on the carboxymethyl cellulose based biopolymer electrolyte. *Journal of Crystallization Process and Technology*, *3*(1), 1.

Chai, M. N., & Isa, M. I. N. (2013). Electrical characterization and ionic transport properties of carboxyl methylcellulose-oleic acid solid polymer electrolytes. *International journal of polymer analysis and characterization*, *18*(4), 280-286.

Chakchouk, N., Louati, B., & Guidara, K. (2018). Electrical properties and conduction mechanism study by OLPT model of NaZnPO$_4$ compound. *Materials Research Bulletin*, *99*, 52-60.

Chandra, A. (2013). Synthesis and dielectric studies of PEO-PVP blended solid polymer electrolytes. *Indian Journal of Pure & Applied Physics,* 788-791.

Chandra, S., Hashmi, S. A., & Prasad, G. (1990). Studies on ammonuim perchlorate doped polyethylene oxide polymer electrolyte. *Solid State Ionics*, *40*, 651-654.

Chen, W., Feng, Q., Zhang, G., Yang, Q., & Zhang, C. (2017). The effect of sodium alginate on the flotation separation of scheelite from calcite and fluorite. *Minerals Engineering*, *113*, 1-7.

Chtchigrovsky, M., Lin, Y., Ouchaou, K., Chaumontet, M., Robitzer, M., Quignard, F., & Taran, F. (2012). Dramatic effect of the gelling cation on the catalytic performances of alginate-supported palladium nanoparticles for the Suzuki–Miyaura reaction. *Chemistry of Materials*, *24*(8), 1505-1510.

Chu, P. P., Jen, H. P., Lo, F. R., & Lang, C. L. (1999). Exceedingly high lithium conductivity in novolac type phenolic resin/PEO blends. *Macromolecules*, *32*(14), 4738-4740.

Davis, T. A., Volesky, B., & Mucci, A. (2003). A review of the biochemistry of heavy metal biosorption by brown algae. *Water research*, *37*(18), 4311-4330.

Devendrappa, H., Rao, U. S., & Prasad, M. A. (2006). Study of dc conductivity and battery application of polyethylene oxide/polyaniline and its composites. *Journal of power sources*, *155*(2), 368-374.

Dey, A., Karan, S., & De, S. K. (2010). Molecular interaction and ionic conductivity of polyethylene oxide–LiClO$_4$ nanocomposites. *Journal of Physics and Chemistry of Solids*, *71*(3), 329-335.

Downs, E. C., Robertson, N. E., Riss, T. L., & Plunkett, M. L. (1992). Calcium alginate beads as a slow- release system for delivering angiogenic molecules in vivo and in vitro. *Journal of cellular physiology*, *152*(2), 422-429.

Dyre, J. C. (1988). The random free- energy barrier model for ac conduction in disordered solids. *Journal of Applied Physics*, *64*(5), 2456-2468.

Eldin, M. M., Hashem, A. E., Tamer, T. M., Omer, A. M., Yossuf, M. E., & Sabet, M. M. (2017). Development of Cross linked Chitosan/Alginate Polyelectrolyte Proton Exchanger Membranes for Fuel Cell Ap plications. *International Journal Electrochemical Sci*ence 12, 3840-3858.

Elliott, S. R. (1978). Errata. *Philos Mag B*, *36*, 129.

Elliott, S. R. (1977). A theory of ac conduction in chalcogenide glasses. *Philosophical Magazine*, *36*(6), 1291-1304.

El Shafee, E. (1996). Dielectric and conductivity relaxation in sodium carboxymethyl cellulose and its acid form. *Carbohydrate polymers*, *31*(1-2), 93-98.

Farid, A. M., Atyia, H. E., & Hegab, N. A. (2005). AC conductivity and dielectric properties of Sb$_2$Te$_3$ thin films. *Vacuum*, *80*(4), 284-294.

Fenton, D. E., Parker, J. M., & Wright, P. V. (1973). Complexes of alkali metal ions with poly (ethylene oxide). *polymer*, *14*(11), 589.

Feuillade, G., & Perche, P. (1975). Ion-conductive macromolecular gels and membranes for solid lithium cells. *Journal of Applied Electrochemistry, 5*(1), 63-69.

Finkenstadt, V. L. (2005). Natural polysaccharides as electroactive polymers. *Applied microbiology and biotechnology*, *67*(6), 735-745.

Fourest, E., & Volesky, B. (1997). Alginate properties and heavy metal biosorption by marine algae. *Applied Biochemistry and Biotechnology*, *67*(3), 215-226.

Freile-Pelegrin, Y., Azamar, J. A., & Robledo, D. (2011). Preliminary characterization of carrageenan from the red seaweed Halymenia floresii. *Journal of aquatic food product technology, 20*(1), 73-83.

Fuzlin, A. F., Rasali, N. M. J., & Samsudin, A. S. (2018). Effect on Ammonium Bromide in dielectric behavior based Alginate Solid Biopolymer electrolytes. In *IOP Conference Series: Materials Science and Engineering 342*(1), 012080. IOP Publishing.

Ganea, C. P. (2012) New approach of the ac electrode polarization during the measurements of impedance spectra. *Romanian Journal of Physics* 57, 664–675.

Gao, C., Pollet, E., & Avérous, L. (2017). Properties of glycerol-plasticized alginate films obtained by thermo-mechanical mixing. *Food Hydrocolloids*, *63*, 414-420.

Ghelichi, M., Qazvini, N. T., Jafari, S. H., Khonakdar, H. A., Farajollahi, Y., & Scheffler, C. (2013). Conformational, thermal, and ionic conductivity behavior of PEO in PEO/PMMA miscible blend: Investigating the effect of lithium salt. *Journal of Applied Polymer Science*, *129*(4), 1868-1874.

Goriparti, S., Miele, E., De Angelis, F., Di Fabrizio, E., Zaccaria, R. P., & Capiglia, C. (2014). Review on recent progress of nanostructured anode materials for Li-ion batteries. *Journal of Power Sources*, *257*, 421-443.

Govindaraj, G., Baskaran, N., Shahi, K., & Monoravi, P. (1995). Preparation, conductivity, complex permittivity and electric modulus in AgI☐ Ag₂O☐ SeO₃☐ MoO₃ glasses. *Solid State Ionics, 76*(1-2), 47-55.

Gurunathan, K., Murugan, A. V., Marimuthu, R., Mulik, U., & Amalnerkar, D. (1999). Electrochemically synthesised conducting polymeric materials for applications towards technology in electronics, optoelectronics and energy storage devices. *Materials Chemistry and Physics, 61*(3), 173-191.

Gurusiddappa, J., Madhuri, W., Suvarna, R. P., & Dasan, K. P. (2016). Conductivity and dielectric behavior of polyethylene oxide-lithium perchlorate solid polymer electrolyte films. *Indian Journal Advances in Chemical Science*, *4*, 14-19.

Hafiza, M. N., & Isa, M. I. N. (2014). Ionic conductivity and conduction mechanism studies of CMC/chitosan biopolymer blend electrolytes. *Research Journal of Recent Sciences* 3(11), 50-56.

Hafiza, M. N., & Isa, M. I. N. (2017). Solid polymer electrolyte production from 2-hydroxyethyl cellulose: Effect of ammonium nitrate composition on its structural properties. *Carbohydrate polymers*, *165*, 123-131.

Hafiza, M. N., & Isa, M. I. N. (2018, October). Conduction mechanism via correlated barrier hopping in EC-plasticized 2-hydroxyehyl cellulose-ammonium nitrate solid polymer electrolyte. In *IOP Conference Series: Materials Science and Engineering 440*(1), 012039. IOP Publishing.

Hamsan, M. H., Shukur, M. F., & Kadir, M. F. Z. (2017). The effect of NH_4NO_3 towards the conductivity enhancement and electrical behavior in methyl cellulose-starch blend based ionic conductors. *Ionics,* 23(5), 1137-1154.

Han, Y. K., Lee, S. U., Ok, J. H., Cho, J. J., & Kim, H. J. (2002). Theoretical studies of the solvent decomposition by lithium atoms in lithium-ion battery electrolyte. *Chemical physics letters*, *360*(3-4), 359-366.

Harun, N. I., Ali, R. M., Ali, A. M. M., & Yahya, M. Z. A. (2012). Dielectric behaviour of cellulose acetate-based polymer electrolytes. *Ionics*, *18*(6), 599-606.

Hashmi, S. A., Kumar, A., Maurya, K. K., & Chandra, S. (1990). Proton-conducting polymer electrolyte. I. The polyethylene oxide+ NH_4ClO_4 system. *Journal of Physics D: Applied Physics*, *23*(10), 1307.

Havriliak, S., & Negami, S. (1966, January). A complex plane analysis of α- dispersions in some polymer systems. In *Journal of Polymer Science: Polymer Symposia* (Vol. 14, No. 1, pp. 99-117). Wiley Subscription Services, Inc., A Wiley Company.

Helmiyati & Aprilliza, M. (2017). Characterization and properties of sodium alginate from brown algae used as an ecofriendly superabsorbent. In *IOP Conference Series: Materials Science and Engineering* (Vol. 188, No. 1, p. 012019). IOP Publishing.

Hema, M., Selvasekerapandian, S., Sakunthala, A., Arunkumar, D., & Nithya, H. (2008). Structural, vibrational and electrical characterization of PVA–NH₄Br polymer electrolyte system. *Physica B: Condensed Matter*, *403*(17), 2740-2747.

Hema, M., Selvasekarapandian, S., Arunkumar, D., Sakunthala, A., & Nithya, H. (2009). FTIR, XRD and ac impedance spectroscopic study on PVA based polymer electrolyte doped with NH$_4$X (X=Cl, Br, I). *Non-Crystalline Solid, 355,* 84-90.

Hema, M., Selvasekarapandian, S., Hirankumar, G., Sakunthala, A., Arunkumar, D., & Nithya, H. (2010). Laser Raman and ac impedance spectroscopic studies of PVA: NH$_4$NO$_3$ polymer electrolyte. *Spectrochimica Acta Part A: Molecular and Biomolecular Spectroscopy*, *75*(1), 474-478.

Hodge, R. M., Edward, G. H., & Simon, G. P. (1996). Water absorption and states of water in semicrystalline poly (vinyl alcohol) films. *Polymer*, *37*(8), 1371-1376.

Hofmann, A., Schulz, M., & Hanemann, T. (2013). Gel electrolytes based on ionic liquids for advanced lithium polymer batteries. *Electrochimica Acta, 89*, 823-831.

Hsu, H. L., Tien, C. F., & Leu, J. (2014). Effect of pore size/distribution in TiO$_2$ films on Agarose gel electrolyte-based Dye-Sensitized Solar Cells. *Journal of Solid State Electrochemistry*, *18*(6), 1665-1671.

Hwang, Y. J., Nahm, K. S., Kumar, T. P., & Stephan, A. M. (2008). Poly (vinylidene fluoride-hexafluoropropylene)-based membranes for lithium batteries. *Journal of Membrane Science*, *310*(1-2), 349-355.

Ibrahim, S., Yassin, M. M., Ahmad, R., & Johan, M. R. (2011). Effects of various LiPF$_6$ salt concentrations on PEO-based solid polymer electrolytes. *Ionics,* 17(5), 399-405.

Idris, N. K., Aziz, N. N., Zambri, M. S. M., Zakaria, N. A., & Isa, M. I. N. (2009). Ionic conductivity studies of chitosan-based polymer electrolytes doped with adipic acid. *Ionics*, *15*(5), 643-646.

Ilie, A., Ghiţulică, C., Andronescu, E., Cucuruz, A., & Ficai, A. (2016). New composite materials based on alginate and hydroxyapatite as potential carriers for ascorbic acid. *International journal of pharmaceutics, 510*(2), 501-507.

Isa, M. I. N., & Samsudin, A. S. (2013). Ionic conduction behavior of CMC based green polymer electrolytes. In *Advanced Materials Research* 802,194-198.

Işıklan, N., Kurşun, F., & İnal, M. (2009). Graft copolymerization of itaconic acid onto sodium alginate using ceric ammonium nitrate as initiator. *Journal of applied polymer science*, *114*(1), 40-48.

Itoh, T., Miyamura, Y., Ichikawa, Y., Uno, T., Kubo, M., & Yamamoto, O. (2003). Composite polymer electrolytes of poly (ethylene oxide)/BaTiO$_3$/Li salt with hyperbranched polymer. *Journal of power sources*, *119*, 403-408.

Itoh, T., Mitsuda, Y., Ebina, T., Uno, T., & Kubo, M. (2009). Solid polymer electrolytes composed of polyanionic lithium salts and polyethers. *Journal of Power Sources, 189*(1), 531-535.

Jacob, M. M. E., Hackett, E., & Giannelis, E. P. (2003). From nanocomposite to nanogel polymer electrolytes. *Journal of Materials Chemistry*, *13*(1), 1-5.

Jayalakshmi, A., & Sivadevi, S. (2018). Structural and conducting properties of proton conducting tri-blend polymer electrolytes. *International Journal of Engineering Development and Research, 6*(1).

Johan, M. R., & Ting, L. M. (2011). Structural, thermal and electrical properties of nano manganese-composite polymer electrolytes. *Int J Electrochem Sci, 6*(10), 4737-4748.

Jung, W.-H. (2002). Non-adiabatic small polaron hopping conduction in Gd1/3Sr^2/3FeO^3. *Materials Letters,* 57(3), 697–702.

Jyothi, A. (2010). Starch graft copolymers: Novel applications in industry. *Composite Interfaces, 17*(2-3), 165-174.

Kadir, M. A., Teo, L. P., Majid, S. R., & Arof, A. K. (2009). Conductivity studies on plasticised PEO/chitosan proton conducting polymer electrolyte. *Materials Research Innovations*, *13*(3), 259-262.

Kadir, M. F. Z., Aspanut, Z., Majid, S. R., & Arof, A. K. (2011). FTIR studies of plasticized poly (vinyl alcohol)–chitosan blend doped with NH$_4$NO$_3$ polymer electrolyte membrane. *Spectrochimica Acta Part A: Molecular and Biomolecular Spectroscopy*, *78*(3), 1068-1074.

Kadir, M. F. Z., & Hamsan, M. H. (2018). Green electrolytes based on dextran-chitosan blend and the effect of NH$_4$SCN as proton provider on the electrical response studies. *Ionics*, *24*(8), 2379-2398.

Kadir, M. F. Z., Majid, S. R., & Arof, A. K. (2010). Plasticized chitosan–PVA blend polymer electrolyte based proton battery. *Electrochimica Acta*, 55(4), 1475-1482.

Kahouli, A., Sylvestre, A., Jomni, F., Yangui, B., & Legrand, J. (2012). Experimental and theoretical study of AC electrical conduction mechanisms of semicrystalline parylene C thin films. *The Journal of Physical Chemistry A*, *116*(3), 1051-1058.

Kam, W., Liew, C.-W., Lim, J., & Ramesh, S. (2014). Electrical, structural, and thermal studies of antimony trioxide-doped poly (acrylic acid)-based composite polymer electrolytes. *Ionics, 20*(5), 665-674.

Kamarudin, K. H., & Isa, M. I. N. (2013). Structural and DC Ionic conductivity studies of carboxy methylcellulose doped with ammonium nitrate as solid polymer electrolytes. *International Journal of Physical Sciences*, *8*(31), 1581-1587.

Kaneko, M., Hoshi, T., Kaburagi, Y., & Ueno, H. (2004). Solid type dye-sensitized solar cell using polysaccharide containing redox electrolyte solution. *Journal of Electroanalytical Chemistry*, *572*(1), 21-27.

Kanti, P., Srigowri, K., Madhuri, J., Smitha, B., & Sridhar, S. (2004). Dehydration of ethanol through blend membranes of chitosan and sodium alginate by pervaporation. *Separation and Purification Technology*, *40*(3), 259-266.

Karthikeyan, S., Selvasekarapandian, S., Premalatha, M., Monisha, S., Boopathi, G., Aristatil, G & Madeswaran, S. (2017). Proton-conducting I-carrageenan-based biopolymer electrolyte for fuel cell application. *Ionics*, *23*(10), 2775-2780.

Karthikeyan, S., Sikkanthar, S., Selvasekarapandian, S. Arunkumar, D & Nithya, H. (2016) structural, electrical and electrochemical properties of polyacrylonitrile-ammonium hexaaflurophosphate polymer electrolyte system *J Polym Res* 23(51).

Kauppinen, J. K., Moffatt, D. J., Mantsch, H. H., & Cameron, D. G. (1981). Fourier self-deconvolution: a method for resolving intrinsically overlapped bands. *Applied Spectroscopy*, *35*(3), 271-276.

Khan, W., Naqvi, A. H., Gupta, M., Husain, S., & Kumar, R. (2011). Small polaron hopping conduction mechanism in Fe doped $LaMnO_3$. *The Journal of chemical physics*, *135*(5), 054501.

Khiar, A., & Arof, A. (2011). Electrical properties of starch/chitosan-NH_4NO_3 polymer electrolyte. *5(3)*, 23-27.

Kim, H., Boysen, D. A., Newhouse, J. M., Spatocco, B. L., Chung, B., Burke, P. J. & Wei, W. (2012). Liquid metal batteries: past, present, and future. *Chemical reviews*, *113*(3), 2075-2099.

Kim, H.-S., Kum, K.-S., Cho, W.-I., Cho, B.-W., & Rhee, H.-W. (2003). Electrochemical and physical properties of composite polymer electrolyte of poly (methyl methacrylate) and poly (ethylene glycol diacrylate). *Journal of Power Sources, 124*(1), 221-224.

Kim, J.-K., Cheruvally, G., Li, X., Ahn, J.-H., Kim, K.-W., & Ahn, H.-J. (2008). Preparation and electrochemical characterization of electrospun, microporous membrane-based composite polymer electrolytes for lithium batteries. *Journal of Power Sources, 178*(2), 815-820.

Kim, J. H., Kang, M.-S., Kim, Y. J., Won, J., Park, N.-G., & Kang, Y. S. (2004). Dye-sensitized nanocrystalline solar cells based on composite polymer electrolytes containing fumed silica nanoparticles. *Chemical communications*(14), 1662-1663.

Kulshrestha, N., Chatterjee, B., & Gupta, P. (2014). Characterization and electrical properties of polyvinyl alcohol based polymer electrolyte films doped with ammonium thiocyanate. *Materials Science and Engineering: B, 184*, 49-57.

Kumar, K. K., Ravi, M., Pavani, Y., Bhavani, S., Sharma, A. K., & Rao, V. N. (2011). Investigations on the effect of complexation of NaF salt with polymer blend (PEO/PVP) electrolytes on ionic conductivity and optical energy band gaps. *Physica B: Condensed Matter*, *406*(9), 1706-1712.

Kumar, M., & Sekhon, S. S. (2002). Role of plasticizer's dielectric constant on conductivity modification of PEO–NH$_4$F polymer electrolytes. *European Polymer Journal*, *38*(7), 1297-1304.

Kumar, M., Tiwari, T., & Srivastava, N. (2012). Electrical transport behaviour of bio-polymer electrolyte system: Potato starch+ ammonium iodide. *Carbohydrate Polymers, 88*(1), 54-60.

Lee, K. Y., & Mooney, D. J. (2012). Alginate: properties and biomedical applications. *Progress in polymer science*, *37*(1), 106-126.

Li, P., Dai, Y. N., Zhang, J. P., Wang, A. Q., & Wei, Q. (2008). Chitosan-alginate nanoparticles as a novel drug delivery system for nifedipine. *International journal of biomedical science: IJBS*, *4*(3), 221.

Li, Q., Chen, J., Fan, L., Kong, X., & Lu, Y. (2016). Progress in electrolytes for rechargeable Li-based batteries and beyond. *Green Energy & Environment, 1*(1), 18-42.

Liew, C. W., Durairaj, R., & Ramesh, S. (2014). Rheological Studies of PMMA–PVC Based Polymer Blend Electrolytes with LiTFSI as Doping Salt. *PloS one, 9*(7), e102815.

Liew, J. W. Y., Loh, K. S., Ahmad, A., Lim, K. L., & Daud, W. R. W. (2017). Synthesis and characterization of modified κ-carrageenan for enhanced proton conductivity as polymer electrolyte membrane. *PloS one*, *12*(9), e0185313.

Liu, L. S., Liu, S. Q., Ng, S. Y., Froix, M., Ohno, T., & Heller, J. (1997). Controlled release of interleukin-2 for tumour immunotherapy using alginate/chitosan porous microspheres. *Journal of Controlled Release*, *43*(1), 65-74.

Linford, R. G. (1988). Experimental technique for studying polymer electrolytes. *Solid State Ionic*, *28*(30), 551-571.

Liu, L., Yang, X., Lv, C., Zhu, A., Zhu, X., Guo, S., & Yang, D. (2016). Seaweed-derived route to Fe_2O_3 hollow nanoparticles/N-doped graphene aerogels with high lithium ion storage performance. *ACS applied materials & interfaces*, *8*(11), 7047-7053.

Lu, N., Ho, Y. M., Fan, C. W., Wang, F. M., & Lee, J. T. (2007). A simple method for synthesizing polymeric lithium salts exhibiting relatively high cationic transference number in solid polymer electrolytes. *Solid state ionics*, *178*(5-6), 347-353.

Lv, C., Yang, X., Umar, A., Xia, Y., Jia, Y. A., Shang, L., & Yang, D. (2015). Architecture-controlled synthesis of M x O y (M= Ni, Fe, Cu) microfibres from seaweed biomass for high-performance lithium ion battery anodes. *Journal of Materials Chemistry A*, *3*(45), 22708-22715.

Ma, X., Yu, J., He, K., & Wang, N. (2007). The effects of different plasticizers on the properties of thermoplastic starch as solid polymer electrolytes. *Macromolecular Materials and Engineering, 292*(4), 503-510.

Ma, X., Yu, J., & Zhao, A. (2006). Properties of biodegradable poly (propylene carbonate)/starch composites with succinic anhydride. *Composites Science and Technology, 66*(13), 2360-2366.

Macdonald, J. R. (1987). WB Johnson in JR MacDonald. *Impedance Spectroscopy, Wiley, New York*, 17.

Macedo, P. B., Moynihan, C. T., & Bose, R. (1972). Dielectric modulus: experiment, application, and interpretation. *J Phy Chem Glasses*, *13*, 171.

Mahakul, P. C., Sa, K., Das, B., & Mahanandia, P. (2017). Structural investigation of the enhanced electrical, optical and electrochemical properties of MWCNT incorporated Poly [3-hexylthiophene-2, 5-diyl] composites. *Materials Chemistry and Physics*, *199*, 477-484.

Maitz, M. F. (2015). Applications of synthetic polymers in clinical medicine. *Biosurface and Biotribology*, *1*(3), 161-176.

Majid S. R., & Arof A. K. (2005) Proton-conducting polymer electrolyte films based on chitosan acetate complexed with NH_4NO_3 salt. *Physica B 355*(1–4):78–82.

Majid, S. R., & Arof, A. K. (2007). Electrical behavior of proton-conducting chitosan-phosphoric acid-based electrolytes. *Physica B: Condensed Matter*, *390*(1-2), 209-215.

Majid, S. R., & Arof, A. K. (2007). Mobility and density of ions in chitosan–orthophosphoric acid–ammonium nitrate electrolytes. *physica status solidi (a)*, *204*(7), 2396-2401.

Majid, S. R., & Arof, A. K. (2008). FTIR studies of chitosan-orthophosphoric acid-ammonium nitrate-aluminosilicate polymer electrolyte. *Molecular Crystals and Liquid Crystals, 484*(1), 117/[483]-126/[492].

Malathi, J., Kumaravadivel, M., Brahmanandhan, G., Hema, M., Baskaran, R., & Selvasekarapandian, S. (2010). Structural, thermal and electrical properties of PVA–$LiCF_3SO_3$ polymer electrolyte. *Journal of Non-crystalline solids, 356*(43), 2277-2281.

Mansour, S. A., Yahia, I. S., & Yakuphanoglu, F. (2010). The electrical conductivity and dielectric properties of CI Basic Violet 10. *Dyes and Pigments*, *87*(2), 144-148.

Mason, R. N., Hu, L., Glatzhofer, D. T., & Frech, R. (2010). Infrared spectroscopic and conductivity studies of poly (N-methylpropylenimine)/lithium triflate electrolytes. *Solid State Ionics*, *180*(40), 1626-1632.

Maurya, K., Srivastava, N., Hashmi, S., & Chandra, S. (1992). Proton conducting polymer electrolyte: II poly ethylene oxide+ NH_4I system. *Journal of materials science, 27*(23), 6357-6364.

Mazuki, N. F., Fuzlin, A. F., Saadiah, M. A., & Samsudin, A. S. (2018). An investigation on the abnormal trend of the conductivity properties of CMC/PVA-doped NH_4Cl-based solid biopolymer electrolyte system. *Ionics,* 1-11.

Michael, M., Jacob, M., Prabaharan, S., & Radhakrishna, S. (1997). Enhanced lithium ion transport in PEO-based solid polymer electrolytes employing a novel class of plasticizers. *Solid State Ionics, 98*(3-4), 167-174.

Migahed, M. D., Bakr, N. A., Abdel- Hamid, M. I., El- Hanafy, O., & El- Nimr, M. (1996). Dielectric relaxation and electric modulus behavior in poly (vinyl alcohol)- based composite systems. *Journal of applied polymer science*, *59*(4), 655-662.

Misenan, M. S. M., Isa, M. I. N., & Khiar, A. S. A. (2018). Electrical and structural studies of polymer electrolyte based on chitosan/methyl cellulose blend doped with BMIMTFSI. *Materials Research Express*, *5*(5), 055304.

Mohamad, A. A., & Arof, A. K. (2007). Plasticized alkaline solid polymer electrolyte system. *Materials Letters*, *61*(14-15), 3096-3099.

Mohapatra, S. R., Thakur, A. K., & Choudhary, R. N. P. (2009). Effect of nanoscopic confinement on improvement in ion conduction and stability properties of an intercalated polymer nanocomposite electrolyte for energy storage applications. *Journal of Power Sources*, *191*(2), 601-613.

Molak, A., Ksepko, E., Gruszka, I., Ratuszna, A., Paluch, M., & Ujma, Z. (2005). Electric permittivity and conductivity of (Na0. 5Pb0$_5$)(Mn0$_5$Nb0. 5) O$_3$ ceramics. *Solid State Ionics*, *176*(15-16), 1439-1447.

Moniha, V., Alagar, M., Selvasekarapandian, S., Sundaresan, B., & Boopathi, G. (2018). Conductive bio-polymer electrolyte iota-carrageenan with ammonium nitrate for application in electrochemical devices. *Journal of Non-Crystalline Solids*, *481*, 424-434.

Monisha, S., Mathavan, T., Selvasekarapandian, S., Benial, A. M. F., Aristatil, G., Mani, N., & Premalatha, M. (2017). Investigation of bio polymer electrolyte based on cellulose acetate-ammonium nitrate for potential use in electrochemical devices. *Carbohydrate polymers*, *157*, 38-47.

Murthy, N. S. (2004). Recent developments in polymer characterization using x-ray diffraction. *parameters, 18*, 19.

Muthupradeepa, R., Sivakumar, M., Subadevi, R., & Suryanarayanan, V. (2017). Sulfonium cation based ionic liquid incorporated polymer electrolyte for lithium ion battery. *Polymer Bulletin*, *74*(5), 1677-1691.

Nath, A. K., & Kumar, A. (2014). Scaling of AC conductivity, electrochemical and thermal properties of ionic liquid based polymer nanocomposite electrolytes. *Electrochimica Acta*, *129*, 177-186.

Navaratnam, S., Ramesh, K., Ramesh, S., Sanusi, A., Basirun, W. J., & Arof, A. K. (2015). Transport mechanism studies of chitosan electrolyte systems. *Electrochimica Acta*, *175*, 68-73.

Ng, L., & Mohamad, A. (2008). Effect of temperature on the performance of proton batteries base on chitosan--NH_4NO_3–EC membrane. *Journal of Membrane Science,* 352(2),653-657.

Ng, L. S., & Mohamad, A. A. (2006). Protonic battery based on a plasticized chitosan-NH_4NO_3 solid polymer electrolyte. *Journal of Power Sources*, *163*(1), 382-385.

Ngai, K. S., Ramesh, S., Ramesh, K., & Juan, J. C. (2016). A review of polymer electrolytes: fundamental, approaches and applications. *Ionics,* 22(8), 1259-1279.

Nicotera, I., Coppola, L., Oliviero, C., Castriota, M., & Cazzanelli, E. (2006). Investigation of ionic conduction and mechanical properties of PMMA–PVdF blend-based polymer electrolytes. *Solid State Ionics, 177*(5-6), 581-588.

Noor, N. A. M. & Isa, M. I. N. (2016). Ionic conductivity and dielectric properties of CMC doped NH_4SCN solid biopolymer electrolytes. *Advanced Materials Research, 1107*(2015), 230-235.

Onishi, S., Farber, H., & Petrucci, S. (1980). Ultrasonic and dielectric relaxation of lithium perchlorate in 1, 2-dimethoxyethane and 1, 3-dioxolane at 25. degree. C. *The Journal of Physical Chemistry, 84*(22), 2922-2927.

Osman, Z., Ibrahim, Z., & Arof, A. (2001). Conductivity enhancement due to ion dissociation in plasticized chitosan based polymer electrolytes. *Carbohydrate Polymers, 44*(2), 167-173.

Othman, M. F. M., Samsudin, A. S., & Isa, M. I. N. (2012). Ionic conductivity and relaxation process in CMC-GA solid biopolymer electrolytes. *Journal of. Current Engineering Research 2*(4), 6-10.

Pandey, G. P., Liu, T., Hancock, C., Li, Y., Sun, X. S., & Li, J. (2016). Thermostable gel polymer electrolyte based on succinonitrile and ionic liquid for high-performance solid-state supercapacitors. *Journal of Power Sources, 328,* 510-519.

Pike, G. E. (1972). AC conductivity of scandium oxide and a new hopping model for conductivity. *Physical Review B*, *6*(4), 1572.

Pradhan, D. K., Choudhary, R., Samantaray, B., Karan, N., & Katiyar, R. (2007). Effect of plasticizer on structural and electrical properties of polymer nanocompsoite electrolytes. *Int. J. Electrochem. Sci, 2*, 861-871.

Pushpamalar, V., Langford, S. J., Ahmad, M., & Lim, Y. Y. (2006). Optimization of reaction conditions for preparing carboxymethyl cellulose from sago waste. *Carbohydrate Polymers*, *64*(2), 312-318.

Radha, K. P., Selvasekarapandian, S., Karthikeyan, S., Hema, M., & Sanjeeviraja, C. (2013). Synthesis and impedance analysis of proton-conducting polymer electrolyte PVA: NH_4F. *Ionics*, *19*(10), 1437-1447.

Rahaman, M. H. A., Khandaker, M. U., Khan, Z. R., Kufian, M. Z., Noor, I. S. M., & Arof, A. K. (2014). Effect of gamma irradiation on poly (vinyledene difluoride)–lithium bis (oxalato) borate electrolyte. *Physical Chemistry Chemical Physics*, *16*(23), 11527-11537.

Rajendran, S., & Uma, T. (2000). Experimental investigations on PVC–$LiAsF_6$–DBP polymer electrolyte systems. *Journal of power sources*, *87*(1-2), 218-222.

Rajendran, S., Sivakumar, M., & Subadevi, R. (2003). Effect of salt concentration in poly (vinyl alcohol)-based solid polymer electrolytes. *Journal of Power Sources*, *124*(1), 225-230.

Rajendran, S., & Sivakumar, P. (2008). An investigation of PVdF/PVC-based blend electrolytes with EC/PC as plasticizers in lithium battery applications. *Physica B: Condensed Matter*, *403*(4), 509-516.

Rajeswari, N., Selvasekarapandian, S., Sanjeeviraja, C., Kawamura, J., & Bahadur, S. A. (2014). A study on polymer blend electrolyte based on PVA/PVP with proton salt. *Polymer bulletin, 71*(5), 1061-1080.

Ramesh, S., & Liew, C.-W. (2012). Exploration on nano-composite fumed silica-based composite polymer electrolytes with doping of ionic liquid. *Journal of Non-crystalline solids, 358*(5), 931-940.

Ramesh, S., Liew, C.-W., & Ramesh, K. (2011). Evaluation and investigation on the effect of ionic liquid onto PMMA-PVC gel polymer blend electrolytes. *Journal of Non-crystalline solids, 357*(10), 2132-2138.

Ramesh, S., & Lu, S. (2012). Enhancement of ionic conductivity and structural properties by BMIMTf ionic liquid in P(VdF-HFP)-based polymer electrolytes. *J Appl Polym Sci, 126*, 484-492.

Ramesh, S., & Wen, L. C. (2010). Investigation on the effects of addition of SiO_2 nanoparticles on ionic conductivity, FTIR, and thermal properties of nanocomposite PMMA–$LiCF_3SO_3$–SiO_2. *Ionics, 16*(3), 255-262.

Ramya, C. S., & Selvasekarapandian, S. (2014). Spectroscopic studies on ion dynamics of PVP–NH_4SCN polymer electrolytes. *Ionics*, *20*(12), 1681-1686.

Ramya, C., Selvasekarapandian, S., Savitha, T., Hirankumar, G., & Angelo, P. (2007). Vibrational and impedance spectroscopic study on PVP–NH_4SCN based polymer electrolytes. *Physica B: Condensed Matter, 393*(1-2), 11-17.

Ramya, C., Selvasekarapandian, S., Savitha, T., Hirankumar, G., Baskaran, R., Bhuvaneswari, M., & Angelo, P. (2006). Conductivity and thermal behavior of proton conducting polymer electrolyte based on poly (N-vinyl pyrrolidone). *European polymer journal, 42*(10), 2672-2677.

Rani, M., Dzulkurnain, N., Ahmad, A., & Mohamed, N. (2015). Conductivity and dielectric behavior studies of carboxymethyl cellulose from kenaf bast fiber incorporated with ammonium acetate-BMATFSI biopolymer electrolytes. *International Journal of Polymer Analysis and Characterization, 20*(3), 250-260.

Rani, M. S. A., Mohamed, N. S., & Isa, M. I. N. (2016). Characterization of proton conducting carboxymethyl cellulose/chitosan dual-blend based biopolymer electrolytes. In *Materials Science Forum* (Vol. 846, pp. 539-544). Trans Tech Publications.

Rao, M., Geng, X., Liao, Y., Hu, S., & Li, W. (2012). Preparation and performance of gel polymer electrolyte based on electrospun polymer membrane and ionic liquid for lithium ion battery. *Journal of Membrane Science, 399*, 37-42.

Raphael, E., Avellaneda, C. O., Manzolli, B., & Pawlicka, A. (2010). Agar-based films for application as polymer electrolytes. *Electrochimica Acta, 55*(4), 1455-1459.

Rasali, N. M. J., Nagao, Y., & Samsudin, A. S. (2018). Enhancement on amorphous phase in solid biopolymer electrolyte based alginate doped NH_4NO_3. *Ionics*, 1-14.

Ravi, M., Pavani, Y., Kumar, K. K., Bhavani, S., Sharma, A. K., & Rao, V. N. (2011). Studies on electrical and dielectric properties of PVP: $KBrO_4$ complexed polymer electrolyte films. *Materials Chemistry and Physics*, *130*(1-2), 442-448.

Ravi, M., Song, S., Gu, K., Tang, J., & Zhang, Z. (2015). Electrical properties of biodegradable poly (ε-caprolactone): lithium thiocyanate complexed polymer electrolyte films. *Materials Science and Engineering: B*, *195*, 74-83.

Reddy, C. V. S., Han, X., Zhu, Q. Y., Mai, L. Q., & Chen, W. (2006). Conductivity and discharge characteristics of (PVC+NaClO₄) polymer electrolyte systems. *European polymer journal*, *42*(11), 3114-3120.

Reddy, C. V. S., Jin, A.-P., Zhu, Q.-Y., Mai, L.-Q., & Chen, W. (2006). Preparation and characterization of (PVP+ NaClO₄) electrolytes for battery applications. *The European Physical Journal E, 19*(4), 471-476.

Rho, Y. H., & Kanamura, K. (2006). Fabrication of all solid-state rechargeable lithium battery and its electrochemical properties. *Journal of power sources*, *158*(2), 1436-1441.

Rosli, N. H. A., Chan, C. H., Subban, R. H. Y., & Winie, T. (2012). Studies on the structural and electrical properties of hexanoyl chitosan/polystyrene-based polymer electrolytes. *Physics Procedia*, *25*, 215-220.

Saaid, F., Rodi, I., & Winie, T. (2017). Effect of temperature on the transport property of PVdF-HFP-MPII-PC/DME gel polymer electrolytes. Paper presented at the AIP Conference Proceedings.

Saadiah, M. A., & Samsudin, A. S. (2018, April). Electrical study on Carboxymethyl Cellulose-Polyvinyl alcohol based bio-polymer blend electrolytes. In *IOP Conference Series: Materials Science and Engineering* 342(1), 012045. IOP Publishing.

Sahu, N., Panigrahi, S., & Kar, M. (2013). Conduction Mechanism by Using CBH Model in Fe3. *Journal of Materials*, 2013.

Saikia, D., Chen-Yang, Y., Chen, Y., Li, Y., & Lin, S. (2008). Investigation of ionic conductivity of composite gel polymer electrolyte membranes based on P (VDF-HFP), LiClO₄ and silica aerogel for lithium ion battery. *Desalination, 234*(1-3), 24-32.

Sakurai, T., Weber, R., Ueno, S., Nishino, J., & Tanaka, M. (2003). Relevance of coplanar PCBs for TEQ emission of fluidized bed incineration and impact of emission control devices. *Chemosphere*, *53*(6), 619-625.

Salleh, N. S., Aziz, S. B., Aspanut, Z., & Kadir, M. F. Z. (2016). Electrical impedance and conduction mechanism analysis of biopolymer electrolytes based on methyl cellulose doped with ammonium iodide. *Ionics*, *22*(11), 2157-2167.

Samsudin, A. S., Aziz, M. I. A., & Isa, M. I. N. (2012). Natural polymer electrolyte system based on sago: Structural and transport behavior

characteristics. *International Journal of Polymer Analysis and Characterization*, *17*(8), 600-607.

Samsudin, A., & Isa, M. (2012). Characterization of carboxy methylcellulose doped with DTAB as new types of biopolymer electrolytes. *Bulletin of Materials Science, 35*(7), 1123-1131.

Samsudin, A. S., & Isa, M. I. N. (2012). Structural and Electrical Properties of Carboxy Methylcellulose-Dodecyltrimethyl Ammonium Bromide-Based Biopolymer Electrolytes System. *International Journal of Polymeric Materials, 61*(1), 30–40.

Samsudin, A. S., & Isa, M. I. N. (2012). Structural and ionic transport study on CMC doped NH4Br: A new types of biopolymer electrolytes. *J. Appl. Sci*, *12*(2), 174-179.

Samsudin, A. S., Khairul, W. M., & Isa, M. I. N. (2012). Characterization on the potential of carboxy methylcellulose for application as proton conducting biopolymer electrolytes. *Journal of Non-crystalline solids*, *358*(8), 1104-1112.

Samsudin, A. S., Kuan, E. C. H., & Isa, M. I. N. (2011). Investigation of the potential of proton-conducting biopolymer electrolytes based methyl cellulose-glycolic acid. *International Journal of Polymer Analysis and Characterization*, *16*(7), 477-485.

Samsudin, A. S., Lai, H. M., & Isa, M. I. N. (2014). Biopolymer materials based carboxymethyl cellulose as a proton conducting biopolymer electrolyte for application in rechargeable proton battery. *Electrochimica Acta*, *129*, 1-13.

Samsudin, A. S., & Saadiah, M. A. (2018). Ionic conduction study of enhanced amorphous solid bio-polymer electrolytes based carboxymethyl cellulose doped NH4Br. *Journal of Non-Crystalline Solids*, *497*, 19-29.

Santos, D. M. F., & Sequeira, C. A. C. (2010). Polymer Electrolytes: Fundamentals and Applications. *Abington: Elsevier Science*.

Saroj AL, Singh RK (2012) Thermal, dielectric and conductivity studies on PVA/Ionic liquid [EMIM][EtSO4] based polymer electrolytes. *J Phys Chem Solids 73*,162–168.

Sawaby, A., Selim, M. S., Marzouk, S. Y., Mostafa, M. A., & Hosny, A. (2010). Structure, optical and electrochromic properties of NiO thin films. *Physica B: Condensed Matter*, *405*(16), 3412-3420.

Schaefer, J. L., Lu, Y., Moganty, S. S., Agarwal, P., Jayaprakash, N., & Archer, L. A. (2012). Electrolytes for high-energy lithium batteries. *Applied Nanoscience, 2*(2), 91-109.

Scrosati, B. (1993). *Applications of electroactive polymers* (Vol. 75): Springer.

Sengwa, R. J., & Choudhary, S. (2014). Dielectric properties and fluctuating relaxation processes of poly (methyl methacrylate) based polymeric nanocomposite electrolytes. *Journal of Physics and Chemistry of Solids*, *75*(6), 765-774.

Selvin, P. C., Perumal, P., Selvasekarapandian, S., Monisha, S., Boopathi, G., & Chandra, M. L. (2018). Study of proton-conducting polymer electrolyte based on K-carrageenan and NH$_4$SCN for electrochemical devices. *Ionics*, 1-8.

Shastry, M. C. R., & Rao, K. J. (1991). Ac conductivity and dielectric relaxation studies in AgI-based fast ion conducting glasses. *Solid State Ionics*, *44*(3-4), 187-198.

Shuhaimi, N. E. A., Majid, S. R., & Arof, A. K. (2009). On complexation between methyl cellulose and ammonium nitrate. *Materials Research Innovations*, *13*(3), 239-242.

Shuhaimi, N. E. A., Teo, L. P., Majid, S. R., & Arof, A. K. (2010). Transport studies of NH$_4$NO$_3$ doped methyl cellulose electrolyte. *Synthetic Metals, 160*(9-10), 1040-1044.

Shujahadeen, B. A. (2012). Electrical and dielectric properties of solid and nanocomposite polymer electrolytes based on chitosan (Doctoral dissertation, University of Malaya).

Shukur, M. F., Ibrahim, F. M., Majid, N. A., Ithnin, R., & Kadir, M. F. Z. (2013). Electrical analysis of amorphous corn starch-based polymer electrolyte membranes doped with LiI. *Physica Scripta*, *88*(2), 025601.

Shukur, M., Ithnin, R., & Kadir, M. (2014). Electrical properties of proton conducting solid biopolymer electrolytes based on starch–chitosan blend. *Ionics, 20*(7), 977-999.

Shukur, M.F., & Kadir, M.F.Z. (2015) Hydrogen ion conducting starch-chitosan blend based electrolyte for application in electrochemical devices. *Electrochimica Acta, 158*, 152-165.

Shriver, D. F., & Bruce, P. G. (1995). Polymer electrolytes I: General principles. In *Solid state electrochemistry* (p. 95). Cambridge University Press Cambridge.

Sim, L. N., Yahya, R., & Arof, A. K. (2016). Blend polymer electrolyte films based on poly (ethyl methacrylate)/poly (vinylidenefluoride-co-hexafluoropropylene) incorporated with 1-butyl-3-methyl imidazolium iodide ionic liquid. *Solid State Ionics*, *291*, 26-32.

Singh, R., Jadhav, N. A., Majumder, S., Bhattacharya, B., & Singh, P. K. (2013). Novel biopolymer gel electrolyte for dye-sensitized solar cell application. *Carbohydrate polymers*, *91*(2), 682-685.

Singh, R., Bhattacharya, B., Rhee, H. W., & Singh, P. K. (2015). Solid gellan gum polymer electrolyte for energy application. *International journal of hydrogen energy*, *40*(30), 9365-9372.

Singh, R., Baghel, J., Shukla, S., Bhattacharya, B., Rhee, H. W., & Singh, P. K. (2014). Detailed electrical measurements on sago starch biopolymer solid electrolyte. *Phase Transitions*, *87*(12), 1237-1245.

Singh, R., Bhattacharya, B., Tomar, S. K., Singh, V., & Singh, P. K. (2017). Electrical, optical and electrophotochemical studies on agarose based biopolymer electrolyte towards dye sensitized solar cell application. *Measurement*, *102*, 214-219.

Singh, T. J., & Bhat, S. (2003). Morphology and conductivity studies of a new solid polymer electrolyte:(PEG) x LiClO$_4$. *Bulletin of Materials Science, 26*(7), 707-714.

Sit, Y. K., Samsudin, A. S., & Isa, M. I. N. (2012). Ionic conductivity study on Hydroxyethyl Cellulose (HEC) doped with NH$_4$Br based biopolymer electrolytes. *Research Journal of Recent Sciences 1*(11), 16-21.

Sohaimy, M. I. H., & Isa, M. I. N. (2017). Ionic conductivity and conduction mechanism studies on cellulose based solid polymer electrolytes doped with ammonium carbonate. *Polymer Bulletin*, *74*(4), 1371-1386.

Solanki, H. K., & Shah, D. A. (2016). Formulation optimization and evaluation of probiotic Lactobacillus sporogenes-loaded sodium alginate with carboxymethyl cellulose mucoadhesive beads using design expert software. *Journal of Food Processing*, *2016*.

Song, A., Huang, Y., Liu, B., Cao, H., Zhong, X., Lin, Y., & Zhong, W. (2017). Gel polymer electrolyte based on polyethylene glycol composite lignocellulose matrix with higher comprehensive performances. *Electrochimica Acta*, *247*, 505-515.

Stephan, A. M., & Nahm, K. S. (2006). Review on composite polymer electrolytes for lithium batteries. *Polymer*, *47*(16), 5952-5964.

Stoeva, Z., Martin-Litas, I., Staunton, E., Andreev, Y. G., & Bruce, P. G. (2003). Ionic conductivity in the crystalline polymer electrolytes PEO6: LiXF6, X= P, As, Sb. *Journal of the American Chemical Society*, *125*(15), 4619-4626.

Sun, J., Lv, C., Lv, F., Chen, S., Li, D., Guo, Z. & Guo, S. (2017). Tuning the shell number of multishelled metal oxide hollow fibers for optimized lithium-ion storage. *ACS nano*, *11*(6), 6186-6193.

Suthanthiraraj SA & Johnsi M 2017 Nanocomposite polymer electrolytes. *Ionics*, 23(10), 2531–2542.

Sudhakar, Y. N., Selvakumar, M., & Bhat, D. K. (2014). Tubular array, dielectric, conductivity and electrochemical properties of biodegradable gel polymer electrolyte. *Materials Science and Engineering: B*, *180*, 12-19.

Taib, N. U., & Idris, N. H. (2014). Plastic crystal–solid biopolymer electrolytes for rechargeable lithium batteries. *Journal of Membrane Science*, *468*, 149-154.

Tao, R., Zhao, Y., & Fujinami, T. (2007). Lithium borate–PEO polymer electrolytes characterized with high lithium ion transference numbers. *Materials Science and Engineering: B*, *137*(1-3), 69-73.

Teeters, D., Neuman, R. G., & Tate, B. D. (1996). The concentration behavior of lithium triflate at the surface of polymer electrolyte materials. *Solid State Ionics*, *85*(1-4), 239-245.

Tripathy, T., & Singh, R. P. (2001). Characterization of polyacrylamide- grafted sodium alginate: A novel polymeric flocculant. *Journal of Applied Polymer Science*, *81*(13), 3296-3308.

Wang, H., Zhang, S., Zhu, M., Sui, G., & Yang, X. (2018). Remarkable heat-resistant halloysite nanotube/polyetherimide composite nanofiber membranes for high performance gel polymer electrolyte in lithium ion batteries. *Journal of Electroanalytical Chemistry*, *808*, 303-310.

Winie, T., & Arof, A. (2004). Dielectric behaviour and AC conductivity of LiCFSO$_3$ doped H-chitosan polymer films. *Ionics, 10*(3-4), 193-199.

Williams, C. J., & Edyvean, R. G. (1997). Ion exchange in nickel biosorption by seaweed materials. *Biotechnology progress*, *13*(4), 424-428.

Woo, H. J., Majid, S. R., & Arof, A. K. (2012). Dielectric properties and morphology of polymer electrolyte based on poly(ε-caprolactone) and ammonium thiocyanate. *Materials Chemistry and Physics, 134,* 755-761.

Woo H. J., Majid S. R., Arof A. K. (2013) Effect of ethylene carbonate on proton conducting polymer electrolyte based on poly(e-caprolactone) (PCL). Solid State *Ionics 252*, 102–108.

Wright, P. V. (1975). Electrical conductivity in ionic complexes of poly (ethylene oxide). *British Polymer Journal, 7*(5), 319-327.

Wu, H. B., Chan, M. N., & Chan, C. K. (2007). FTIR characterization of polymorphic transformation of ammonium nitrate. *Aerosol Science and Technology*, *41*(6), 581-588.

Uma, T., Mahalingam, T., & Stimming, U. (2005). Conductivity studies on poly (methyl methacrylate)–Li_2SO_4 polymer electrolyte systems. *Materials Chemistry and Physics, 90*(2-3), 245-249.

Vahini, M., & Muthuvinayagam, M. (2018). AC impedance studies on proton conducting biopolymer electrolytes based on pectin. *Materials Letters, 218*, 197-200.

Varshney, P. K., & Gupta, S. (2011). Natural polymer-based electrolytes for electrochemical devices: a review. *Ionics, 17*(6), 479-483.

Verma, R., Vinoda, K., Papireddy, M., & Gowda, A. (2016). Toxic Pollutants from Plastic Waste-A Review. *Procedia Environmental Sciences, 35*, 701-708.

Vieira, D. F., Avellaneda, C. O., & Pawlicka, A. (2007). Conductivity study of a gelatin-based polymer electrolyte. *Electrochimica Acta, 53*(4), 1404-1408.

Vignarooban, K., Kushagra, R., Elango, A., Badami, P., Mellander, B.-E., Xu, X., Kannan, A. (2016). Current trends and future challenges of electrolytes for sodium-ion batteries. *International Journal of Hydrogen Energy, 41*(4), 2829-2846.

Vijaya, N., Selvasekarapandian, S., Hirankumar, G., Karthikeyan, S., Nithya, H., Ramya, C., & Prabu, M. (2012). Structural, vibrational, thermal, and conductivity studies

on proton-conducting polymer electrolyte based on poly (N-vinylpyrrolidone). *Ionics, 18*(1-2), 91-99.

Vijaya, N., Selvasekarapandian, S., Malathi, J., Iwai, Y., Nithya, H. &, Kawamura, J. (2013) NMR study on PVP-NH$_4$Cl based- proton conducting polymer electrolyte. *Indian Journal of Applied Research, 3,* 506-510.

Vincent, C. A. (1987). Polymer electrolytes. *Progress in solid state chemistry*, *17*(3), 145-261.

Yang, D. J., Fu, X. K., & Gong, Y. F. (2008). Study on the preparation and performances of P (VAc-MMA) polymer electrolytes for lithium ion battery. *Chinese Journal of Polymer Science*, *26*(04), 375-380.

Yang, J. M., Wang, N. C., & Chiu, H. C. (2014). Preparation and characterization of poly (vinyl alcohol)/sodium alginate blended membrane for alkaline solid polymer electrolytes membrane. *Journal of Membrane Science*, *457*, 139-148.

Yap, K. S. (2012). *Characteristics of pmma-grafted natural rubber polymer electrolytes/Yap Kiat Sen* (Doctoral dissertation, University of Malaya).

Zainuddin, N. K., & Samsudin, A. S. (2018). Investigation on the Effect of NH$_4$Br at Transport Properties in K–Carrageenan Based Biopolymer Electrolytes via Structural and Electrical Analysis. *Materials Today Communications*, *14,* 199-209.

Zang, L., Luo, J., Guo, J., Liu, H., & Ru, J. (2010). Preparation and characterization of poly (ethylene glycol)/organo-vermiculite nanocomposite polymer electrolytes. *Polymer bulletin, 65*(7), 669-680.

Zhang, J., Yuan, Y., Shen, J., & Lin, S. (2003). Synthesis and characterization of chitosan grafted poly (N, N-dimethyl-N-methacryloxyethyl-N-(3-sulfopropyl) ammonium) initiated by ceric (IV) ion. *European Polymer Journal*, *39*(4), 847-850.

Zhang, P., Yang, L., Li, L., Ding, M., Wu, Y., & Holze, R. (2011). Enhanced electrochemical and mechanical properties of P (VDF-HFP)-based composite polymer electrolytes with SiO$_2$ nanowires. *Journal of Membrane Science, 379*(1-2), 80-85.

Zhang, Q., Liu, K., Ding, F., & Liu, X. (2017). Recent advances in solid polymer electrolytes for lithium batteries. *Nano Research*, 1-36.

Zhao, Y., Zhang, Y., Gosselink, D., Sadhu, M., Cheang, H. J., & Chen, P. (2012). Polymer electrolytes for lithium/sulfur batteries. *Membranes*, *2*(3), 553-564.

Zhou, L., Wu, N., Cao, Q., Jing, B., Wang, X., Wang, Q., & Kuang, H. (2013). A novel electrospun PVDF/PMMA gel polymer electrolyte with in situ TiO_2 for Li-ion batteries. *Solid State Ionics*, *249*, 93-97.
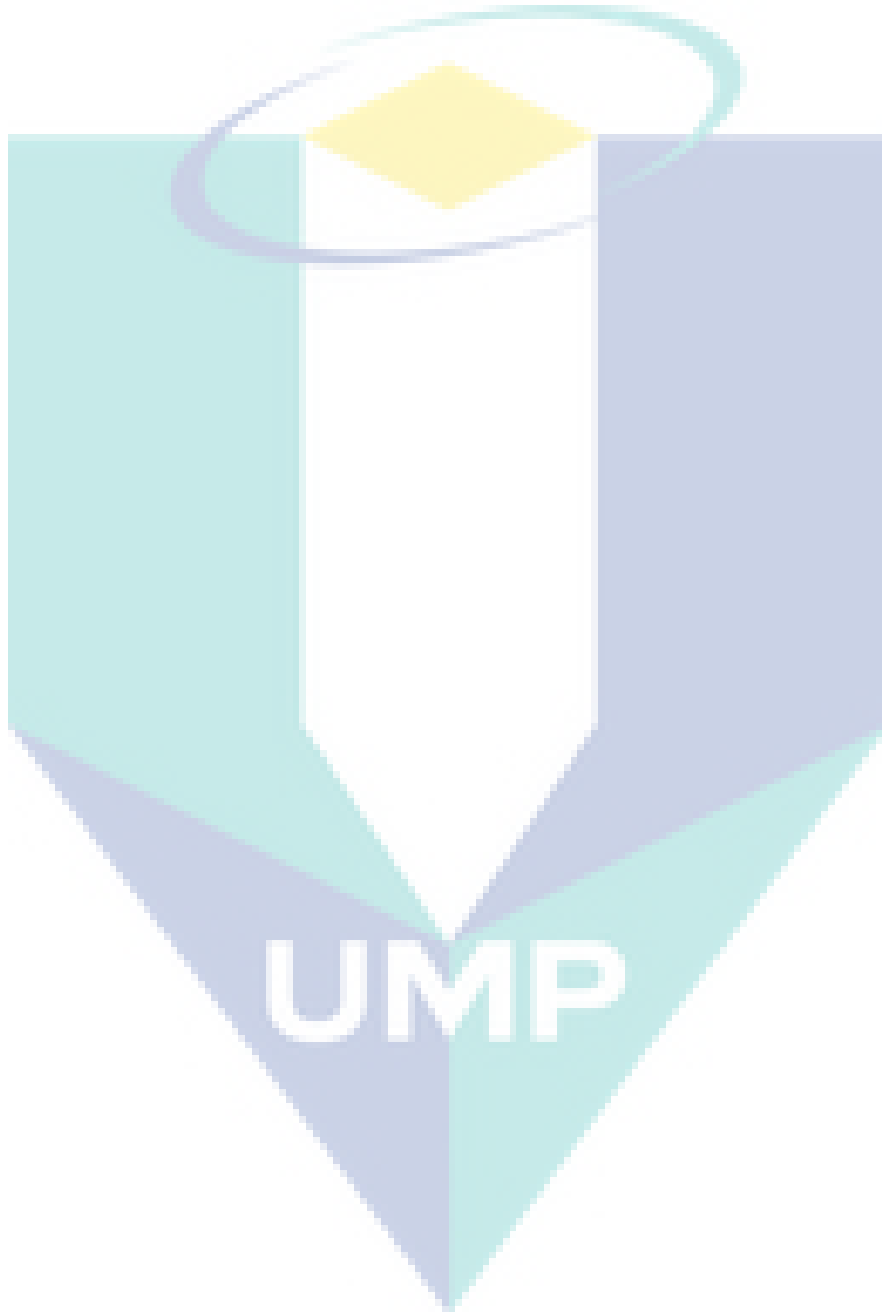
APPENDIX A

LISTS OF PUBLICATION AND CONFERENCE PROCEEDING

Published and under reviewed

1. **N. M. J. Rasali**, S. K. Muzakir and A. S. Samsuddin (2017). "A Study on Dielectric Properties of The Cellulose Derivative-NH4Br-Glycerol- Based The Solid Polymer Electrolyte System". *MAKARA Journal of Technology*, 21(2), 65-69.

2. **N. M. J. Rasali** and A. S. Samsuddin (2018). "Ionic transport properties of protonic conducting solid biopolymer electrolytes based on enhanced carboxymethyl cellulose - NH4Br with glycerol". *Ionics*, 24(6), 1639-1650.

3. N. K. Zainuddin, **N. M. J. Rasali** and A. S. Samsudin (2018). "Study on the effect of PEG in ionic transport for CMC-NH4Br-based solid polymer electrolyte". *Ionics*, 1-14.

4. **N. M. J. Rasali**, Y. Nagao and A. S. Samsuddin (2018). "Enhancement on amorphous phase in solid biopolymer electrolyte based alginate doped NH4NO3". Ionics, 1-14.

5. Fuzlin, A. F., **Rasali, N. M. J**., & Samsudin, A. S. (2018, April). Effect on Ammonium Bromide in dielectric behavior based Alginate Solid Biopolymer electrolytes. Materials Science and Engineering 342(1), 012080. IOP Publishing.

6. Mazuki, N. F., **Rasali, N. M. J**., Saadiah, M. A., & Samsudin, A. S. (2018, November). Irregularities trend in electrical conductivity of CMC/PVA-NH4Cl based solid biopolymer electrolytes. 2030(1), 020221. AIP Publishing.

7. **N. M. J. Rasali**, N.K. Zainuddin, M. A. Saadiah, Y. Nagao, and A.S. Samsudin (2018). "Ionic conduction properties analysis via theoretical and experimental approach on solid bio-polymer electrolytes based carboxymethyl cellulose doped NH4CH3CO2". Under review (Electrochimica Acta)

Conference Proceedings

1. **N. M. J. Rasali**, S. K. Muzakir and A. S. Samsuddin (2016). "A Study on Dielectric Properties of The Cellulose Derivative-NH$_4$Br-Glycerol- Based The Solid Polymer Electrolyte System". Proceeding in International Collaborative Conference on Technology 2016, 17th October 2016, Bandung, Indonesia.

2. **N. M. J. Rasali** and A. S. Samsuddin (2017). "Investigation on Dielectric Properties of Cellulose Derivative-NH$_4$Br-Glycerol for application as Solid Polymer Electrolyte System". Proceeding in National Workshop on Functional Materials (NWFM 2017), 17-18th January 2017, Physics Department, University of Malaya, Kuala Lumpur.

3. **N. M. J. Rasali** and A. S. Samsuddin (2017). "Effect on the electrical properties of plasticized cellulose derivative-NH$_4$Br solid polymer electrolytes system via impedance analysis". Proceeding in ASIA International Multidisciplinary Conference 2017, 1st-2nd May 2017, Universiti Teknologi Malaysia (UTM), Johor.

4. **N. M. J. Rasali** and A. S. Samsuddin (2017). "Ionic transport studies of bio-polymer electrolytes on cellulose derivative doped NH$_4$CH$_3$CO$_2$". Proceeding in 6th International Conference on Functional Materials & Devices (ICFMD 2017), 15-18th August 2017, Bayview Hotel, Melaka.

5. A. F. Fuzlin, **N. M. J. Rasali** and A. S. Samsuddin (2018). "Effect on Ammonium Bromide in Dielectric Behavior based alginate solid biopolymer electrolytes". Proceeding in International Conference on Innovative Technology, Engineering and Sciences (iCITES 2018), 1st-2nd March 2018, Universiti Malaysia Pahang, Pekan, Pahang.

6. **N. M. J. Rasali** and A. S. Samsuddin (2018). "Characterization on Ionic Conductivity of Solid Bio-Polymer Electrolytes System Based Alginate Doped Ammonium Nitrate via Impedance Spectroscopy". Proceeding in 6th International Conference on Advanced Material Engineering & Technology (ICAMET) 2018, 29-30th April 2018, Ho Chi Minh, Vietnam.

7. N. F. Mazuki, **N. M. J. Rasali**, M. A. Saadiah and A. S. Samsuddin (2018). "Irregularities trend in electrical conductivity of CMC/PVA-NH$_4$CI based solid biopolymer electrolytes". Proceeding in 6th International Conference on Advanced Material Engineering & Technology (ICAMET) 2018, 29-30th April 2018, Ho Chi Minh, Vietnam.